Aalto-yliopisto
Insinööritieteiden
korkeakoulu

Janne Heiskari

On the design criteria of large insulating glass structures in cruise ships

Thesis submitted for examination for the degree of Master of Science in Technology

Espoo, Finland 18.09.2020

Supervisors

Prof. Jani Romanoff, Aalto University
(Prof. Jonas Ringsberg, Chalmers University of Technology)

Advisors

M.Sc. Aleksi Laakso
M.Sc. Ari Niemelä

Aalto University
School of Engineering

Aalto University, P.O. BOX 11000, 00076 AALTO
www.aalto.fi

Abstract of master's thesis

Author Janne Matias Heiskari

Title of thesis On the design criteria of large insulating glass structures in cruise ships

Master programme Nordic Master Programme in Maritime Engineering **Code** ENG214

Thesis supervisor Professor Jani Romanoff

Thesis advisors M.Sc. Aleksi Laakso, M.Sc. Ari Niemelä

Date 18.09.2020 **Number of pages** 63+20 **Language** English

Abstract

Insulating glass units (IGUs) consist of two glass panes separated by a hermetically sealed gas. IGUs are used in ships to save energy by reducing heat losses. From a structural point of view, research has shown that the gas transfers loads between the glass panes, which increases the IGU's structural performance. This load sharing effect is not yet considered in ship classification rules by different classification societies, which may result in thicker glass constructions than necessary. Thus, this thesis studies the load sharing effect for evaluating the sufficiency of the current design criteria for glass pane thickness determination.

This thesis presents a Finite Element (FE) model for calculating the response of a rectangular IGU using Ansys. The glass is modelled with structural shell elements (SHELL181) and the gas is modelled with hydrostatic fluid elements (HSFLD242). The former is based on Mindlin-Reissner plate theory, while the latter is based on Ideal Gas Law. The interaction between the glass panes is determined by considering the volume change of the gas.

The response is first calculated on a linear basis, considering small loads that are frequently applied to ship structures. The linear FE model is validated by Betti's Analytical Method. However, occasionally the windows are subjected to increased loads that result in large deflections of thin glass plates, i.e. geometrically nonlinear behavior is observed. The linear FE model is extended for nonlinear analysis. The model is validated by experimental results from open scientific literature.

The presented nonlinear FE model is used to calculate the minimum required thickness of glass panes in an IGU, with respect to standard stress limit. The same thicknesses are also calculated according to classification rules by Lloyd's Register. The obtained thicknesses are compared. The results indicate that the thickness of the glass panes can be reduced up to 52 percent when the load sharing effect is considered. The reduction is based on maximum principal stress reduction that is a benefit of both panes carrying the load instead of one. This reduction is the largest when the geometric nonlinearities are apparent.

Based on the results, this study concludes that the current glass pane thickness determination criteria by the classification societies are insufficient. Cruise ships have hundreds of square meters of IGUs and therefore the load sharing should be considered, to reduce weight or to allow for larger windows. Furthermore, the findings of this study are important as the classification rules are based on linear assumptions and very little information is available in the open scientific literature about IGU FE modelling.

Further research is needed to obtain more experimental results for IGUs with different boundary conditions as they appeared to have significant effect on the performed analyses.

Keywords Design criteria, insulating glass unit, load sharing, hydrostatic fluid element

Acknowledgements

This thesis was written for Meyer Turku Oy in the department of hull basic design and marks the ending of my joint Master's programme in the Nordic Master in Maritime Engineering.

I would like to thank my thesis supervisors Jani Romanoff from Aalto University and Jonas Ringsberg from Chalmers University of Technology for all their guidance. I would also like to show my gratitude to the thesis advisors at Meyer Turku, Aleksi Laakso and Ari Niemelä for providing the thesis subject and helping me along the project.

Lastly, I want to thank my family, friends and fellow students at Chalmers University of Technology for their support, especially Gustav and Linda.

Espoo 18.9.2020

Janne Heiskari

Contents

Nomenclature

A	[mm²]	area of glass pane
D_i	[Nmm]	flexural rigidity of glass pane
E	[MPa]	Young's Modulus of glass
LS_1	[%]	load carrying percentage of glass pane 1
T_0	[K]	reference absolute temperature in cavity at time of sealing
$\overline{\Delta T}$	[K]	temperature variation of gas in cavity with respect to T_0
V_0	[mm³]	reference volume of the cavity at time of sealing
a	[mm]	length of glass plate in x-direction
b	[mm]	length of glass plate in y-direction
$\bar{f}_1(x,y)$	[N]	force acting on glass pane 1
$\bar{f}_2(x,y)$	[N]	force acting on glass pane 2
h_1	[mm]	thickness of glass pane 1
h_2	[mm]	thickness of glass pane 2
$\bar{p}$	[N]	applied uniform pressure on pane 1
p_0	[MPa]	reference pressure of the gas in the cavity at time of sealing
s	[mm]	thickness of IGU spacer
t_0	[mm]	thickness of glass pane according to class rules
$w_1(x,y)$	[mm]	deflection of glass pane 1 at specified point
$w_2(x,y)$	[mm]	deflection of glass pane 2 at specified point
$w_{1\,max}$	[mm]	maximum deflection of glass pane 1
$w_{2\,max}$	[mm]	maximum deflection of glass pane 2
Δp_1	[MPa]	cavity pressure variation due to atmospheric pressure change
$\overline{\Delta p}$	[MPa]	atmospheric pressure change
$\Delta p_{barometric}$	[MPa]	pressure acting on one pane due to atmospheric pressure change
$\Delta p_{external}$	[MPa]	cavity pressure variation due to external pressure
$\Delta p_{temperature}$	[MPa]	cavity pressure variation due to temperature change
Δp_{total}	[MPa]	superimposed cavity pressure variation
σ_{p+}	[MPa]	maximum principal stress
ν	[-]	Poisson's ratio of glass
$\bar{\psi}_A$	[-]	mean value of shape function on the area
$\psi(x,y)$	[-]	shape function for the deflection of a simply supported plate under uniform pressure

Abbreviations

BAM	Betti's Analytical Method
BC	Boundary condition
DIGU	Double-glazed insulating glass unit
DNVGL	Det Norske Veritas and Germanischer Lloyd
DOF	Degree of freedom
FEM	Finite Element Method
HSFLD242	3-D Hydrostatic fluid element
IGU	Insulated glass unit
LG	Laminated glass
LR	Lloyd's Register
LSG	Laminated safety glass
PVB	Polyvinyl butyral
RINA	Registro Italiano Navale
SG	SentryGlas®
TIGU	Triple-glazed insulating glass unit

1 Introduction

The advancements in glazing technology has increased the usage of glass in structures. Glass is a rigid material that is known for its transparency and brittle behavior. However, owing to the modern post processing techniques, it is even used as a load bearing material e.g. in cars and skyscrapers. For building architecture, the recent market trends show that i) more glass is used for more transparency; ii) demand of complex glass geometries has increased; iii) larger individual glass panes are manufactured [1].

The development of the trends is important as cruise line companies use other industries as one source of inspiration for attracting passengers in a competing business. The companies are always on a lookout for new "wow" factors that will make the customer to choose their ship for the next holiday cruise instead of the competitor's.

Ship architecture is one key "wow" factor. The passengers want a hotel-like luxurious experience that also enables immersion with the marine environment [2]. Therefore, the usage of glass has increased significantly in cruise ships. In particular, the size and the number of windows has increased but also large glass structures are built (Figure 1).

Figure 1. SkyDome of MS Iona, a flagship of P&O cruises, built by Meyer Werft in Papenburg [3].

The increasing glass usage in combination with light-weight steel structures requires special attention. Light-weight structures are used to increase operational efficiency, reduce building cost and gain better stability, to name a few. As the ship structure is built as lightweight and invisible as possible, the proportion of glass increases in weight and volume. Therefore, considering glass in structural design has become more important. Several studies have been conducted recently for ship windows.

Fricke and Gerlach [4] studied the contribution of large bonded and clamped windows on the shear stiffness of ship's side wall. The side walls have multiple windows and consequently large cut-outs with slender mullions in between. Therefore, the stiffness of the windows can be significant on the total stiffness of the side wall. The study demonstrated how the shear stiffness of clamped or bonded windows can be considered in the global Finite Element model. It was concluded that the shear stiffness increases with windows. The

authors highlighted the significance of adequate Finite Element mesh quality in the connection between the window and the hull.

Wiegard et al. [5] studied bonded windows on the strength and vibration analysis of ship structure. The authors challenged the common assumption that neglecting the windowpanes in the global analysis is a conservative approach. They conducted full-scale experiments and Finite Element analyses. It was found that the stresses in the mullions between two windows increased in some cases. These findings are important as they proved that neglecting the windows in the strength analysis is not always conservative. Furthermore, they concluded that the windowpanes have negligible effect on the global stresses and deformations of the ship structure. However, the authors recommend including the windowpanes in the strength analysis for assessing the correct structural stresses.

Gerlach et al. [6] studied the response of window subjected to wave loads as incidents have occurred where superstructure windows have broken due to a wave impact. Some of these incidents have led to loss of lives. The event is complex and hence it was studied experimentally and numerically. The numerical studies included first computational fluid dynamics for determining shape and velocity of water mass just before the impact. Then the impact was simulated using hydrodynamics and Finite Element Method. The presented method is able to predict the failure probability of windows in wave impact.

Wave impact can be experienced in severe sea state or when rogue waves are encountered. These rogue waves are steep and larger than the surrounding waves and hence are very dangerous for ships and offshore structures. Bitner-Gregersen and Gramstad [7] studied the rogue waves and their impact on marine structures. Because these waves are rare, the study seeks answer to question whether they should be accounted for in the design and if so, how. The study concluded that rogue waves can be expected to occur more than once during ships lifetime. In that sense, they should be accounted for in the design, but it is not clear how. The implication for window design is that larger loads can occur during ship's lifetime than expected for.

Gerlach and Fricke [8] studied the response of windows subjected to quasi-static pressure loads. An example of such load case is MS Estonia. The reason for the extremely fast sinking was suspected to be related to broken windows that enabled massive inflow of water as a consequence of capsizing. The authors conducted experimental studies using water filled bags that represent the load. Additionally, nonlinear Finite Element analysis was performed which showed good agreement with the experiments. Large deflections were observed in the glass pane and in the surrounding metal structure which led the glass pane to slip-out from the frame in some cases. These findings highlight the importance of nonlinear analysis and correct assessment of the boundary conditions.

Vergassola and Boote [9] and by Van Antwerpen et al. [10] studied the effect of large openings in passenger comfort onboard. Passenger comfort in cruise ships is essential and its significance has increased in the recent years. The focus in the studies was to reduce noise and vibration that are a consequence of having large windows. The latter paper analyzes the windows using Finite Element Method and experiments. The former also conducts experiments but uses dynamic effective thickness in the numerical analyses. The dynamic effective thickness is a convenient way to model laminated glasses as an alternative to

conventional layered shell or solid FE models. These methods can be used in the early design phases. This is important as modifying existing structures is difficult and expensive.

Verbaas [11] discussed glass as a structural material in ships and identified challenges that they have onboard. The challenges are summarized in Table 1, which demonstrates how glass differs from conventional building materials, e.g. from steel. Therefore, special care must be practiced in designing glass structures in ships.

Table 1. Design challenges with glass in ships [11].

	Design challenge
1.	Glass is brittle material with linear stress-strain curve until it breaks without any plasticity. Therefore, permissible strain under design load has to be chosen well below the breaking strain
2.	The load bearing capacity of glass does not remain constant throughout its lifetime
3.	Glass is susceptible to surface damage
4.	Any surface damage may lead to instantaneous failure without any sign of warning
5.	The strength of glass has a relatively large variation. Thus, large number of tests have to be conducted with statistical processing to determine it

Verbaas [12] further discussed the identified challenges. He concluded that the disadvantages of glass as a structural material can be overcome with good engineering. The best way to do so is to use the technology, materials and standards from building industry. However, the building industry uses Eurocodes for designing. Verbaas [13] studied what could be adapted from the building industry and hence trying to establish a foundation for a design code of structural glass in ships.

1.1 Classification of ship windows

Yet to date, no design code such as Eurocode exist for ship's glass structures. Therefore, the design is done according to the rules and regulations by different classification societies. Three common classification societies are Lloyd's Register (LR) [14], DNV GL [15] and RINA [16]. The former two have almost identical rules for glass design while RINA has slightly less specific rules (Table 2). Lloyd's Register is used as a reference hereinafter.

The current LR's guidelines (July 2019) for windows in cruise ships are given in "Pt 3, Ch 11, 6.5" and "Pt 4, Ch 2, 11" [14]. First of all, it is defined that the windows are thermally toughened safety glass. Chemically strengthened glass can be used if it is demonstrated to have at least equivalent strength to that of thermally toughened glass. Furthermore, chemically strengthened glass can be only used in laminated construction. Laminated glasses are sandwich structures with at least two panes of glass and one polymeric interlayer [17].

The required thickness for a single rectangular thermally toughened glass pane is calculated according to Equation 12 (Appendix 1). If laminated construction is used, then the total thickness of the laminated glass has to be greater than required for equivalent sized toughened safety glass (Equation 13 in Appendix 1). As an example, if a toughened safety glass with thickness of 10 mm is replaced with laminated glass consisting of two equally thick toughened glasses, the total thickness of the laminated construction has to be about 14 mm. The formula therefore assumes the "worst case" scenario where the interlayer is neglected (no shear transfer). The design pressure acting on the window is defined depending on the vertical location of the window as well as whether it is located on the sides, aft or front (Figure 41 in Appendix 1).

Table 2. Design of glass panes according to classification societies. See Appendix 1 for more detailed explanation of Lloyd's Register's equations.

	Lloyd's Register [14]	DNV GL [15]	RINA [16]
Glass type	Thermally toughened/ chemically strengthened	Thermally toughened	Thermally toughened
Configuration	Monolithic/laminated	Monolithic/laminated	Monolithic
Thickness for single glass pane	$t_0 = b\sqrt{\frac{H_d\beta}{4000}}$	$t_r = \frac{b}{200}\sqrt{\beta P}$	Prescribed depending on window size
Thickness for laminated glass	${T_S}^2 = {T_{L1}}^2 + {T_{L2}}^2 + \cdots + {T_{Ln}}^2 \geq t_0$	$t_e = \sqrt{\frac{\sum_i^n = 1t_i^3}{t_{max}}} \geq t_r$	N/A
Maximum size	N/A	N/A	1100 x 800 mm

Other design pressures and thickness arrangements are accepted given that they are according to equivalent nationally or internationally recognized standards. Specifications for rectangular ship windows are given in ISO 3903 [18]. The thickness of thermally toughened window complying ISO 3903 can be calculated according to ISO 21005 [19]. However, the specifications are only valid up to window size of 1100x800 mm. Larger windows have to be tested with typically safety factor of four with respect to the characteristic failure strength of glass [20]. In case of laminated glass, the recently adopted standard ISO 11336-1 [21] considers the contribution of the interlayer (shear transfer). However, the standard is made only for large yachts up to 3000 gross tonnage. Hence, the laminated glasses are often tested according to EN 1288-3 [22].

1.2 Research problem

Most of windows in cruise ships (e.g. in Figure 1) are insulated glass units (IGUs) consisting of at least two glass panes separated by hermetically sealed space (Figure 2). The space is often filled with air or argon. The IGUs are commonly used in every industry due to their ability to reduce heat losses and provide noise insulation. Furthermore, often the IGUs in ships are built with laminated glasses consisting of thermally toughened safety glass and ionomer interlayer.

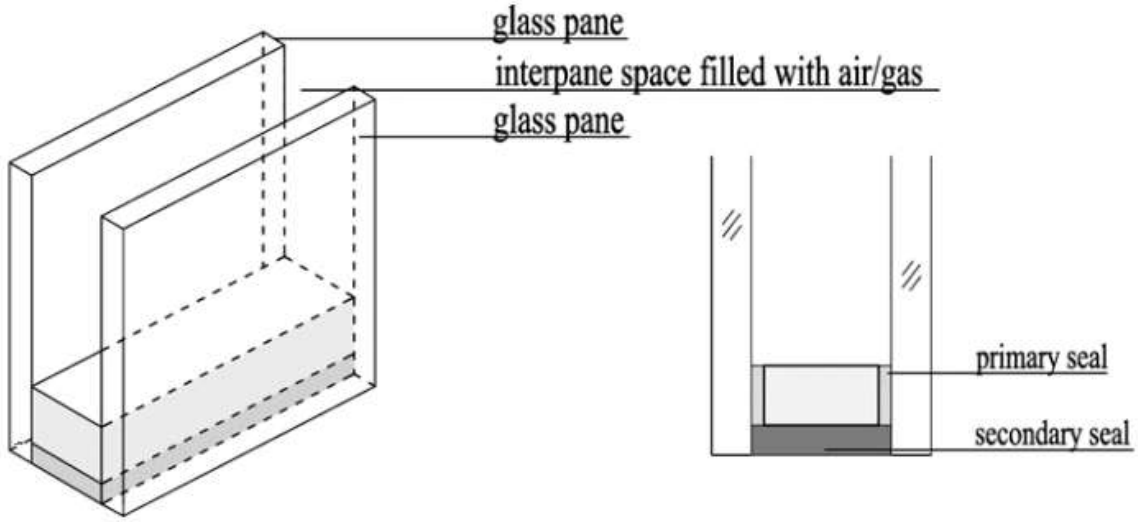

Figure 2. Insulating glass unit consisting of monolithic glasses [23].

Special for IGUs from structural point of view is that load is shared between the glass panes via the gas. The load sharing is beneficial for the structure and its significance has been proven experimentally by McMahon et al. [24]. The implication of considering the load sharing is that the thickness of individual glass panes could be reduced, or potentially larger glass panes could be designed.

In the building industry, the load sharing effect is recognized in the upcoming Eurocode for glasses [25] and in other standards [26, 27, 28, 29]. However, it is not yet considered in the aforementioned standards for ships nor in the classification rules. The thickness determination is only prescribed for monolithic glasses and laminated glasses. This contradicts the ideology of having as lightweight and economical structure as possible considering that largest cruise ships have hundreds of square meters of IGUs. Hence, it is established that the current classification rules may provide insufficient design criteria for determining the thickness of glass panes in insulating glass units.

1.3 Objective

The objective of this thesis is to evaluate the sufficiency of the current design criteria of glass pane thickness determination set by the classification societies. The criteria can be evaluated by presenting a Finite Element model for calculating the response of rectangular insulating glass units used in cruise ships. Therefore, this thesis presents a literature study to obtain comprehensive understanding of glass in structures, and the load sharing effect. Part of the study is presented in the appendices in more detail.

1.4 Limitations

The case consists of an insulating glass unit located in ship so that is separates the indoor and outdoor. The insulating glass unit is therefore subjected to multiple loads. These include ship motions, temperature changes, wind load, water particle splashes, snow load, impact, wave blast etc. The loading condition in this study is limited to uniform pressure with short loading time, e.g. a wind load. The behavior of glass in impact, blast and extreme loads is studied e.g. in [30, 31, 32, 33].

The insulating glass unit consist of laminated glass, gas, edge seal system and a frame. The IGU is connected to a larger structure via mechanical or adhesive connection. The connections can be linear or local. In the analysis, only rectangular monolithic glasses and the gas is considered with linear simply support around its four edges. The model is sufficient to demonstrate the load sharing effect. The implications of laminated glass, glass connections and edge seal system on the mechanical behavior are discussed.

2 Structural glass

Different type of glass materials exists. Most common ones are silicate glasses, which cover 95% of all the glass production [34]. Silicate glasses can be further divided into subsets depending on the chemical composition. This thesis will focus on soda-lime silicate glasses hereinafter, as they are the most commonly used variety in structures in the form of flat glass.

Flat glass includes all the glasses that have been produced as a flat piece of glass by different manufacturing methods. Float glass is a subset of flat glass and will be the focus on this thesis. Float glass is a product of manufacturing method, floating, and annealing process, hence the name annealed float glass. Nowadays it covers 90% of all flat glass production [17] and 35% of all glass production [34].

Annealed float glass is the base for most of the structural glasses. Glasses by casting in structural applications have been also studied but they are expensive and lack standardization [35]. This chapter describes the basic glass products and their properties and behavior.

2.1 Float glass

The novel floating process was invented in 1959 by the Pilkington Brothers. This process is described in Figure 3. The raw material is melted in the furnace and then poured on to a pool of molten tin. The molten glass floats on the liquid tin and spreads across, forming a sheet with equilibrium thickness of 7 mm. The formed smooth sheet is drawn to an annealing lehr, where the glass is slowly cooled to 100 °C. The cooling process prevents any unwanted residual stresses from inducing inside the glass. The thickness is controlled by the speed of the rollers that draw the glass sheet in to the annealing lehr. Thicknesses that can be produced vary from 2 mm to 25 mm [17]. The dimensional and quality requirements are specified in EN 572-2 [36]. Finally, the product is cooled to room temperature, inspected and cut.

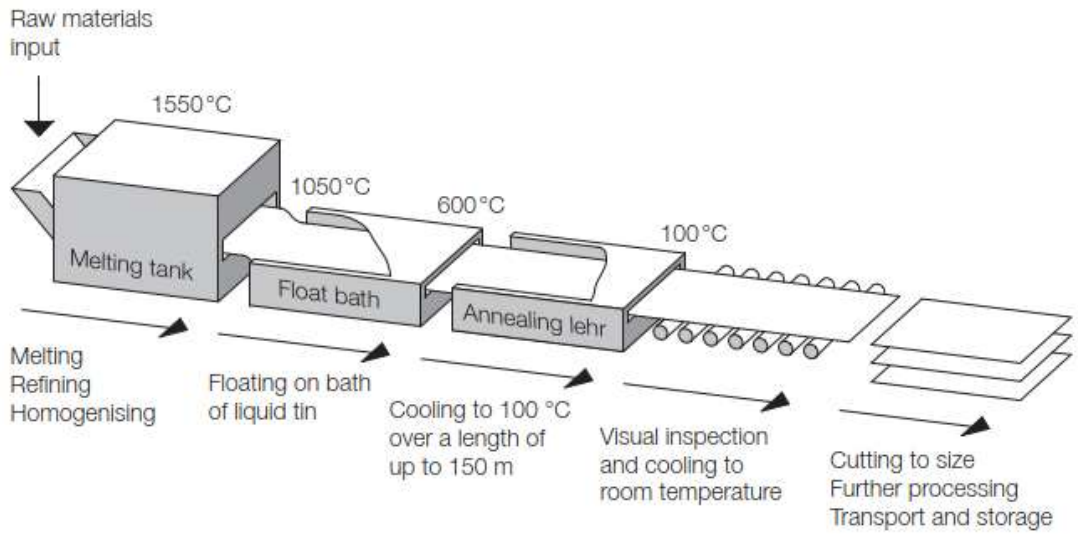

Figure 3. Principle sketch of the floating process [34].

The side of the float glass that is in contact with the molten tin is called tin side. Similarly, the other side is called air side. The sides are not identical because some tin atoms have diffused on the surface [37]. The tin side is also in contact with the conveying steel rollers. The rollers cause surface flaws that alters the mechanical properties of that side [38], e.g. decrease the mechanical strength [17].

Glass is a non-crystalline solid, also called amorphous solid, that show short-range order atoms i.e. they are not periodically ordered [39]. Glass transforms from brittle and hard state to molten viscous/rubber-like state as temperature is increased. This is called glass transition. The transition does not have an exact point but happens over a temperature range [17]. The constituents of soda-lime silicate glass are presented in Table 3. It should be noted that the chemical composition of soda-lime silicate glass is defined by proportion by mass of elements (oxides excluded).

Table 3. Principal constituents by mass proportions of soda-lime silicate glass according to EN 572-1 [40].

Constituents	Proportion by mass of elements
Silicon (Si)	32% - 35%
Calcium (Ca)	3.5% - 10.1%
Sodium (Na)	7.4% - 11.9%
Magnesium (Mg)	0% - 3.7%
Aluminium (Al)	0% - 1.6%
Others [a]	< 5%

[a] Properties other than photometric characteristics shall not be significantly altered by these other components.

The important general characteristics of soda-lime silicate glass are presented in Table 4.

Table 4. General characteristics of soda-lime silicate glass according to EN 572-1 [40].

Characteristics	Symbol	Value and unit
Density (at 18°C)	ρ	2500 kg/m^3
Hardness (Knoop)	$HK_{0,1/20}$	6 GPa [a]
Young's modulus (modulus of elasticity)	E	70 GPa
Poisson's ratio	μ	0.2[b]
Specific heat capacity	c_p	0.72 x 10^3 J/(kg · K)
Resistance against temperature differential and sudden temperature change		40 K[c]
Thermal conductivity	λ	1 W/(m · K)
Emissivity (corrected)	ε	0.837

[a] Knoop Hardness in accordance with ISO 9385
[b] Values of 0.22 to 0.24 are typically used in practice [17]
[c] Generally accepted value that is influenced by edge quality and glass type.

2.2 Prestressed glass

Behavior of annealed float glass is dependent on the surface properties i.e. on surface cracks. Consequently, it has low tensile strength and fractures to large fragments in a brittle manner. This is associated with high risk of injury [34].

Heat and chemical treatments are used to overcome these shortcomings. The treatments create residual stress field (prestress) on the glass: tensile in the core and compressive on the surfaces. The compressive prestress ensures that the surface cracks do not propagate during loading [17]. This principle is described in Figure 4.

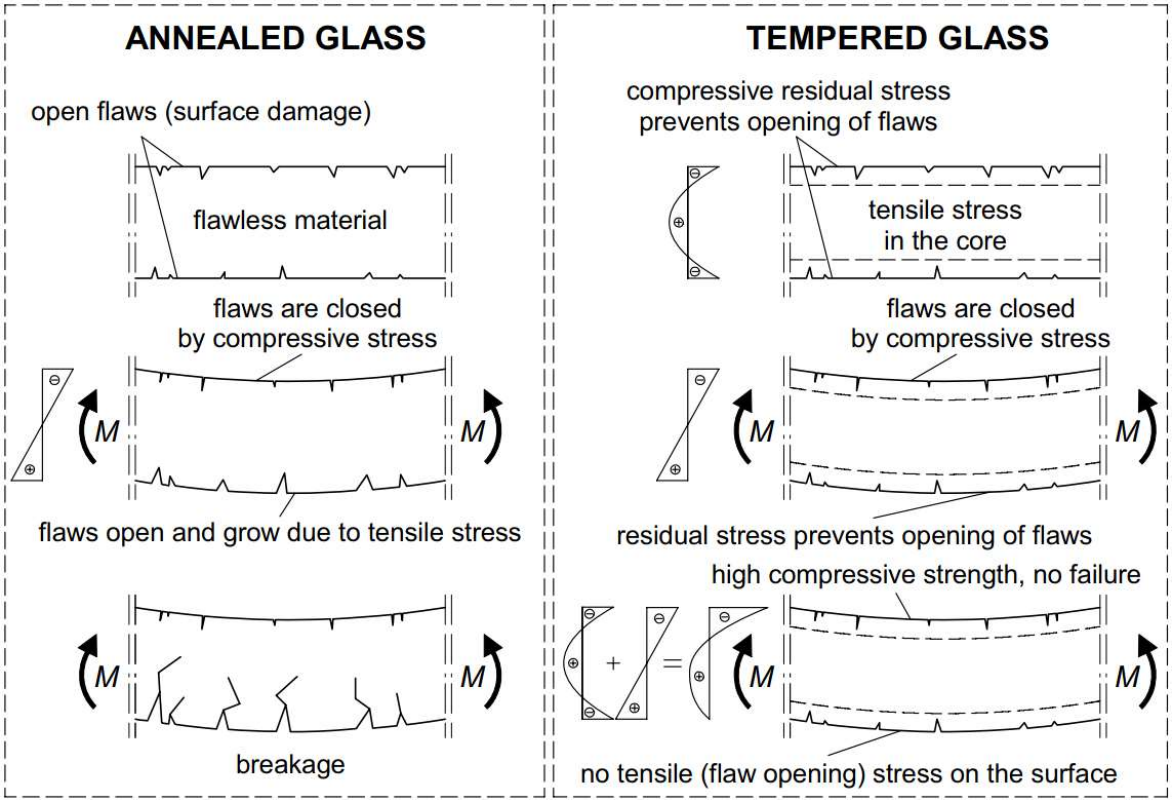

Figure 4. Behavior of annealed glass and tempered glass in bending [17].

Fully tempered glass, also called as **thermally toughened glass**, has been heated above its glass transition temperature and then cooled rapidly with bursts of cold air. The cooling process is called quenching. The cold air causes the surfaces to cool and contract faster than the core, resulting in the characteristic residual stress field. Consequently, the stored energy changes the fracture pattern. Fully tempered glass has the highest residual stress and breaks into small and relatively harmless pieces (~100 mm²) [17]. Therefore, it is also called as safety glass. Minimum values for the count of broken particles are given in EN 12150-1 [41]. Float glass with thicknesses from 2 mm to 25 mm can be fully tempered [41].

Fully tempered glass can experience spontaneous breakage after it has been manufactured [17]. This is due to Nickel Sulfide (Nis) inclusions (impurities) that convert into form with smaller specific volume during the heating process. The inclusions are not able to convert back to their normal state during the rapid cooling. However, when the glass is exposed e.g. to solar radiation, the supplied energy is sufficient to cause the inclusions to expand back to their original state. The volume change of the inclusions creates stresses that act together with the high tensile stress in the core [17]. The combination of the stresses can cause spontaneous failure.

The risk of failure can be reduced by **heat soak test**. Fully tempered glass is heated to a holding temperature of 260°C±10°C for several hours. Present Nickel Sulfide inclusions will expand and break the glass during the testing. The procedure is presented in EN 14179-1 [42], where the residual risk of breakage is estimated to be 1 per every 400 tonnes of heat soaked glass.

Heat strengthened glass undergoes the same procedure as fully tempered glass with the exception of slower cooling rate. Therefore, the residual stress field and the achieved tensile

strength are lower than for fully tempered glass. However, the lower stored energy leads to larger broken particles (Figure 5). Float glasses with thicknesses up to 12 mm can be heat strengthened [43].

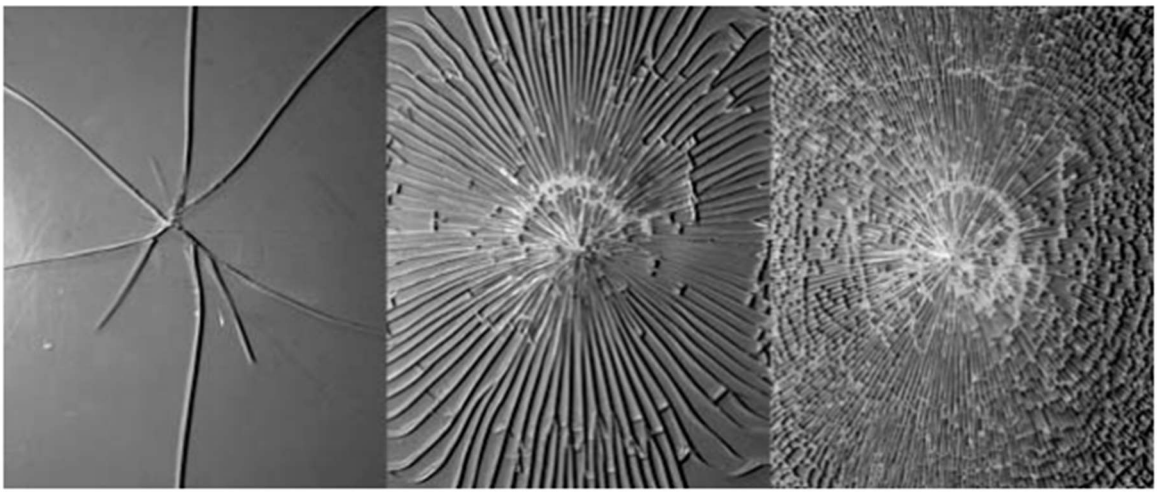

Figure 5. Fracture patterns of annealed glass, heat strengthened glass and fully tempered glass, respectively [17].

The residual stress field can be alternatively achieved with **chemical strengthening**. However, chemically strengthened glasses are less common in structural applications [34, 17] due to higher expenses and thickness limitations. Curved and thin glasses are often chemically strengthened, especially if they should withstand impact or high velocities, e.g. aircraft windshields [44]. The sodium ions on the surface of the glass are replaced by potassium ions through an ion exchange process. The potassium ions are larger than the sodium ions and therefore compression on the surfaces is created. The exchange of ions occurs only close to the surface, which results in different residual stress field than in tempering (Figure 6). Karlsson and Jonson [44] present a detailed review of chemical strengthening and comparison to the other methods. Float glass with thicknesses up to 12 mm can be chemically strengthened [45].

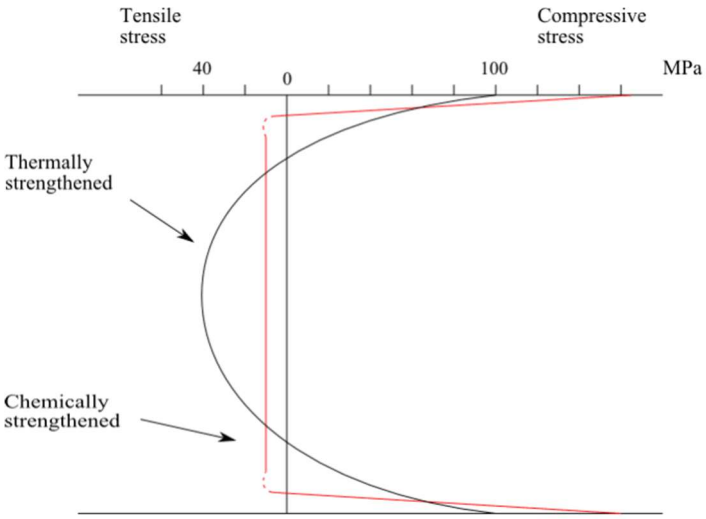

Figure 6. Residual stress field comparison between tempered glass and chemically strengthened glass [44].

2.3 Laminated glass

Laminated glass (LG) is a composite structure consisting of at least of two panes of glass and one polymeric interlayer [17]. The most common polymeric interlayers are presented in Appendix 2. Laminated glasses are typically used in applications where the structural integrity of a single glass pane is insufficient (Figure 7). The panes can be annealed glass, heat treated glass, chemically strengthened glass or a combination of two or more. Similarly, the thickness of the panes can be unequal or equal. Combination of differently treated glasses and thicknesses are used to obtain better structural performance [46]. These hybrid solutions are also used in a "sacrificial ply" concept, where one extra glass ply is used to collect the live loads but does not have any structural role in the design i.e. it is considered broken [47].

Manufacturing of laminated glass can be divided to dry and wet method. In dry method, heat and pressure are applied to ensure bonding between the interlayer and the glass [17, 48]. The wet method and its liquid resins are less common in structures. The quality of bonding has a great influence on the behavior of laminated glass.

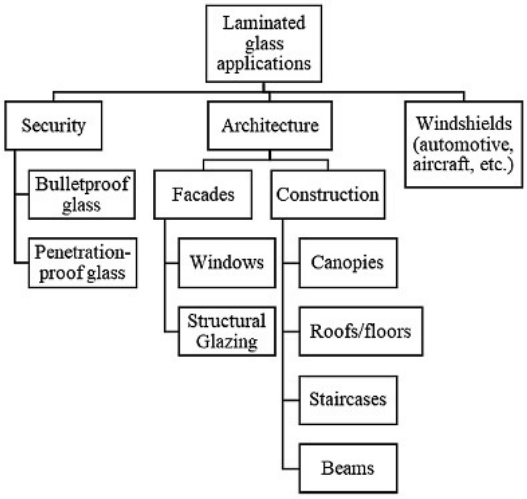

Figure 7. Applications of laminated glass [49].

The interlayer adheres the glass fragments in case of failure, preventing them from falling and posing a risk of injury. The adhered fragments provide improvement in the post-breakage capacity, which is dependent on the fragmentation and the fragment size [17]. The post-breakage behavior of laminated glasses is presented in Appendix 3. Laminated glass is classified as "laminated safety glass" if the aforementioned properties fulfil the requirements of ISO 12543-2 [50].

2.4 Strength assessment of glass

Glass does not have a single strength value. Thus, maximum stress criterion is often unsuited, or large safety factors are used. Glass behavior is isotropic and almost perfectly linear. Due to its inability to yield plastically, no redistribution of stress concentration by local yielding occurs which can lead to a sudden fracture [17]. This is one of the most important structural property of glass compared to steel.

The failure strength of prestressed glasses is dependent on the prestress (compression) level on the surfaces, edge quality, aspect ratio and orientation of glass relative to load. In four-point bending experiments by Veer et al. [51], the failure strength varied from 54.9 MPa to

167.0 MPa and 72.6 MPa to 205.1 MPa for heat strengthened glass and fully tempered glass, respectively, depending on the glass sample and the load orientation.

Defining the minimum failure strength value is difficult due to the randomness. Therefore, the strength parameters are analyzed using statistics, i.e. most commonly with two-parameter Weibull distribution [52]. For practical design, standard EN 16612 [28] gives a surface prestress values (Table 5) for each type of prestressed glass for calculating the bending strength. On the other hand, standard ISO 11336-1 [21] defines characteristic failure strength of 160 MPa for fully tempered and chemically strengthened glass with safety factor of 4. The resulting design bending strength is then 40 MPa.

Table 5. Surface prestress values for prestressed glasses according to EN 16612 [28].

Glass type	$f_{b;k}$ [a] (MPa)
Heat-strengthened	70
Fully tempered	120
Chemically strengthened	150

[a] Including the characteristic strength of float glass (45 MPa)

The bending strength according to EN 16612 is

$$f_{g;d} = \frac{k_{mod} k_{sp} f_{g;k}}{\gamma_{M;A}} + \frac{k_v \left(f_{b;k} - f_{g;k} \right)}{\gamma_{M;v}} \quad (1)$$

where k_{mod} is factor for load duration
k_{sp} is factor for glass surface profile
k_v is factor for strengthening of prestressed glass
$f_{b;k}$ is characteristic bending strength of prestressed glass
$f_{g;k}$ is characteristic bending strength of annealed glass
$\gamma_{M;A}$ is material partial factor for annealed glass
$\gamma_{M;v}$ is material partial factor for surface prestress.

2.5 Mechanical modelling

Numerical simulations are often used to estimate the design parameters of glass panes [53]. The numerical models are based on theoretical concepts i.e. on plate theories in this case. These include First-order shear deformation theory (FSDT), Higher-order shear deformation theory (HSDT), Classical Lamination Theory (CLT), Zigzag Theory (ZZT), Layer-wise Lamination Theory (LLT) and 3D Elasticity Theory. Classical Lamination Theory is an extension of classical plate theory i.e. Kirchhoff plate theory. The advantages and disadvantages of the plate theories are summarized in Table 6. It should be noted that the table discusses laminated glasses while the modelling in this thesis is limited to monolithic glasses. Regardless, the information is valid.

Table 6. Laminated plate (LP) theories, advantages and disadvantages [53].

LP theory	Advantages	Assumptions/limitations
FDST	(a) Suitable for analyzing the thin plate; for moderate thick and thicker LPs (except for LPs subjected to the transverse shear effects). (b) Less complex equations and computation.	(a) The displacement w is considered constant through the thickness and displacements u and v vary linearly through the thickness of each layer. (b) Assumes constant transverse shear stress. (c) Requires shear correction factor to satisfy the plate boundary conditions. (d) Shear correction factor determines accuracy of the results. (e) The normal lines to the mid-plane before deformation remain straight and normal to the plane after deformation. (f) Unable to predict edge defect.
HDST	(a) More accurate calculation of transverse shear than FDST. (b) Satisfy all boundary conditions. (c) Effectively analyze the behavior of complicated thick LPs under different loads. (d) Capable of representing the section warping in the deformed configuration.	(a) Complex equation and more computation than FDST. (b) Based on an assumption of nonlinear stress variation through the thickness.
CLT	(a) The simplest Equivalent single layer LP theory Based on the displacement field. (b) The quick and simple predictions especially for the behavior of thin plated structures. (c) Suitable for structures that consist of a symmetric and balanced laminate subjected to pure tension or pure bending.	(a) The shear strains across the interfaces between adjacent laminate are not continuous. (b) Ignores the effects of the transverse shear strains on the deformation of the elastic 2D structure. (c) Ignores some of the deformation mode constraints by reducing the model to a single degree of freedom results. (d) Neglecting shear stresses leads to a reduction or removal of the normal force, bending moment and twisting couple along free edges. (e) Neglects transverse shear strains, under estimate the values of deflections and over predict the natural frequencies and buckling loads. (f) The bending, buckling stresses are not predicted well.
ZZT	(a) Suitable for thick LPs having the free edges, corners or holes. (b) Suitability to through-the-thickness piece-wise behavior of stresses and displacement. (c) The compatibility of the displacements and the interlaminar equilibrium of the transverse stresses in the thickness direction are assured	(a) Computationally expensive but lesser than LLT.
LLT	(a) Best suited for the closed-form analysis of layered plates having no-edge effects. (b) Comparatively accurate results than earlier developed theories. (c) Accurately captures the local state of stress for all LPs, for different plate thickness.	(a) Require many different unknowns for multilayered plates. (b) Computationally time-consuming and expensive.
3D elasticity theory	(a) Suitable for problems related to the vibration in the LPs. (b) Usable for calculating bending and buckling of simply supported thick LPs.	

Choosing the theory depends on the situation. Complex models use more resources, but they do not necessarily give better results. When a monolithic glass pane with thickness to width ratio less than 1/10 [54] in bending is considered, then classical plate theory (Kirchhoff) is sufficient. The Kirchhoff plate theory assumes that

- thickness of the plate does not change during deformation
- straight lines drawn normal to the mid surface remain straight
- straight lines drawn normal to the mid surface remain normal [54].

Thin plates are often modelled using shell elements in commercial Finite Element software (Appendix 8). The shell elements are typically based on First-order shear deformation theory (Mindlin-Reissner) by default. The Mindlin-Reissner plate theory includes shear deformation through the thickness [54]. The theory assumes that

- thickness of the plate does not change during deformation
- straight lines drawn normal to the mid surface remain straight
- straight lines drawn normal to the mid surface **are not** normal (Figure 8) [54].

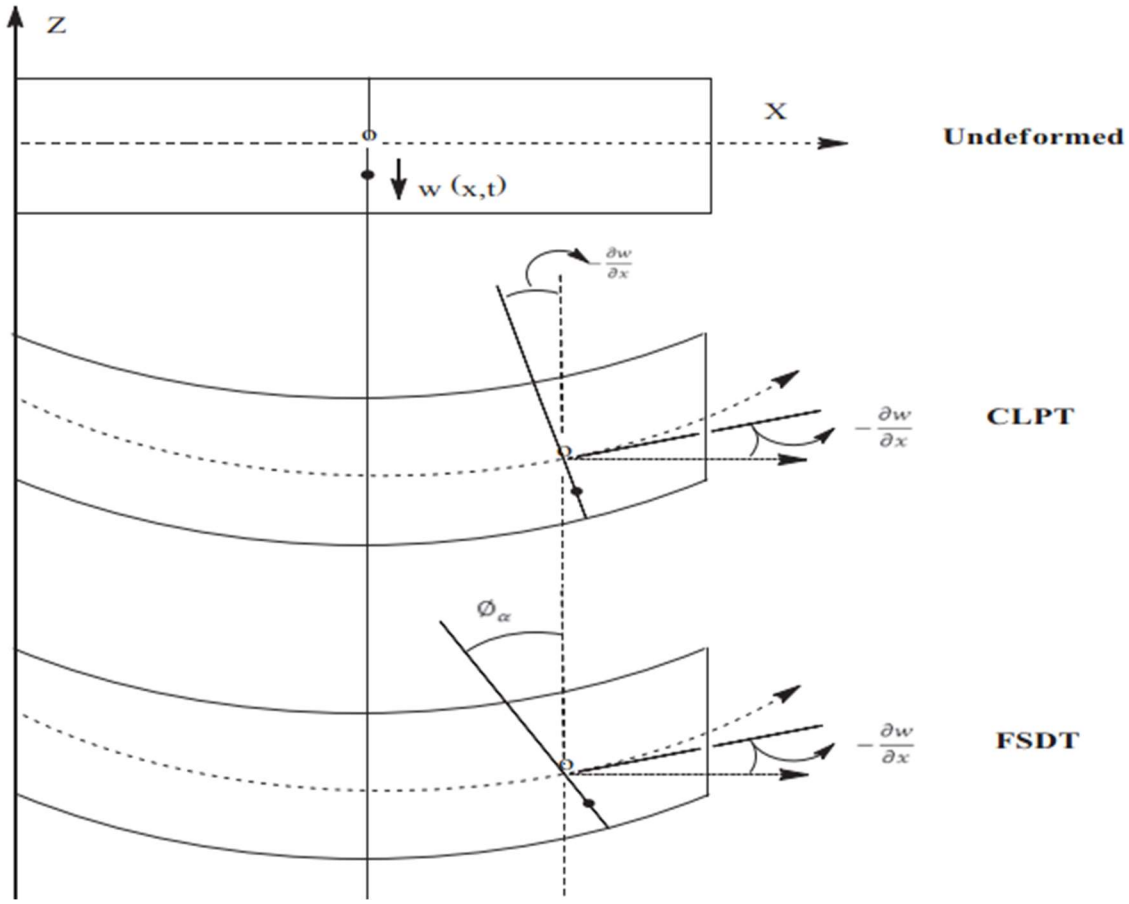

Figure 8. Deformation of plate in theoretical models. Classical plate theory (CLPT) i.e. Kirchhoff and First-order shear deformation theory (FSDT) i.e. Mindlin-Reissner [54].

The transverse shear deformation is negligible if the thickness of the plate is small. In that case, the theories should have practically the same solution.

2.6 Geometric nonlinearity

Glass panes often experience large deflections before breaking. A glass pane with translational restraints on its edges develops membrane (in-plane) stresses in the mid-plane as it stretches when subjected to lateral load. This membrane effect results in increase of the glass pane's stiffness. Linear analysis cannot capture this geometrically nonlinear behavior and thus overestimates the deflection (Figure 9). As a consequent, the actual tensile stresses are overestimated and underestimated for a given load and deflection, respectively. Therefore, geometrically nonlinear analysis is required in case of large deflections [17].

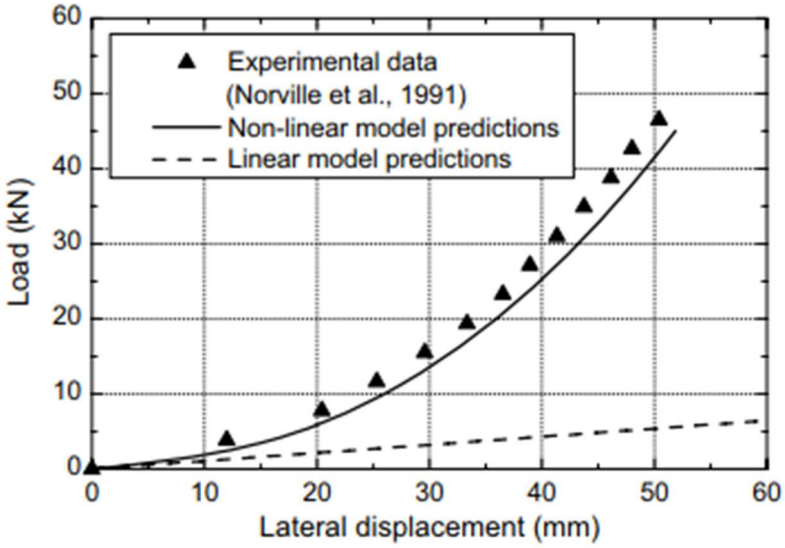

Figure 9. Load-deflection relationship of a fully tempered glass plate [17].

Often the thickness of glass pane has been determined using linear plate theory. This is beneficial for large and relatively thin glasses as they gain extra load carrying capacity compared to the lateral design pressures [20]. Only very recently adopted standard EN 16612 [28] requires consideration of nonlinear plate bending theory.

3 Insulating glass unit (IGU)

An insulating glass unit (IGU) consists of at least two glass panes separated by hermetically sealed space (Figure 10) [17]. The main functions of the IGU is to reduce heat losses (Appendix 4) and provide sound insulation (Appendix 5). The IGUs also enhances fire safety (Appendix 6). The unit is referred as double-glazed insulating unit (DIGU) or triple-glazed insulating unit (TIGU) when two or three glass panes are used, respectively. The panes can be monolithic glass, laminated glass or a combination. The glasses themselves can be any of the products discussed in section 2.

The enclosed space is sealed along its perimeter with an edge seal system and often filled with some inert gas, typically argon, krypton or xenon [55]. The inert gases are often used instead of air to achieve better thermal insulation. The gas can be inserted through a hole in the edge seal while the replaced air escapes from another hole [56]. Hence, the enclosed space has some initial gas pressure, volume and temperature. The initial gas pressure and temperature corresponds to the atmospheric pressure and temperature at the time of the sealing and thus the glass panes are in equilibrium (no initial deflection).

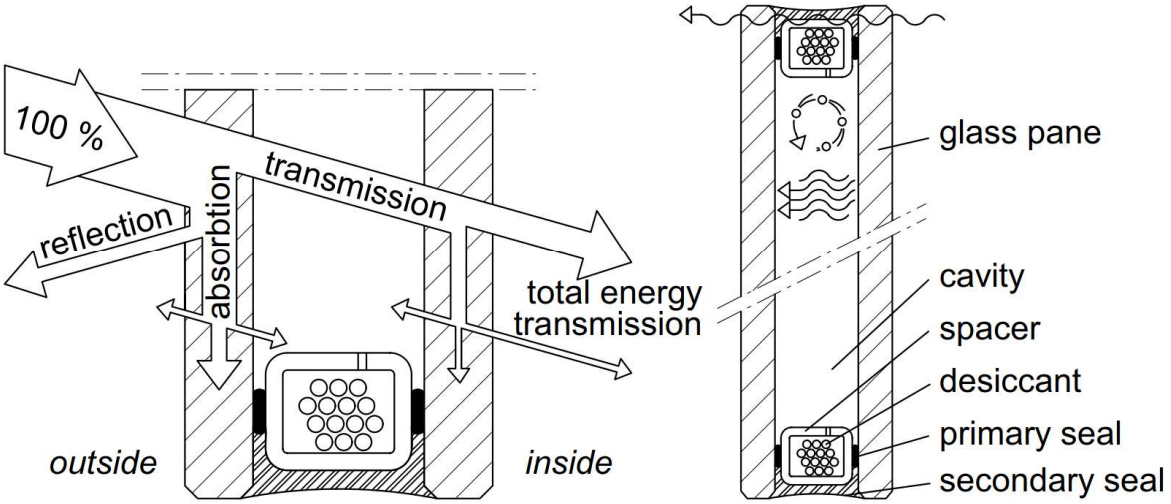

Figure 10. Principal structure of double-glazed insulating glass unit [17].

The edge seal system consists of spacer bar, sealants and desiccant and its main purpose is to separate the glass panes with equal distance and isolate the space [23]. The spacer commonly accommodates the panes 12 mm up to 22 mm [25] apart with hollow metallic or solid non-metallic profile. The hollow profile can be filled with desiccant, which is used to prevent fogging due to condensation of moisture vapor or organic vapor. Moisture vapor could be trapped during manufacture or be a sign of leaking primary seal. The secondary seal is used to structurally bond the glass panes and the spacer bar together and prevent any excessive movement. The primary seal is typically polyisobutylene (PIB) while main materials for the secondary seal are Polyurethane (PU), silicone (Si) and polysulfide (PS). Review by van den Berg et al. [23] gives a comprehensive description of the edge seal system and its components, properties, manufacturers and performance requirements.

Two aspects are often considered for structural performance of IGUs: 1) internal loads are generated due to changes in environment; 2) actions are transmitted between the panes, also known as load sharing.

3.1 Internal pressure loads

The edge seals and the glass panes are subjected to internal pressure loads due to the pressure difference between the atmosphere and the enclosed space [17]. The pressure differences are also called climate loads and they are generated by 1) altitude difference between manufacturing (sealing) and operation location; 2) meteorological air pressure changes; 3) temperature changes inside the enclosed space [57]. These result in the characteristic concave and convex shape of the IGU (Figure 11). In case the cavity is filled with air, the climate loads can possibly be avoided by using a pressure release system [58].

The daily variations in the atmospheric pressure depends on the location. Typical range (from minimum to maximum) for the variation is 0.03 kPa and 0.3 kPa in polar regions and in the tropics, respectively [59]. Therefore, the daily changes are insignificant while seasonal changes are larger. Standard DIN 18001-1 [60] suggests -2.0 kPa and +4.0 kPa change in the atmospheric pressure during summer and winter, respectively. Similarly, the same standard suggests +20 K and -25 K temperature change for summer and winter time, respectively.

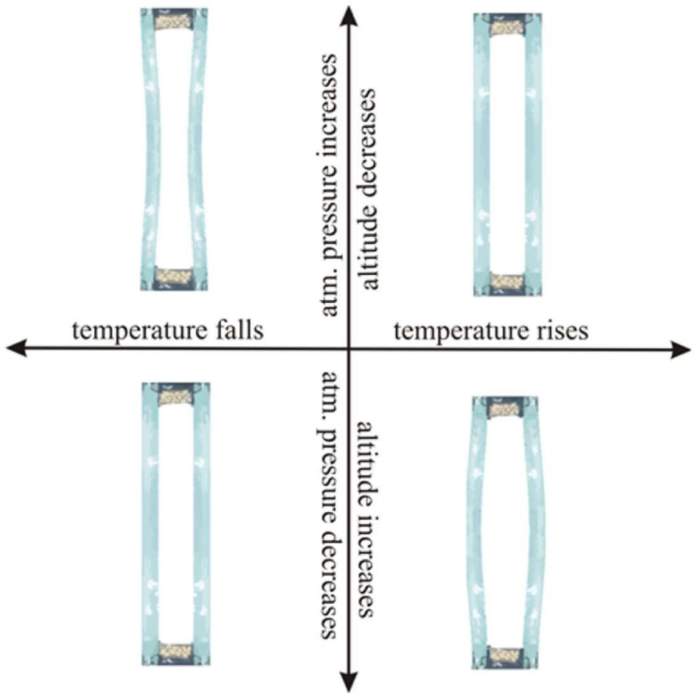

Figure 11. Influence of the climate changes on the insulating glass unit [57].

The amount of stresses the climatic loads can create is dependent on the volume change of the cavity, thus on the glass pane's lateral stiffness and the flexibility of the edge seal system. The edge seal system is often assumed immovable for conservative results [57]. The resulting stresses from climate loads are normally critical only for small glasses as they exhibit high lateral stiffness.

Buddenberg et al. [57] presents numerical and experimental investigation of the climate loads and the contribution of the edge seal system. Respondek and Major [61] presents an experimental testing device for studying deflection of the glass panes due to the climate loads.

3.2 Load sharing

Load sharing is a beneficial interaction between the gas and the glass panes that enhances the load bearing capacity of the IGU [55]. Some amount of the load applied externally to one pane is transferred to the other(s) pane(s) via the gas in the enclosed cavity (Figure 12). When the directly loaded pane deflects, the volume of the cavity decreases and consequently the gas pressure increases. The increased gas pressure acts on the second pane and causes it to deflect. McMahon et al. [24] investigated the load sharing experimentally.

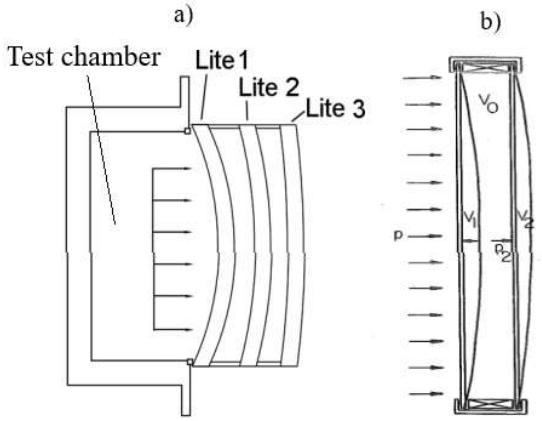

Figure 12. Load sharing in insulating glass unit: a) test chamber in [24]; b) deformation of the panes due to external pressure and the corresponding volume changes [62].

The experiments were conducted to symmetric and asymmetric DIGUs and TIGUs with two different glass sizes and cavity thickness (Table 7). The test chamber ("a" in Figure 12) was over pressurized to simulate uniformly distributed loading condition.

Table 7. Test sample dimensions in [19] given in millimeters and inches (brackets). Abbreviations: "S" is small (1260x750mm); "L" is large (1930x965mm); "D" is DIGU; "S" is symmetric; "A" is asymmetric. Note that configurations with 3 panes are hidden.

Specimen ID				
Small	Large	Lite 1	Airspace 1	Lite 2
SDS1	LDS1	3.1 (0.122)	8.0 (0.315)	3.1 (0.122)
SDS2	—	5.7 (0.224)	8.0 (0.315)	5.7 (0.224)
SDS3	—	5.7 (0.224)	13.0 (0.512)	5.7 (0.224)
SDA4	LDA4	3.1 (0.122)	13.0 (0.512)	5.7 (0.224)
—	LDA5	5.7 (0.224)	13.0 (0.512)	10.0 (0.394)

The deflection of both panes, the applied pressure and the pressures in the cavities were measured. In case of DIGU, the percentage of the total load that the directly loaded pane carry was calculated using Equation 2.

$$LS_1 = \frac{P_{frame} - ASP_1}{P_{frame}} * 100 \qquad (2)$$

where LS_1 is the percentage of total load that directly loaded pane carry
ASP_1 is the measured pressure in the cavity
P_{frame} is the applied load.

The deflections and pressures were measured for multiple pressures, P_{frame}. The final deflections and load sharing percentages at the target loads are presented in Table 8. The target loads were approximately 1.5-2.0 times larger than suggested by ASTME E1300-16 [27]. However, the exact amplitudes of the target loads are not reported and therefore these valued cannot be used later on. The asymmetric specimens were tested with thinner being directly loaded and thicker being directly loaded, denoted with load orientation A and load orientation B, respectively.

Table 8. Final deflections and load sharing percentages at the target load for different specimens in [19]. Abbreviations: "S" is small (1260x750mm); "L" is large (1930x965mm); "D" is DIGU; "S" is symmetric; "A" is asymmetric. Thinner pane is directly loaded in Load Orientation A.

Symmetric IGU Lite Deflections at Target Loads

	Deflection at target load		
Specimen ID	Lite 1	Lite 2	Lite 3
SDS1	15.7 (0.62)	14.7 (0.58)	—
LDS1	19.0 (0.75)	17.8 (0.70)	—
SDS2	8.6 (0.34)	7.4 (0.29)	—
SDS3	8.6 (0.34)	7.6 (0.30)	—

Asymmetric IGU Lite Deflections at Target Loads

	Deflection at target load					
	Load Orientation A			Load Orientation B		
Specimen ID	Lite 1	Lite 2	Lite 3	Lite 1	Lite 2	Lite 3
SDA4	8.1 (0.32)	7.1 (0.28)	—	7.4 (0.29)	6.6 (0.27)	—
LDA4	14.2 (0.56)	13.7 (0.54)	—	14.0 (0.55)	10.2 (0.4)	—
LDA5	8.9 (0.35)	7.4 (0.29)	—	7.6 (0.30)	7.1 (0.28)	—

Symmetric IGU Load-Share Percentages

	Percentage of total load carried		
Specimen ID	Lite 1	Lite 2	Lite 3
SDS1	51	49	—
SDS2	60	40	—
SDS3	55	45	—

Asymmetric IGU Load-Share Percentages

	Percentage of total load carried					
	Load Orientation A			Load Orientation B		
Specimen ID	Lite 1	Lite 2	Lite 3	Lite 1	Lite 2	Lite 3
SDA4	33	67	—	85	15	—

From the results it can be seen that the load sharing is significant for all the cases. In symmetric specimens the glass panes carry the load almost equally. From the asymmetric specimen, SDA4, it can be observed that the thicker pane carries more load (67% and 85%) regardless of the load orientation.

The deflection of both panes for specimen SDS3 are presented in Figure 13. Similarly, the results for specimen SDA4 are presented in Figure 14 for both load orientations. Note the significance of the orientation on the results. The results from both of these tables are used in section 5.2.

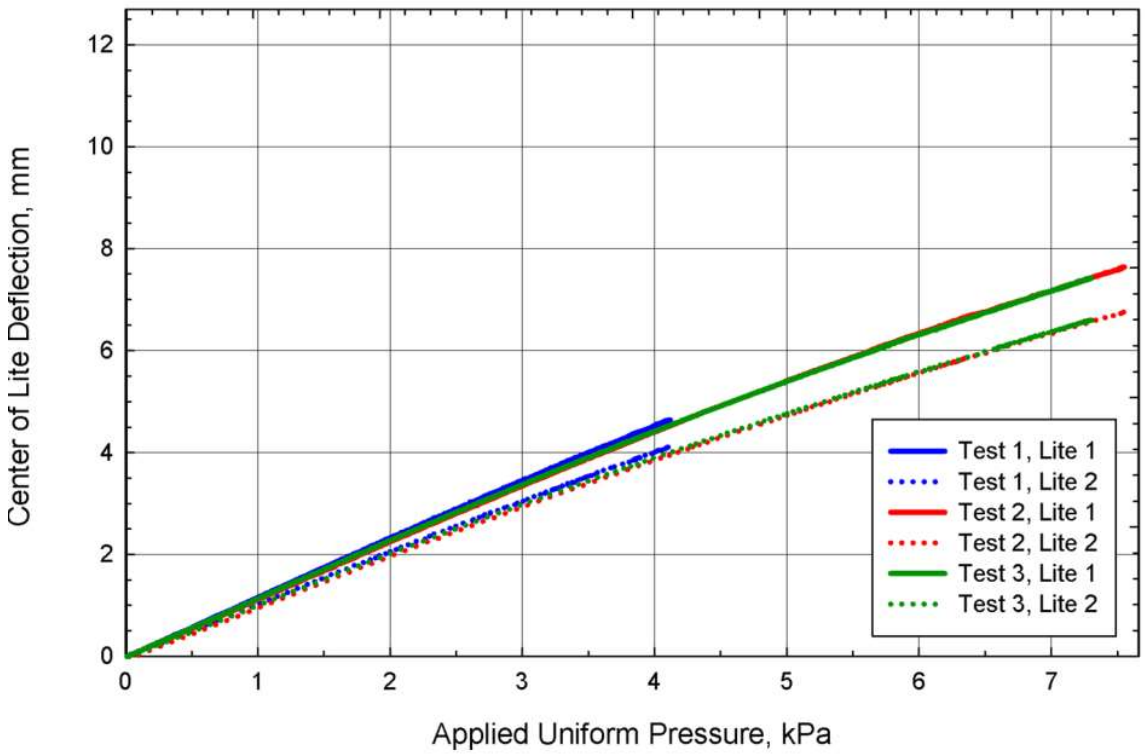

Figure 13. Specimen SDS3 (1260x750 / 5.7+13+5.7 mm) - Center of pane deflection versus applied load [24]. The results from test 2 (red) are used in section 5.2.

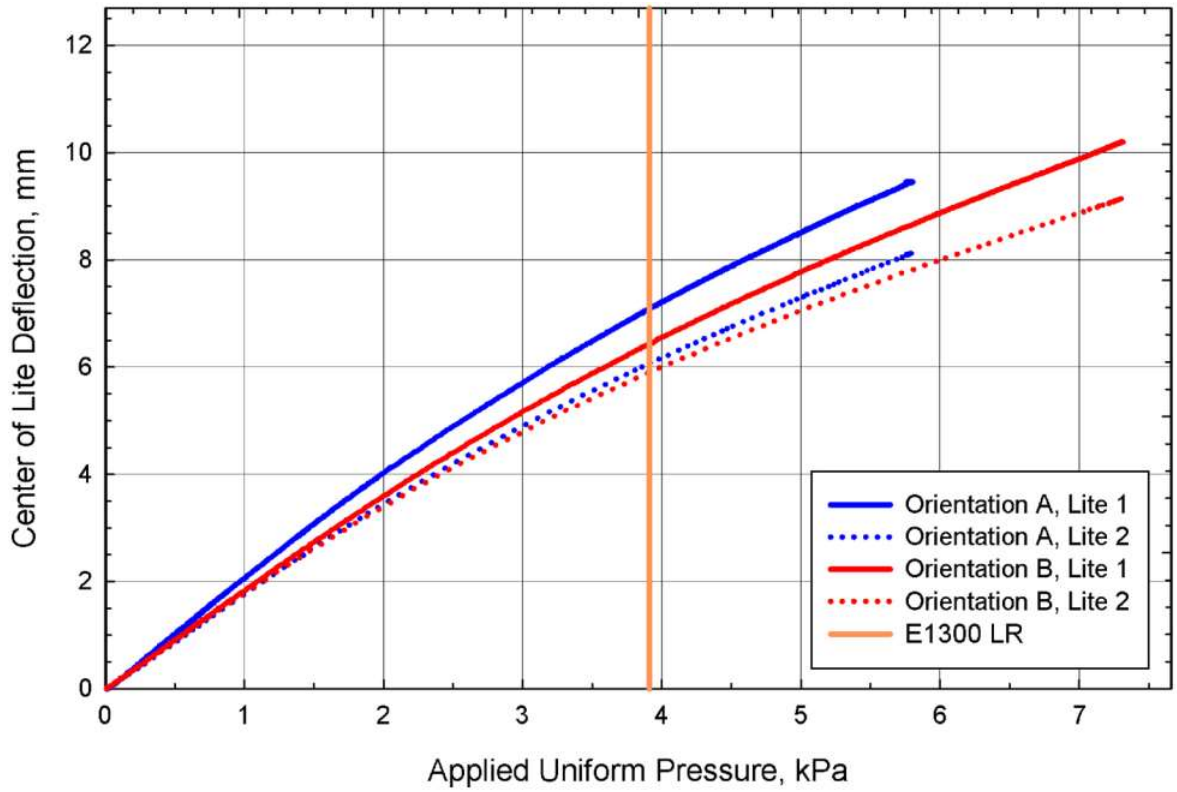

Figure 14. Specimen SDA4 (1260x750 / 5.7+13+3.1 mm) - Center of pane deflection versus applied load for both load orientations [19]. Thinner pane was directly loaded in Load Orientation A. Results from load orientation B are used in section 5.2.

In the design process, the load sharing is usually considered through standards. Common glass design standards ASTME E1300-16 [27], AS 1288 [26], EN 16612 [28] and DIN 18008-2 [29] provide means for estimation but their respective approaches differ from one another.

The first two standards use “thickness cubed” method that assumes that each pane carries load that is proportional to its respective flexural stiffness. This approach is often considered insufficient. The stiffness of the individual panes also governs the load sharing in method prescribed by EN 16612, but an insulating unit factor is used to correct the results. This factor depends on the dimensions of the IGU, thickness of the panes and the cavity, climate loads and the volume change of the cavity. The factor is presented with tables valid only for rectangular IGUs. Similar approach is proposed in DIN 18002-2.

The standards consider only simply supported boundary condition with unrestrained edge rotations. However, real IGU constructions often behave in a stiffer manner as the frame and the edge sealing restrict the edge rotation. This could be a reason for if smaller deflections are observed in experiments than anticipated.

3.3 Betti’s Analytical Method

Methods for calculating load sharing has been already proposed in the years 1986 [62] and 1993 [63]. However, these have limitations and are not easy to implement. A more recent paper by Galuppi and Royer-Carfagni [55] proposes a Betti’s Analytical Method (BAM) for evaluating the load sharing in double glazed insulating units. The method is based on Reciprocal Work Theorem by Enrico Betti [64].

The advantage of BAM is that only the deformation of a simply supported linear-elastic plate with the same shape as the glass pane under uniform pressure has to be solved. Based on this, variations in gas pressure can be calculated for other load cases and boundary conditions without having to determine the corresponding deformation. Possible load cases are uniform pressure, point load and line load, while the simply support can be continuous or a point type. The method therefore provides a flexible way to evaluate different cases and glass shapes.

The Betti’s Analytical Method is described for a rectangular insulating glass unit subjected to external uniform pressure and internal pressure loads. Double-glazed unit is presented in Figure 15. The unit consist of directly loaded pane, 1, and indirectly loaded pane, 2, that are divided by a spacer with thickness “s”. The panes have thicknesses “h_1” and “h_2”. Only the final equations are shown here while their derivations can be found in [55]. However, it should be mentioned that the solutions are based on linear elasticity theory and Kirchhoff theorem (see chapter 2.5).

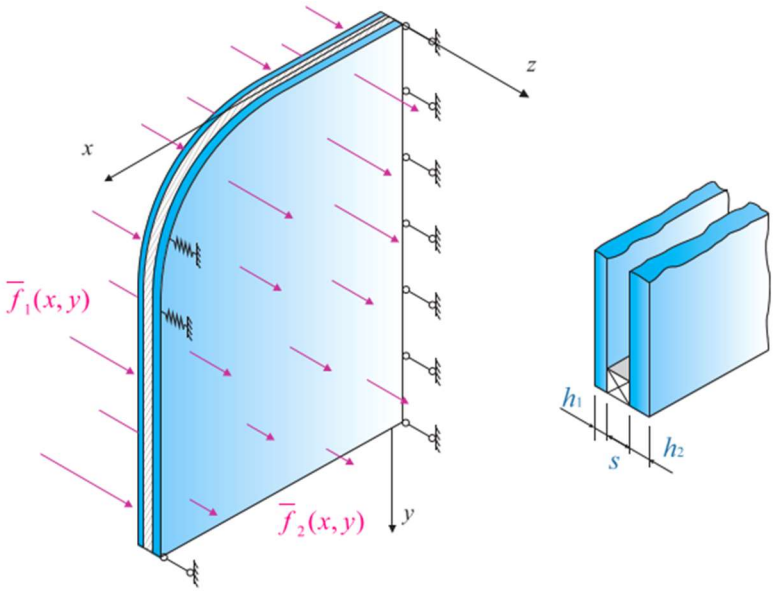

Figure 15. Double-glazed unit schematic for various support conditions with arbitrary glass shape subjected to external forces per unit area f1(x,y) and f2(x,y) on panes 1 and 2, respectively [55].

First, the cavity pressure variation, Δp, due to applied uniform pressure, $\bar{p}$, is determined using Equation 3. If the climate loads are not considered, then $\bar{f_1}(x,y) = \bar{p},\ \bar{f_2}(x,y) = 0$. The resulting deflections of panes 1 and 2 are $w_1(x,y)$ and $w_2(x,y)$, respectively.

$$\Delta p_{external} = \frac{h_2^3\,\bar{\psi}_A}{(h_1^3 + h_2^3)\bar{\psi}_A + \frac{E}{12(1-\nu^2)} h_1^3 h_2^3 \frac{V_0}{A^3 p_0}} \bar{p} \tag{3}$$

where
$\Delta p_{external}$ is cavity pressure variation [MPa]
h_1 is thickness of pane 1 [mm]
h_2 is thickness of pane 2 [mm]
E is Young's modulus of glass [MPa]
ν is Poisson's ratio of glass [-]
V_0 is reference volume of the cavity at the time of sealing [mm³]
A is area of glass panel [mm²]
p_0 is reference pressure of the gas in the cavity at the time of sealing [MPa]
$\bar{p}$ is the applied uniform pressure on pane 1 [MPa]
$\bar{\psi}_A$ is the mean value of shape function on the area [-].

The mean value of the shape function for rectangular plate is

$$\bar{\psi}_A = \frac{64a^2b^2}{\pi^8} \sum_{m=1}^{\infty} \sum_{n=1}^{\infty} \frac{1}{m^2 n^2 (m^2 b^2 + n^2 a^2)^2} \tag{4}$$

where
a is pane dimension in x-direction [mm]
b is pane dimension in y-direction [mm]
m,n=1,3,5.

The calculated cavity pressure presents a load that is applied directly to glass pane 2. The pressure acting on glass pane 1 is the applied pressure minus the calculated cavity pressure. At this point any commercial FE software can be used to determine the response of either pane caused by this pressure. The deflection of the panes can be calculated using Equation 5.

$$w_1(x,y) = \frac{\bar{p} - \Delta p}{D_i} A^2 \psi(x,y)$$
$$w_2(x,y) = \frac{\Delta p}{D_i} A^2 \psi(x,y) \quad (5)$$

where D is the plate's flexural rigidity [Nmm]; $D_i = \frac{E h_i^3}{12(1-\nu^2)}$

$\psi(x,y)$ is the shape function for the deflection of a simply supported plate under uniform pressure [-].

For rectangular plate, the shape function is

$$\psi(x,y) = \frac{16a^2b^2}{\pi^6} \sum_{m=1}^{\infty} \sum_{n=1}^{\infty} \frac{sin\frac{m\pi x}{a} sin\frac{n\pi y}{b}}{mn(m^2b^2 + n^2a^2)^2} \quad (6)$$

where x is the point of interest in x-direction (a/2 for maximum) [mm]
y is the point of interest in y-direction (b/2 for maximum) [mm]
m,n=1,3,5.

Cavity pressure variation due to atmospheric pressure variation is calculated with Equation 7. The variations in the atmospheric pressure can be considered as a uniform pressure, $\overline{\Delta p}$, acting externally on both panes. $\overline{\Delta p}$ is positive when it is larger than the reference pressure p_0. The resulting loading is $\bar{f}_1(x,y) = -\bar{f}_2(x,y) = \overline{\Delta p}$, and the generated cavity pressure is

$$\Delta p_1 = \frac{\bar{\psi}_A}{\bar{\psi}_A + \frac{E}{12(1-\nu^2)} \frac{h_1^3 h_2^3}{h_1^3 + h_2^3} \frac{V_0}{A^3 p_0}} \overline{\Delta p}. \quad (7)$$

The resulting pressure variation acting on one pane is

$$\Delta p_{barometric} = \Delta p_1 - \overline{\Delta p}. \quad (8)$$

Similarly, the generated cavity pressure due to temperature variation, $\overline{\Delta T}$, is

$$\Delta p_{temperature} = -\frac{1}{2}\left[p_0 + \frac{E}{12(1-\nu^2)}\frac{h_1^3 h_2^3}{h_1^3+h_2^3}\frac{V_0}{A^3\bar{\psi}_A} - \frac{\sqrt{T_0^2\left(A^3 p_0\bar{\psi}_A + \frac{E}{12(1-\nu^2)}\frac{h_1^3h_2^3}{h_1^3+h_2^3}V_0\right)^2 + \frac{E}{3(1-\nu^2)}\frac{h_1^3h_2^3}{h_1^3+h_2^3}A^3\,\overline{\Delta T}T_0V_0p_0\bar{\psi}_A}}{A^3T_0\bar{\psi}_A}\right] \quad (9)$$

where T_0 is reference absolute temperature in the cavity at the time of sealing [K]
$\overline{\Delta T}$ is temperature variation of the gas in the cavity with respect to T_0 [K].

The calculated pressure variations may be superimposed as the whole system is assumed to be linear elastic so that resulting total cavity pressure variation is

$$\Delta p_{total} = \Delta p_{external} + \Delta p_{barometric} + \Delta p_{temperature}. \quad (10)$$

3.4 MEPLA ISO

MEPLA ISO [65] is a freeware software for calculating the response of insulating glass units. The software works on linear basis and uses analytical approach of double Fourier Series to calculate maximum deflections and maximum principal stresses. The accuracy is based on classical plate theory (Kirchhoff). Furthermore, because the geometric nonlinearities (see chapter 2.6) are neglected, the solution is valid for deflections smaller than half the plate thickness ($w_{max}<t/2$). The solution of the software is validated in [55].

The software can be used for DIGUs or TIGUs with rectangular shape and simply supported boundary condition. Possible load cases include uniform pressure, point load and line load. Additionally, changes in atmospheric pressure and cavity temperature can be included. The cavity volume change is based on Ideal Gas Law. An automatically generated report by MEPLA ISO is presented in Figure 51 (Appendix 10).

4 IGU Finite Element model

A finite element model for insulating glass unit is presented. The model consists of two glass panes and four spacers that form an enclosed space. The enclosed space is filled with a gas. A 2-D schematic of the model is presented in Figure 16.

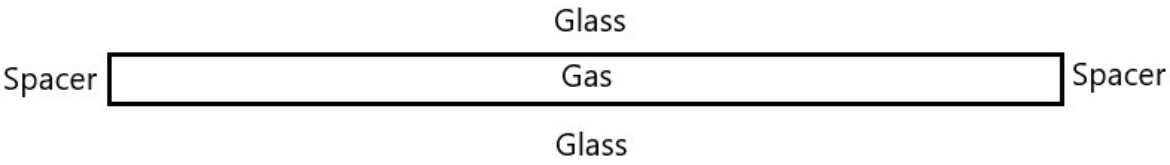

Figure 16. 2-D schematic of insulating glass unit.

4.1 Glass element

The glasses in Ansys are modelled with shell elements. The elements by default are structural 4-node SHELL181 elements (Figure 17) that are based on Mindlin-Reissner plate theory. Hence, they are suitable for analyzing thin to moderately thick shell structures. The full element description is given in Ansys element reference library [66].

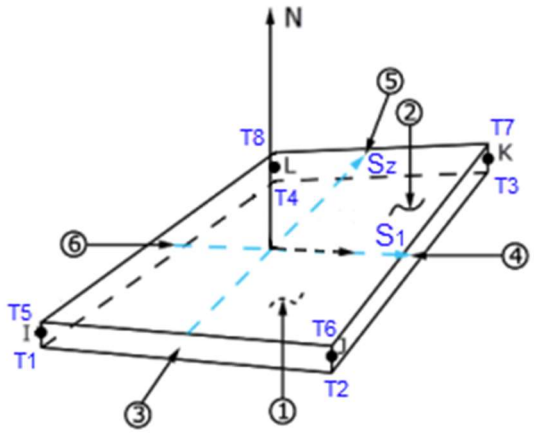

Figure 17. 4-node structural SHELL181 element, Ansys [66].

The analytical methods described in sections 3.3 and 3.4 use Kirchhoff plate theory. The Kirchhoff and Mindlin-Reissner theories should give practically the same results for thin glass plates, as mentioned in chapter 2.5. To confirm this, SHELL63 elements can be used that are based on Kirchhoff plate theory [67]. A single glass plate of 1260x750x5.7 mm (Table 7) is modelled with simply supported boundary conditions and subjected to uniform pressure of 1.0 kPa in a linear static structural analysis. The results are presented in Figure 18 in terms of deflection.

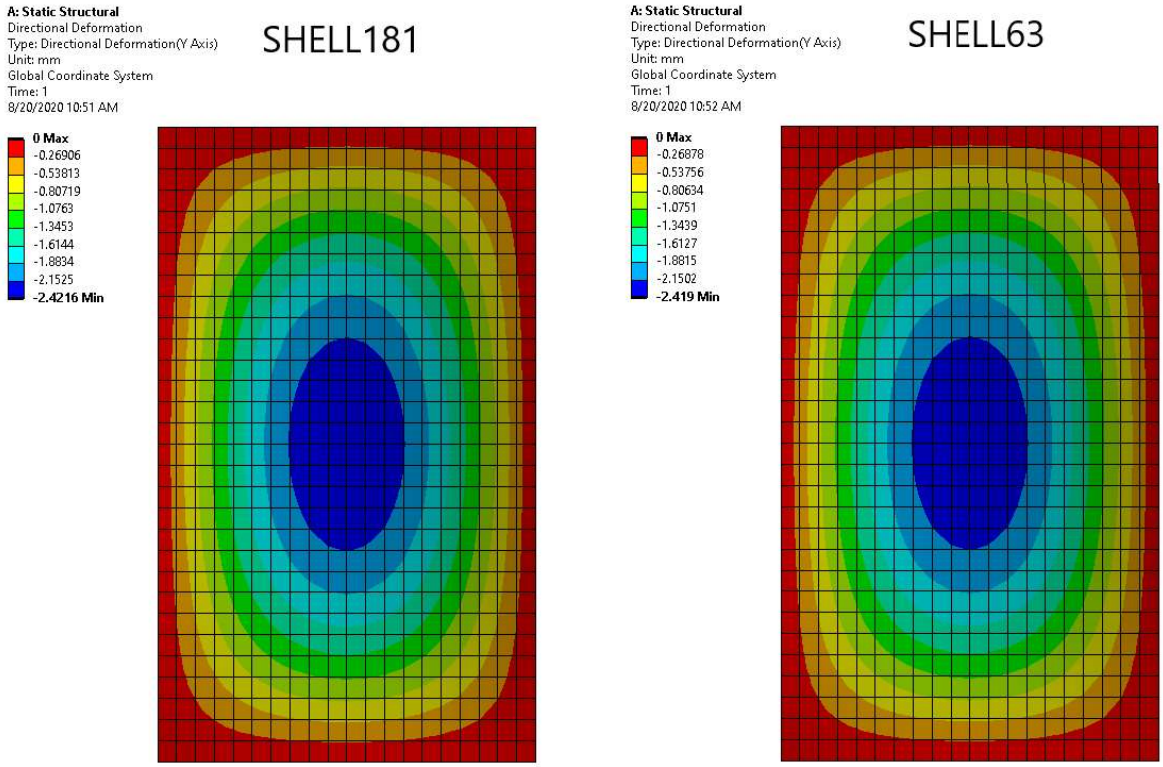

Figure 18. Ansys, deflection comparison between SHELL181 (Mindlin-Reissner) and SHELL63 (Kirchhoff) elements in a linear static structural analysis with simply supported boundary condition and 1 kPa external pressure. The plate dimensions are 1260x750x5.7 mm. Maximum deflections for SHELL181 and SHELL63 are 2.4216 mm and 2.419 mm, respectively.

It can be concluded that the results are correct as SHELL63 is slightly stiffer as it neglects the transverse shear. The relative error between the result is 0.11% and hence SHELL181 elements can be used.

4.2 Ideal gas element

In Ansys, the gas can be modelled with hydrostatic fluid elements (HSFLD). Generally, they are designed to model fluid enclosed by solids. These elements are presented in Figure 19.

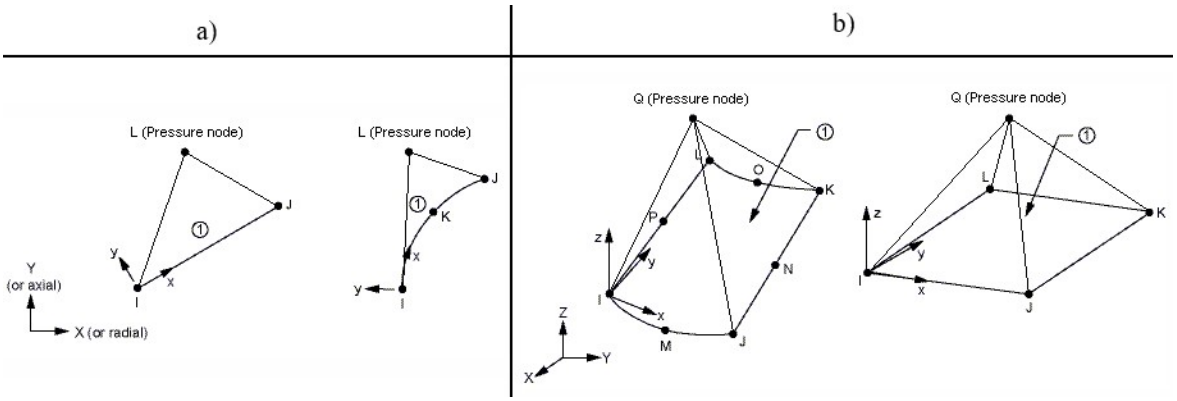

Figure 19. Hydrostatic fluid elements in Ansys; a) HSFLD241 (2-D); b) HSFLD242 (3-D) [68].

The hydrostatic fluid elements were introduced in Ansys 13.0 in 2010. The implication from the product brochure is that the elements were created to model inflated car tires. In fact, the demonstration case study by Ansys has been made for a car tire rolling over a bump (Figure

20). This could not be modelled before as the “normal” fluid element (FLUID79/80) has linear stiffness relationship [69].

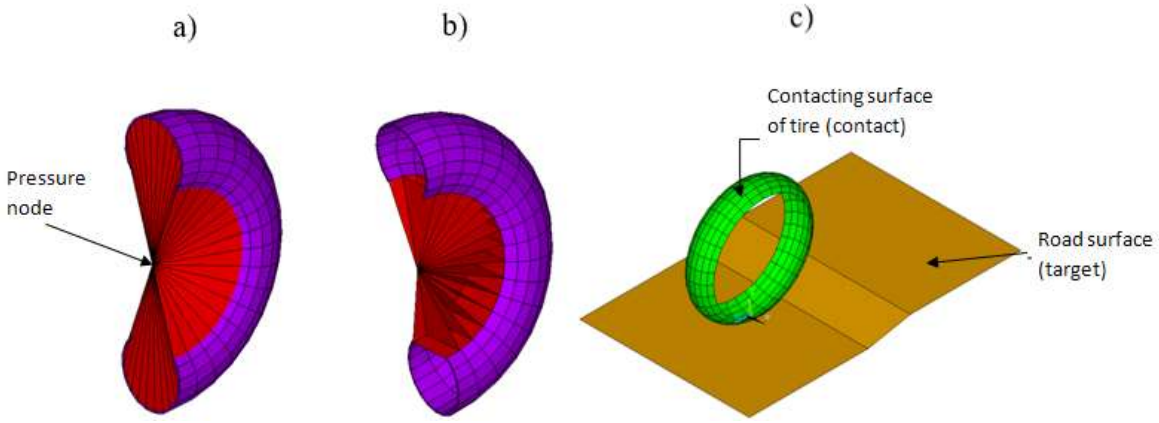

Figure 20. Ansys technology demonstration guide - Hydrostatic fluid analysis of an inflating and rolling tire: a) HSFLD242 elements (red) connected to pressure node; b) the "empty" part in the middle modelled with negative volume; c) the road-tire model [70].

The HSFLD elements fill the enclosed space by connecting the structural element faces with the pressure node presented in Figure 19 and Figure 20. Hence, all the structural elements are connected to one point and therefore the enclosed space has uniform pressure, temperature and density. Furthermore, because the space is completely filled up, there are no free surface effects (e.g. sloshing).

The element has pressure node “Q” that has a HDSP (hydrostatic pressure) DOF. The other nodes that are on the surface of the structural element faces have only translational DOFs. The pressure in the node “Q” is calculate based on the volume change of the HSFLD elements. This pressure is further applied to the structural elements it is attached to. New pressure is calculated because the cavity volume may change. Therefore, it is suggested to have nonlinear analysis activated due to the nonlinear nature of the element [69].

In the case of compressible gas, the behavior of the element is based on the Ideal Gas Law PV=nRT, where P is the pressure of the gas, V is the volume of the gas, T is the temperature of the gas, n is the moles in the substance and R is the ideal gas constant. The inputs for the elements are initial gas density, reference pressure, offset temperature and reference temperature. Furthermore, temperature and pressure loads can be inserted that would represent the climate loads. Alternatively, the atmospheric pressure can be represented with conventional surface pressures. Detailed description of the inputs, outputs and limitations are given in the Ansys element library [68]. The element’s governing equations are described in the Ansys theory reference [71].

The elements have to be inserted using Ansys parametric design language (APDL) command as is not available in Ansys graphical user interface. The HSFLD element implementation routine is presented in Appendix 9. The elements do not require similar meshing as normal elements do. The structural element surfaces facing the cavity are “coated” with the hydrostatic elements using ESURF command. If the cavity is fully modelled, then the pressure node can be inserted anywhere in the cavity as it will be automatically centered. If symmetry planes exist, then the pressure node has to be inserted there.

The user has to be cautious of negative volumes as presented in Figure 20, section “b”. In the case of insulate glass unit, there are no negative volumes thanks to its geometry. Although, depending on the modelling technique, some elements might have normal in direction away from the cavity that results in negative volume. Then, the elements having negative volumes have to be reversed. Furthermore, Ansys gives a warning of negative volumes in the output file.

An alternative finite element modelling of the gas is presented in [72]. A four-node element is formed that is also based on the Ideal Gas Law so that each node has 10 DOFs. The element only considers volumetric strain as ideal gas is unable to resist shear deformation. The advantage of the element is said to be that an IGU with more than one cavity can be modelled. However, IGUs with more than one cavity can also be modelled with HSFLD elements. Since the 4-node element is not available in Ansys, the HSFLD element is used.

4.3 IGU FE model and post-processing

A 2-D schematic of insulating glass unit model with the structural elements and hydrostatic fluid elements are presented in Figure 21.

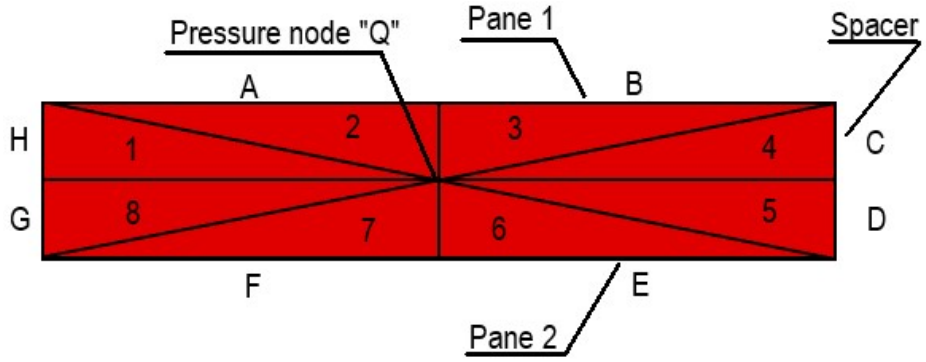

Figure 21. Insulating glass unit 2-D schematic with hydrostatic fluid elements. Numbered triangular elements, 1-8, represent HSFLD elements while line elements with letters, A-H, represent the structural elements. The pressure node is located in the middle of the cross-section.

In Ansys, the model requires all six surfaces to calculate the volume of the cavity. Therefore, the vertical surfaces that represent the spacer are modelled with dummy elements with low stiffness, so they do not contribute to the total stiffness of the structure. Furthermore, the spacer elements have all their nodes restrained so that they do not deform, i.e. they do not participate in volume change. The meshed model is presented in Figure 22.

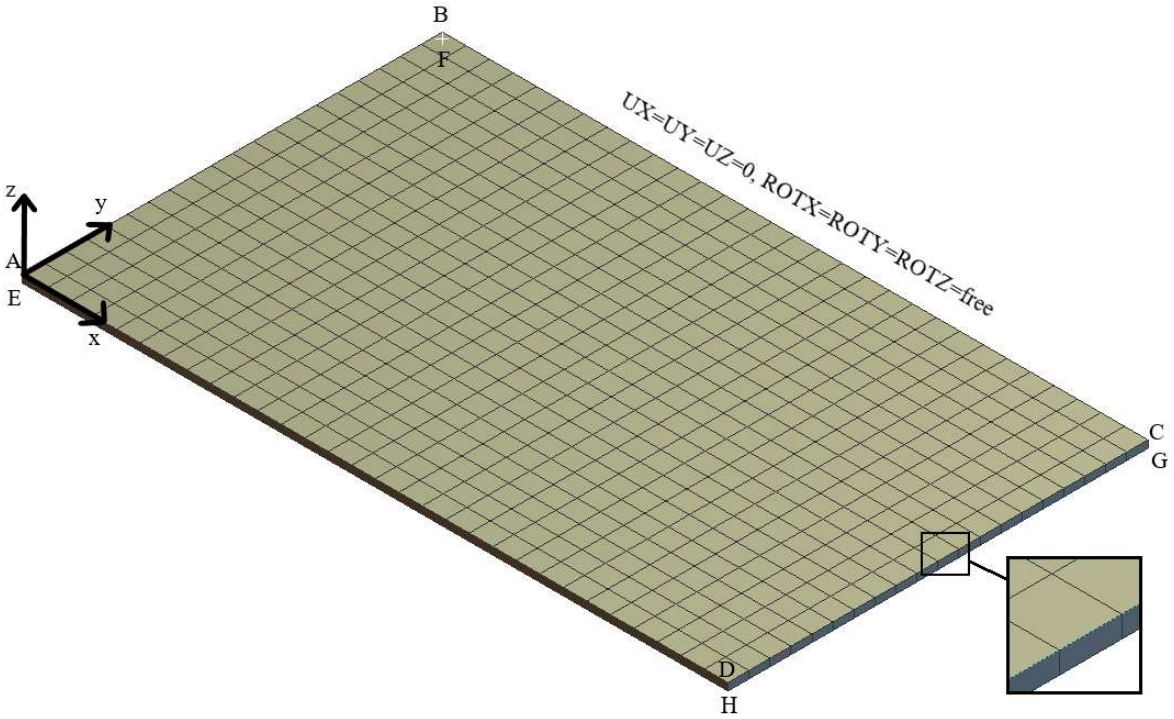

Figure 22. Meshed IGU model with SHELL181 elements in Ansys (HSFLD242 elements not visible). Dark elements represent the spacers with low stiffness (E≈0, ν≈0). The same boundary conditions are applied to all 8 horizontal edges. "U" is translation and "ROT" is rotation. Dimensions are 1260x750/5.7+13+5.7 (SDS3).

The behavior of the presented model can be analyzed by using simply supported boundary condition and 1.0 kPa uniform pressure on surface ABCD in linear static analysis. The resulting deflection of the panes are presented in Figure 23 and Figure 24.

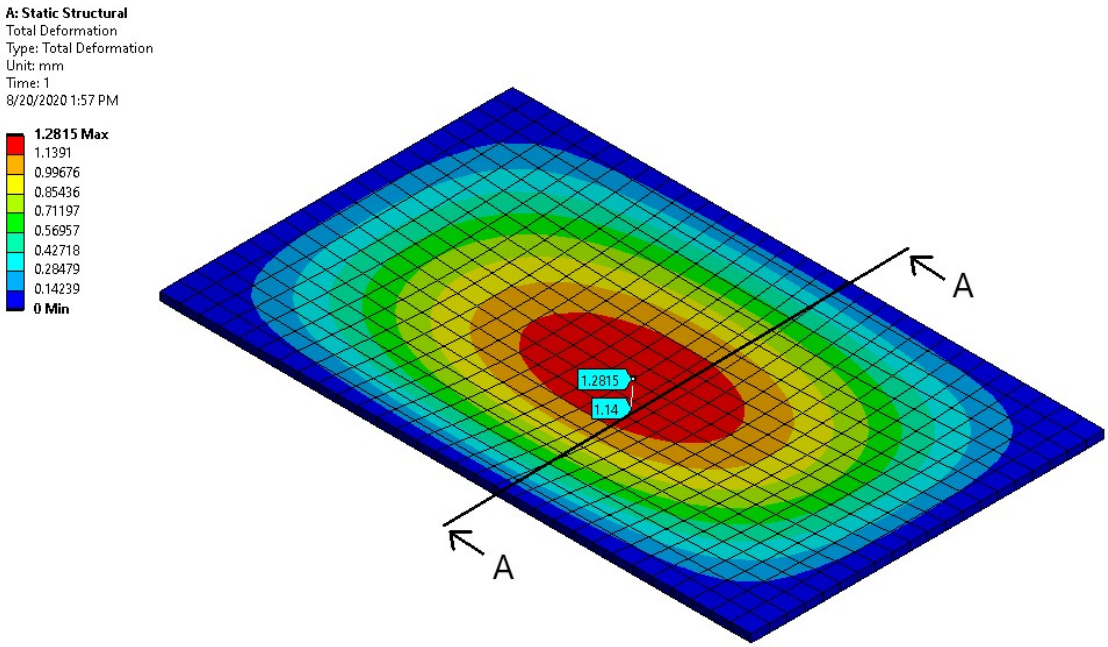

Figure 23. Deflection of simply supported IGU (1260x750/5.7+13+5.7) in a linear static analysis subjected to 1.0 kPa uniform pressure. The maximum deflection of pane 1 and pane 2 is 1.2815 mm and 1.14 mm, respectively. Section A-A is at the middle of the insulating glass unit.

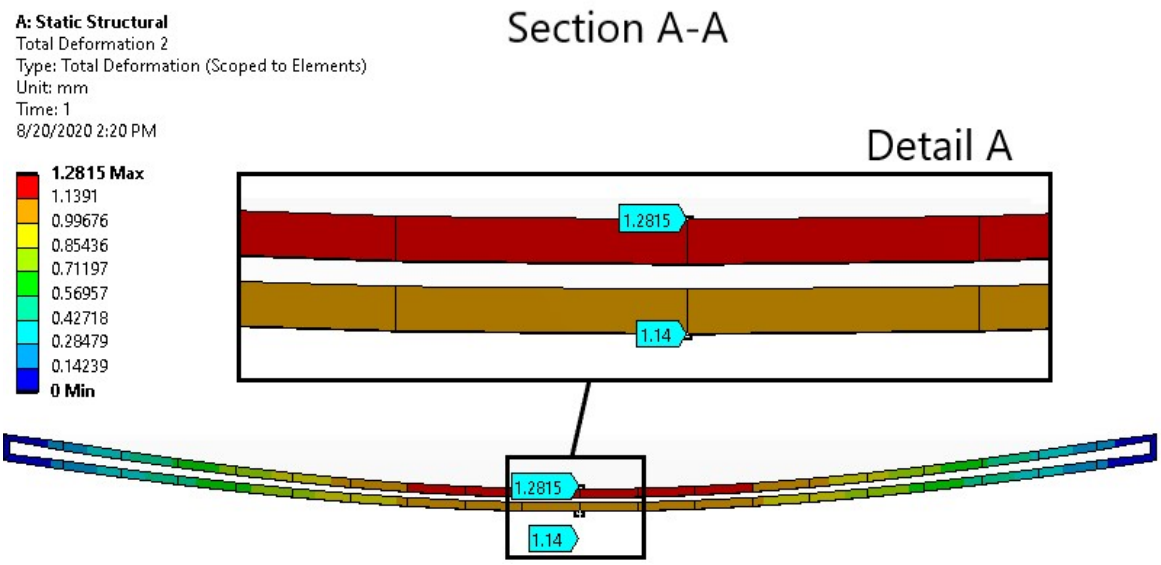

Figure 24. Section view A-A (Figure 23) of deflection of simply supported IGU (1260x750/5.7+13+5.7) in a linear static analysis subjected to 1.0 kPa uniform pressure. The maximum deflection of pane 1 and pane 2 is 1.2815 mm and 1.14 mm, respectively.

The results are intuitive as the indirectly loaded pane deflects less. This happens because the gas is compressible.

The stresses are obtained from Ansys. The maximum principal stress should be used when we recall that glass fails if the prestress value (compression) on the surface is exceeded. The maximum principal stresses on top and bottom of the shell elements are presented in Figure 25.

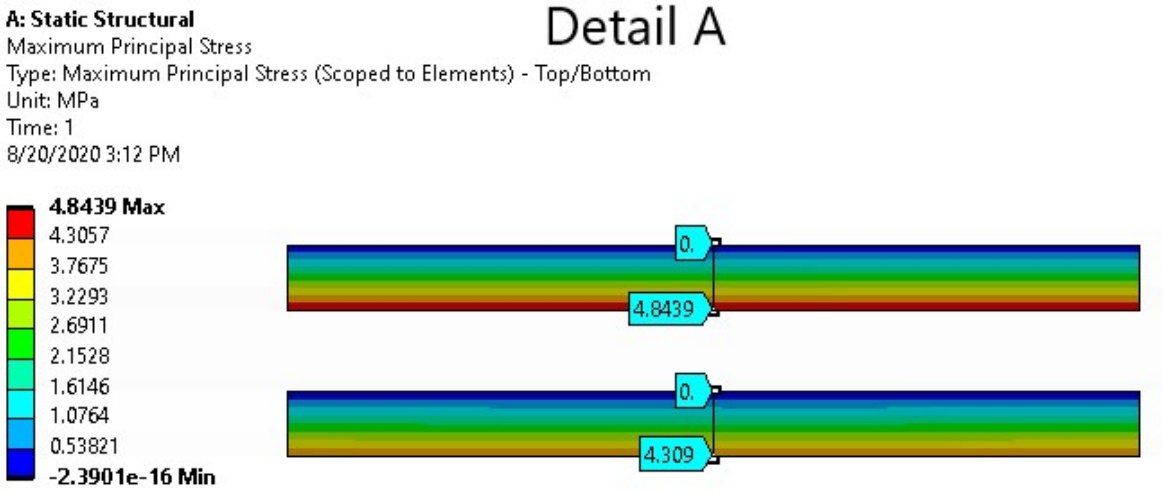

Figure 25. Detail view A-A (Figure 23) of maximum principal stress on top and bottom of the shells of simply supported IGU (1260x750/5.7+13+5.7) in a linear static analysis subjected to 1.0 kPa uniform pressure.

The maximum principal stress is at the bottom of the directly loaded pane. The stress is zero on the top of surface of the indirectly loaded pane which is correct as the ideal gas is unable to resist shear deformation. The results are intuitive.

For nonlinear analysis, Ansys use Newton-Raphson procedure. It is an iterative process for solving the nonlinear equations. The procedure is described in Ansys theory reference [73].

5 Case study

The workflow of this chapter is as follows:

- The presented Finite Element model is validated on a linear basis
- The presented Finite Element model is validated on a nonlinear basis
- The validated models are used to study nonlinear cavity pressure variation
- A parametric study is conducted to prove the significance of load sharing in large IGUs
- The climate loads are implemented to the validated Finite element models
- Design example is performed to demonstrate the benefit of considering load sharing.

5.1 Validation of linear model

Finite element model according to chapter 4 and analytical models according to chapter 3.3 and 3.4 are used with the same IGU dimensions as in [24]. The dimensions are chosen so it is convenient to use the same models later on for comparing obtained result with the experimental results by McMahon et al. [24]. Two specimen IDs are chosen, SDS3 and SDA4. Parameters for the model are presented in Table 9.

Table 9. Parameters for the analytical and numerical models.

Symbol	Meaning	SDS3	SDA4
a [mm]	Length in x-direction	1260	1260
b [mm]	Length in y-direction	750	750
h_1 [mm]	Thickness of pane 1	5.7	5.7
h_2 [mm]	Thickness of pane 2	5.7	3.1
s [mm]	Thickness of spacer	13	13
E [MPa]	Young's modulus, glass	70000	
ν [-]	Poisson's ratio, glass	0.23	
m, n [-]		1,3,5,..,31	
$\overline{\Delta T}$ [K]	Temperature variation	0	
$\overline{\Delta p}$ [MPa]	Atmospheric pressure variation	0	
p0 [MPa]	Reference pressure	0.101325	
ρ_{gas} [Kg/mm³]	Gas density (only in Ansys)	1.7e-9	

The model is simply supported so that all the horizontal edges have translational DOFs restrained and rotational DOFs unrestrained (Figure 26). This boundary conditions abbreviated as BC1. These correspond to the boundary conditions in chapters 3.3 and 3.4. It should be noted that the FE model has 8 horizontal edges that have these boundary conditions.

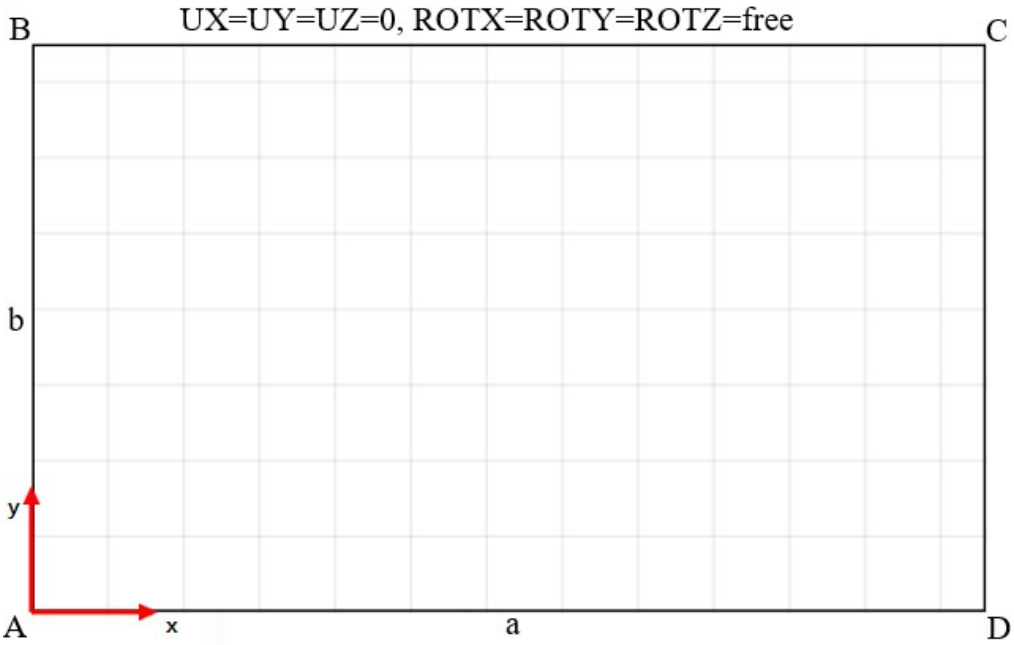

Figure 26. The boundary conditions (BC1) and coordinate system for the IGU model. The same BCs are applied to all horizontal edges. "U" is translation and "ROT" is rotation.

Uniform pressure of 1.0 kPa is applied to surface ABCD. The cavity pressure variation according to BAM is calculated using Equation 3 and the deflection of the panes using Equation 5. The nodal deflections are extracted every 42 mm along the line b/2 on the surface of both panes. The results are presented in Figure 27 and Figure 28 for SDS3 and SDA4, respectively.

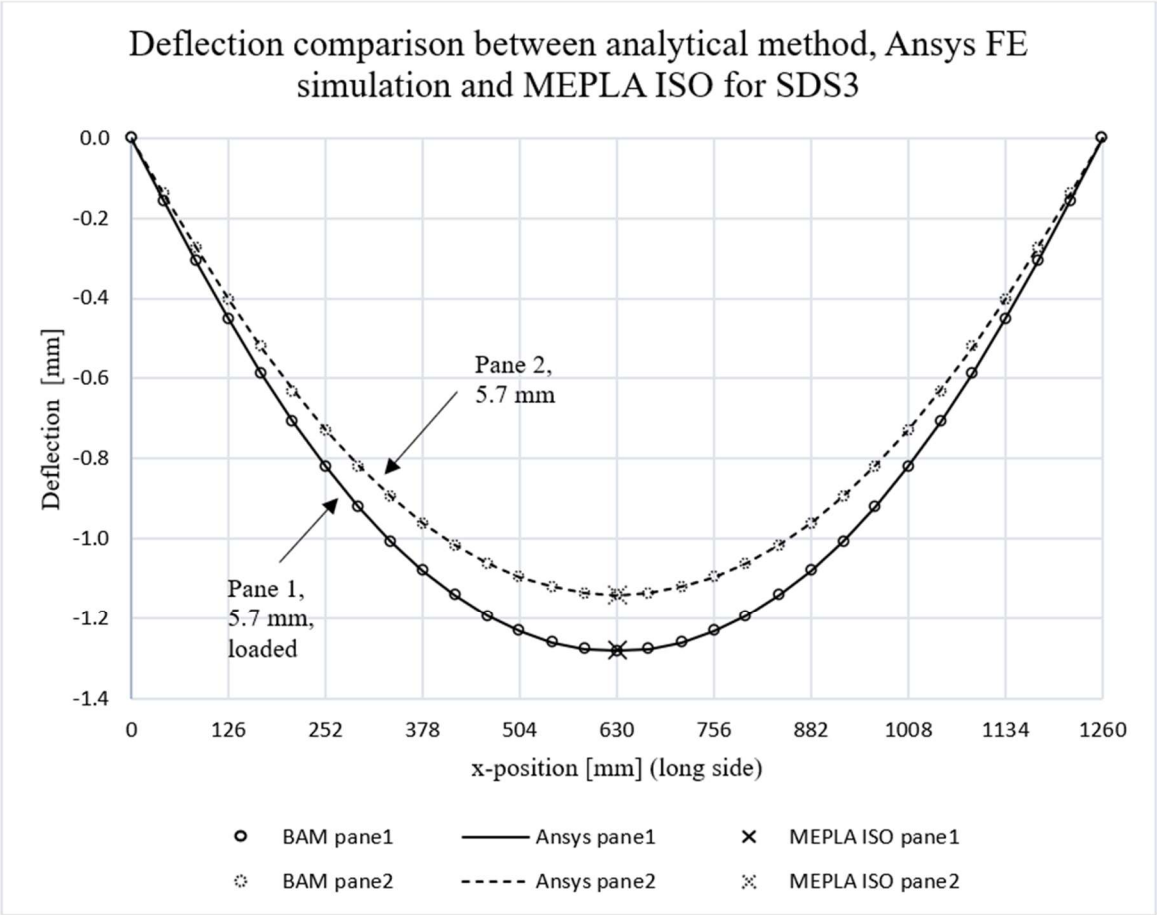

Figure 27. SDS3 (1260x750/5.7+13+5.7) – Deflection comparison of pane 1 and pane 2 along line b/2 for 1.0 kPa external pressure, linear results, between Betti's Analytical Method (BAM), Ansys and MEPLA ISO. MEPLA ISO [65] is a freeware software for insulating glass units.

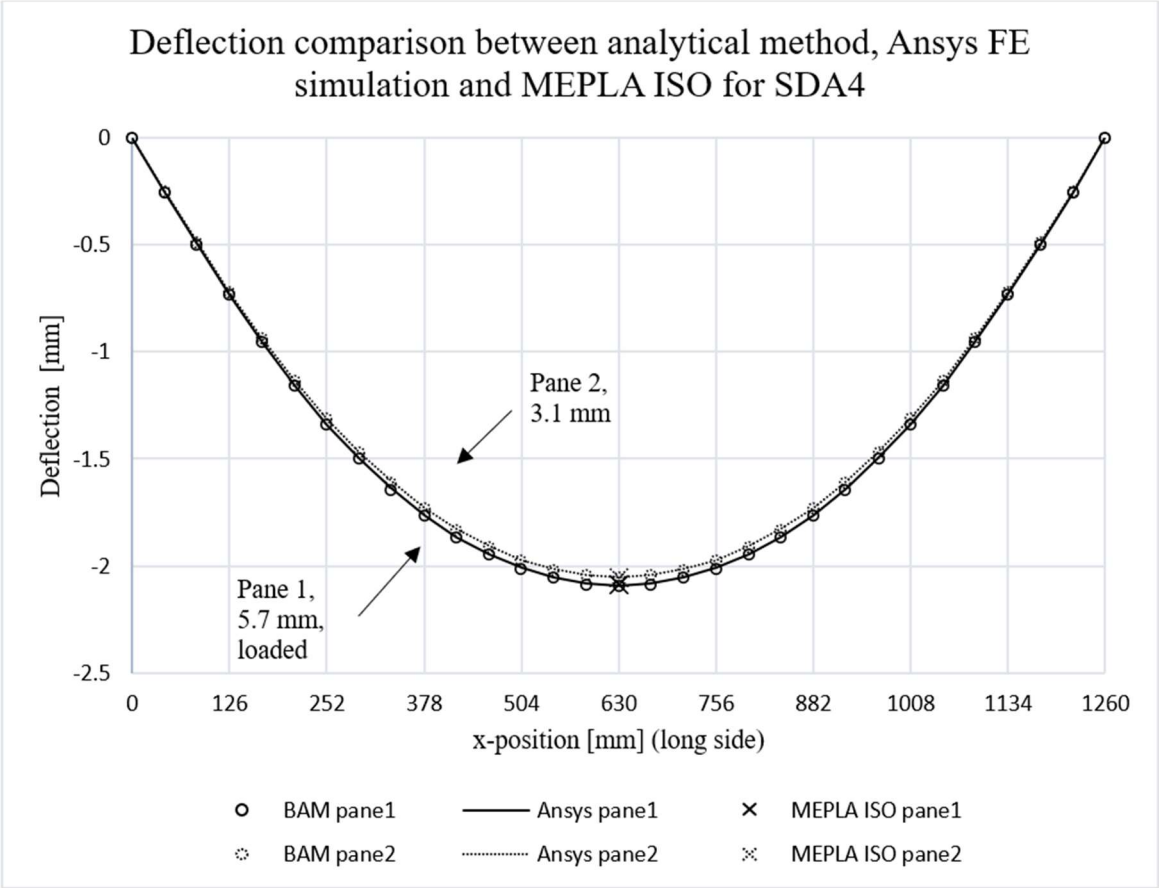

Figure 28. SDA4 (1260x750/5.7+13+3.1) – Deflection comparison of pane 1 and pane 2 along line b/2 for 1.0 kPa external pressure, linear results, between Betti's Analytical Method (BAM), Ansys and MEPLA ISO. MEPLA ISO [65] is a freeware software for insulating glass units.

In both IGU sizes, SDS3 and SDA4, the relative error in the middle of the pane is 0.08 % and 0.09 % between Ansys and BAM for pane 1 and pane 2, respectively. The largest relative error is right next to the boundary edge, being 0.28%. Furthermore, the deflection result from MEPLA ISO at the middle (a/2, b/2) is in very good agreement. Similar results were obtained along line a/2 (y-direction). The pressure variation in the cavity is presented in Table 10. Note that MEPLA ISO does not provide this information.

*Table 10. Comparison of pressure variation in the cavity between Ansys and Betti's Analytical Method (linear results). Relative error is (BAM-Ansys)/BAM*100.*

	SDS3 (1260x750/5.7+13+5.7)			SDA4 (1260x750/5.7+13+3.1)		
Pressure [kPa]	Ansys [kPa]	BAM [kPa]	Error [%]	Ansys [kPa]	BAM [kPa]	Error [%]
1.0	0.47080	0.47083	0.0064	0.13623	0.13630	0.0514

Since the second pane in SDA4 is 2.6 mm thinner than in SDS3, it is less stiff and hence deflects more, which results in smaller pressure variation in the cavity. For the same reason, the difference in deflection between the panes in SDA4 is smaller than in SDS3. The results are therefore intuitive.

Now considering that the analytical solution follows [55] and is in good agreement with MEPLA ISO, it can be concluded that the linear Ansys model is validated as the relative error in deflections and pressures variation are very small. However, the presented model is

valid only for small deflections as the geometric nonlinearities are pronounced for larger loads.

5.2 Validation of nonlinear model

The nonlinear model can be validated using the experimental results obtained by McMahon et al. (Figure 13 and Figure 14) [24]. These results are chosen as no other IGU experimental results are available. It is mentioned in the experimental test setup that the boundary condition does not restrain in-plane or rotational DOFs (sliding allowed). Therefore, the BCs are changed as presented in Figure 29. In this way the plate deforms symmetrically and has no in-plane restrains on its edges. This boundary conditions abbreviated as BC2.

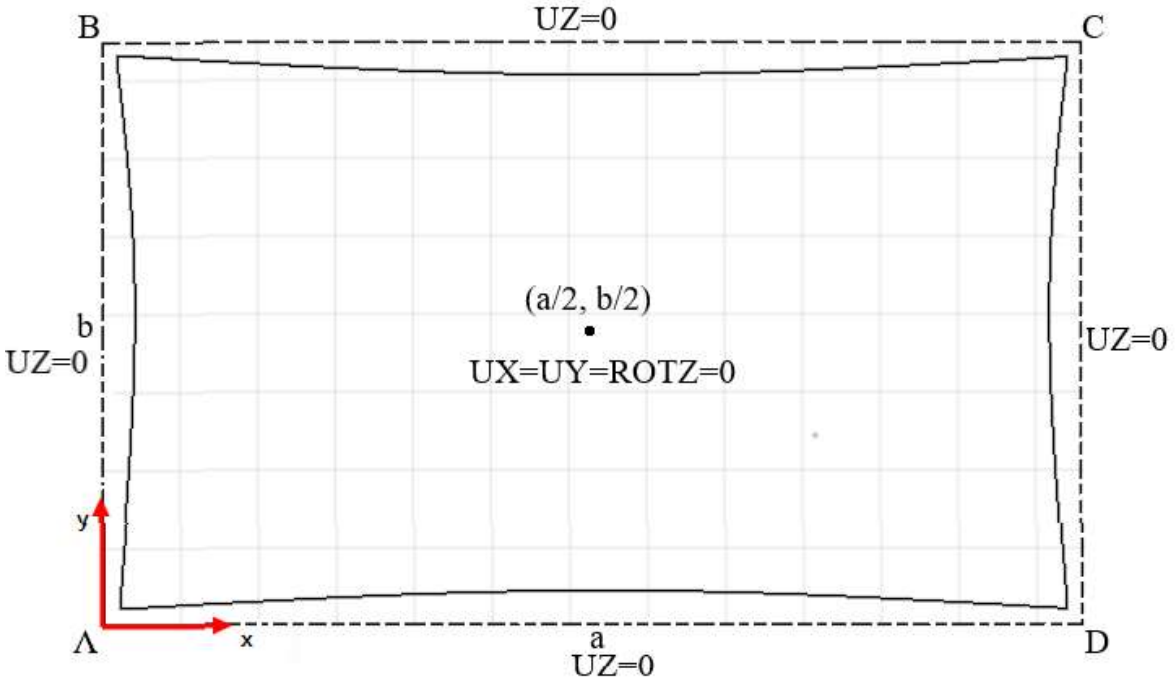

Figure 29. Modified boundary conditions (BC2) for the nonlinear Ansys analysis. Dashed lines represent the original shape and the solid line the deformed shape (exaggerated). The edge BCs apply for all the 8 horizontal edges. Nodal BC is applied to middle node of both panes. "U" is translation and "ROT" is rotation.

The geometric nonlinearity is activated from Ansys by setting "large deflections" on in the analysis settings. External pressure is increased from 1.0 kPa to 7.0 kPa with increments of 0.5 kPa. The maximum deflection of both panes is recorded for each load. Furthermore, linear results for the directly loaded pane are presented to demonstrate the importance of nonlinearity. Similarly, the significance of the boundary conditions is highlighted. The results are presented in Figure 30, Figure 31, Figure 32 and Figure 33.

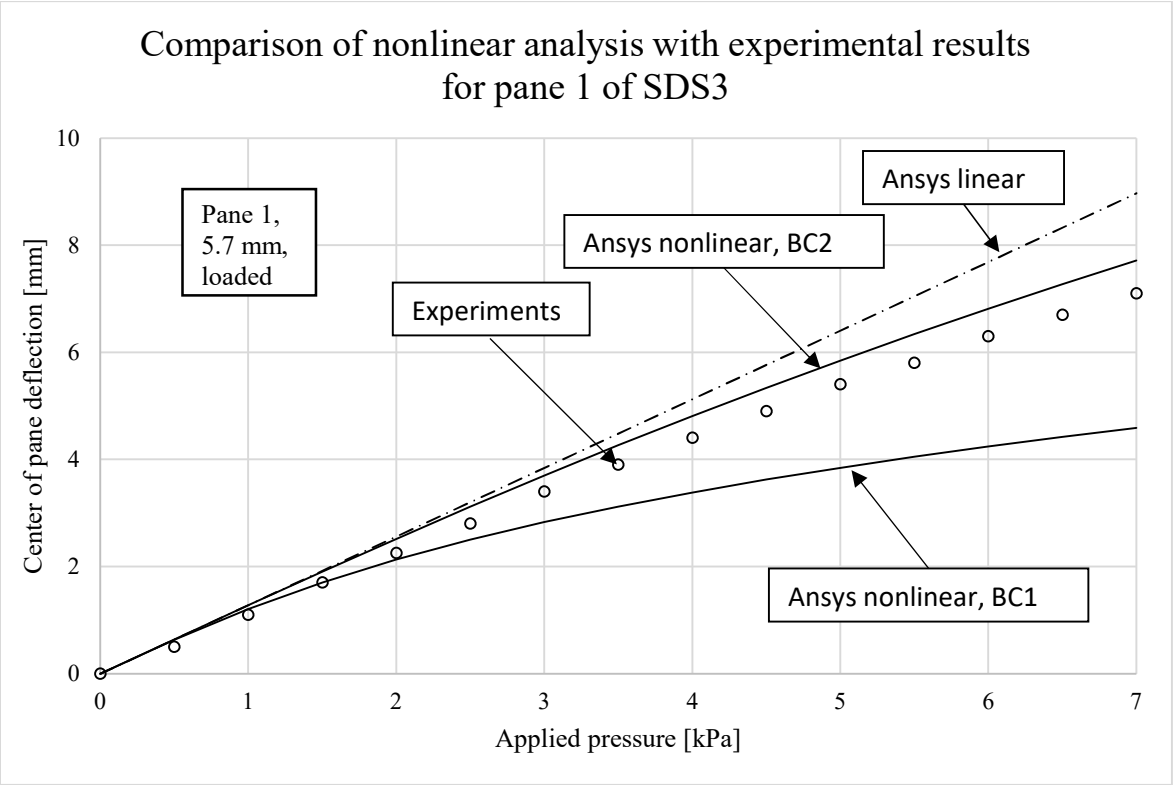

Figure 30. SDS3 (1260x750/5.7+13+5.7) - Comparison of Ansys nonlinear analysis results with experimental results from [24]. The dashed line represents the significance of geometric nonlinearities. BC1 is model with in-plane restraints (Figure 26) and BC2 is model without in-plane restraints (Figure 29).

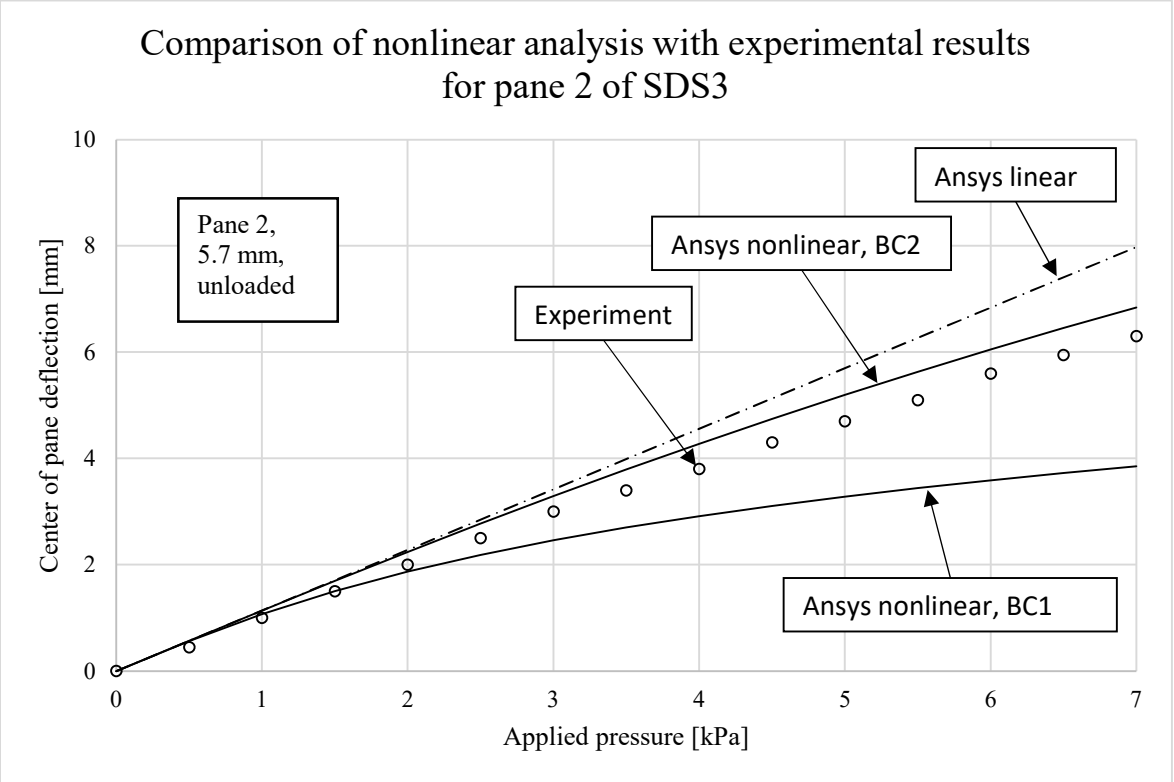

Figure 31. SDS3 (1260x750/5.7+13+5.7) - Comparison of Ansys nonlinear analysis results with experimental results from [24]. The dashed line represents the significance of geometric nonlinearities. BC1 is model with in-plane restraints (Figure 26) and BC2 is model without in-plane restraints (Figure 29).

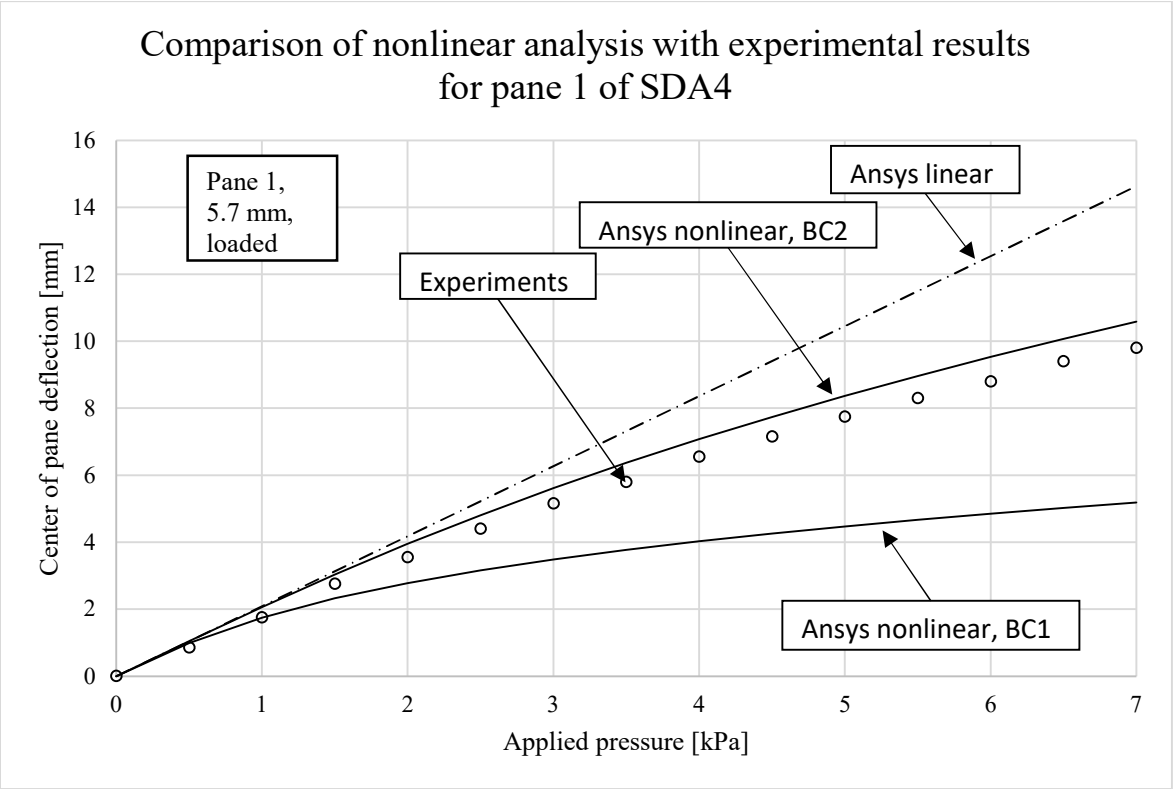

Figure 32. SDA4 (1260x750/5.7+13+3.1) - Comparison of Ansys nonlinear analysis results with experimental results from [24]. The dashed line represents the significance of geometric nonlinearities. BC1 is model with in-plane restraints (Figure 26) and BC2 is model without in-plane restraints (Figure 29).

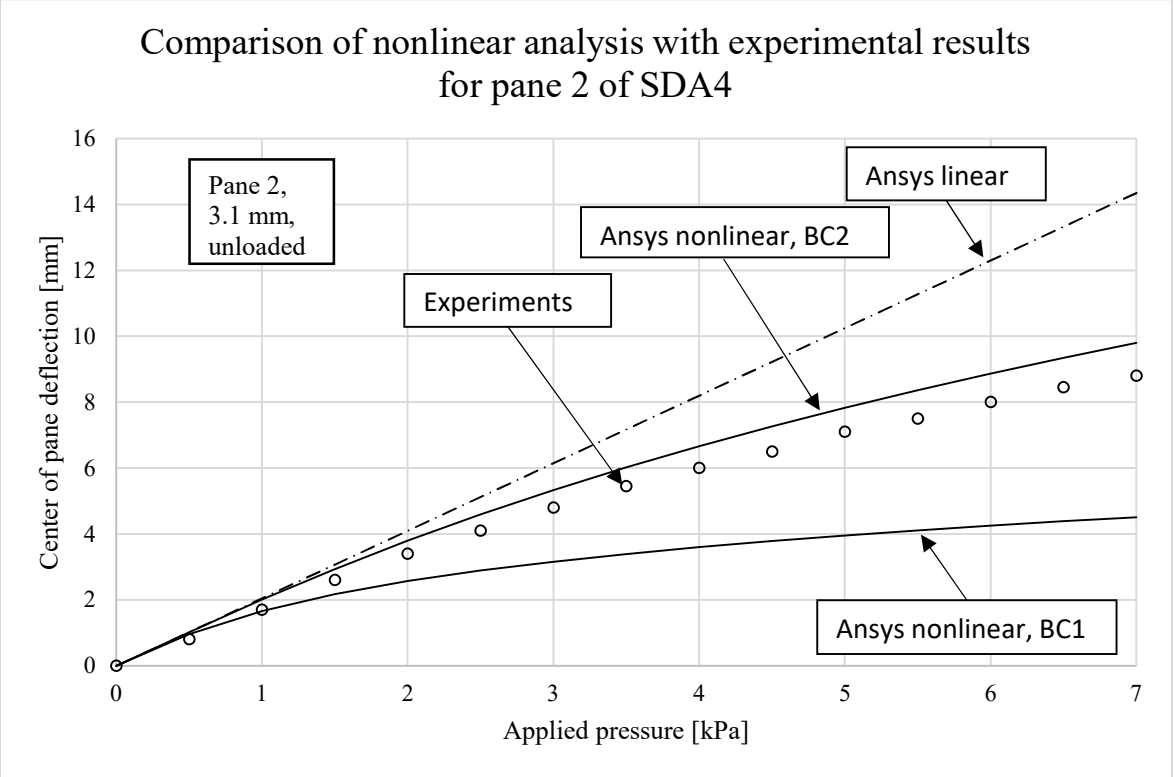

Figure 33. SDA4 (1260x750/5.7+13+3.1) - Comparison of Ansys nonlinear analysis results with experimental results from [24]. The dashed line represents the significance of geometric nonlinearities. BC1 is model with in-plane restraints (Figure 26) and BC2 is model without in-plane restraints (Figure 29).

The results show that the experimental results are close to those of Ansys nonlinear analysis with BC2. The largest absolute error between these two is 0.6 mm (pane 1) and 1.0 mm (pane 2) for SDS3 and SDA4, respectively. These correspond to 8.7 % and 11.4 % in relative error, respectively.

The reason for errors could be from multiple sources. For example, the edge seal system or the frame could provide some rotational or in-plane restraints. Similarly, the IGU could have climate loads present that result in initial deflections. A part of the glass in the test setup schematic is clearly inside the frame and not subjected to the external pressure. Therefore, the effective glass area could be smaller than reported and hence the deflections would be smaller. Furthermore, the study does not report the material parameters or how much the edge seal system participates in the volume change of the cavity.

The Ansys nonlinear model is validated since the general trend of the results are correct, the relative errors are reasonable and the sources for errors are considered.

5.3 Nonlinear pressure variation

It was stated in [55] that the importance of geometric nonlinearities on the load sharing is not clear. Hence, it is studied using the validated models from chapters 5.1 and 5.2. Three cases are considered: i) linear analysis with in-plane restraints (Figure 26); ii) nonlinear analysis with in-plane restraints (Figure 26); iii) nonlinear analysis without in-plane restraints (Figure 29). The external pressure is varied from 1.0 kPa to 15.0 kPa with increments of 1.0 kPa. The pressure variation in the cavity is recorded for each load. The results are presented in Figure 34.

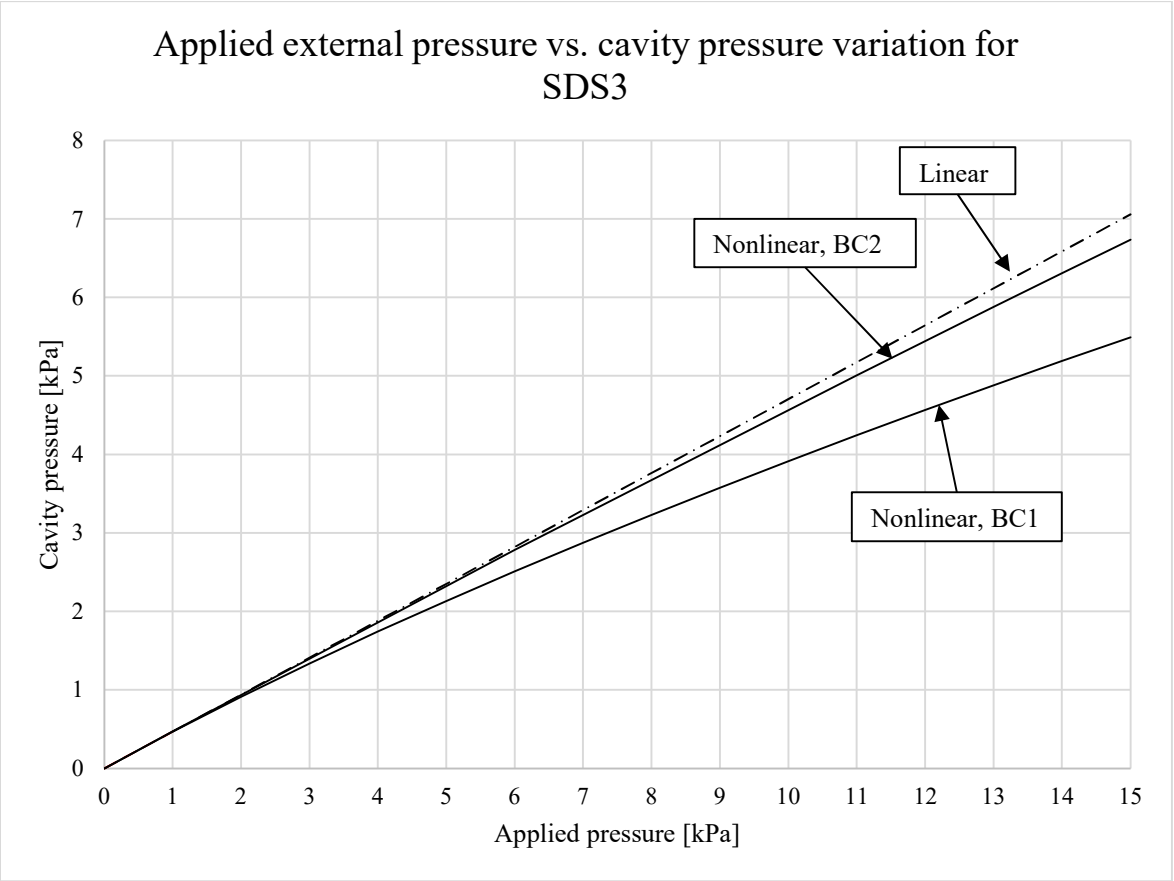

Figure 34. SDS3 (1260x750/5.7+13+5.7) - Comparison of pressure variation in the cavity from Ansys linear and nonlinear analyses. BC1 is model with in-plane restraints (Figure 26) and BC2 is model without in-plane restraints (Figure 29).

The geometric nonlinearity does have an effect on the cavity pressure. The nonlinearity is more pronounced if the edges have in-plane restraints. The nonlinear analysis without in-plane restrains is nearly equal to the linear results. Furthermore, all three cases have nearly the same pressure variation up to 4.0 kPa. Hence, with such boundary conditions or with small loads, one can tentatively use e.g. BAM to determine the pressure variation in the cavity and then use that pressure in nonlinear FE analysis to calculate stress and deflection of a single glass pane. The cavity pressure can be directly applied to pane 2, while the pressure acting on pane 1 is the external pressure minus the cavity pressure (Equation 5). The advantage is that geometric nonlinearities can be included, and only single plate has to be modelled without the gas.

5.4 Parametric study

The Betti's Analytical Method is used to perform parametric study to determine how different factors influence the load sharing. Ship windows are relatively large and therefore it is important to know how the size and the aspect ratio affects the response of the IGU. BAM is used because it is implemented to MATLAB a routine and hence altering parameters is more convenient. The MATLAB routine presented in Appendix 11. The climate loads are not included.

First consider three IGUs with pane thicknesses $h_1=h_2=5$mm, $h_1=h_2=15$mm and $h_1=h_2=25$mm called t5, t15 and t25, respectively. The side lengths are changed so that the

effect of rectangular size and the aspect ratio on the load sharing can be determined. The dimensions of the IGUs are

$a = asp * mul * 100\ [mm]$ (length of longer side)
$b = mul * 100\ [mm]$ (length of shorter side)
$s = \ 10\ [mm]$ (spacer thickness)
$asp = 1.0, 1.2, 1.6, 2.0, 3.0\ [-]$ (aspect ratio)
$mul = 1,2,3, \dots ,20\ [-]$ (size multiplier).

Changing the size multiplier, aspect ratio and the thickness results in 300 specimens. The largest square specimen is 2000x2000 mm with multiplier 20. The largest rectangle is 6000x2000 mm with multiplier 20 and aspect ratio 3. Having an insulating glass unit with 6000x2000 mm and h_1=h_2=25 mm is an extreme case but not impossible. The results are presented in Figure 35 in terms of how much load the directly loaded pane carries (Equation 11).

$$LS_1 = \frac{P_{external} - P_{cavity}}{P_{external}} * 100 \qquad (11)$$

where $P_{external}$ is the applied load [MPa]
P_{cavity} is the pressure variation in the cavity [MPa]
LS_1 is the percentage of total load that pane 1 carry [%].

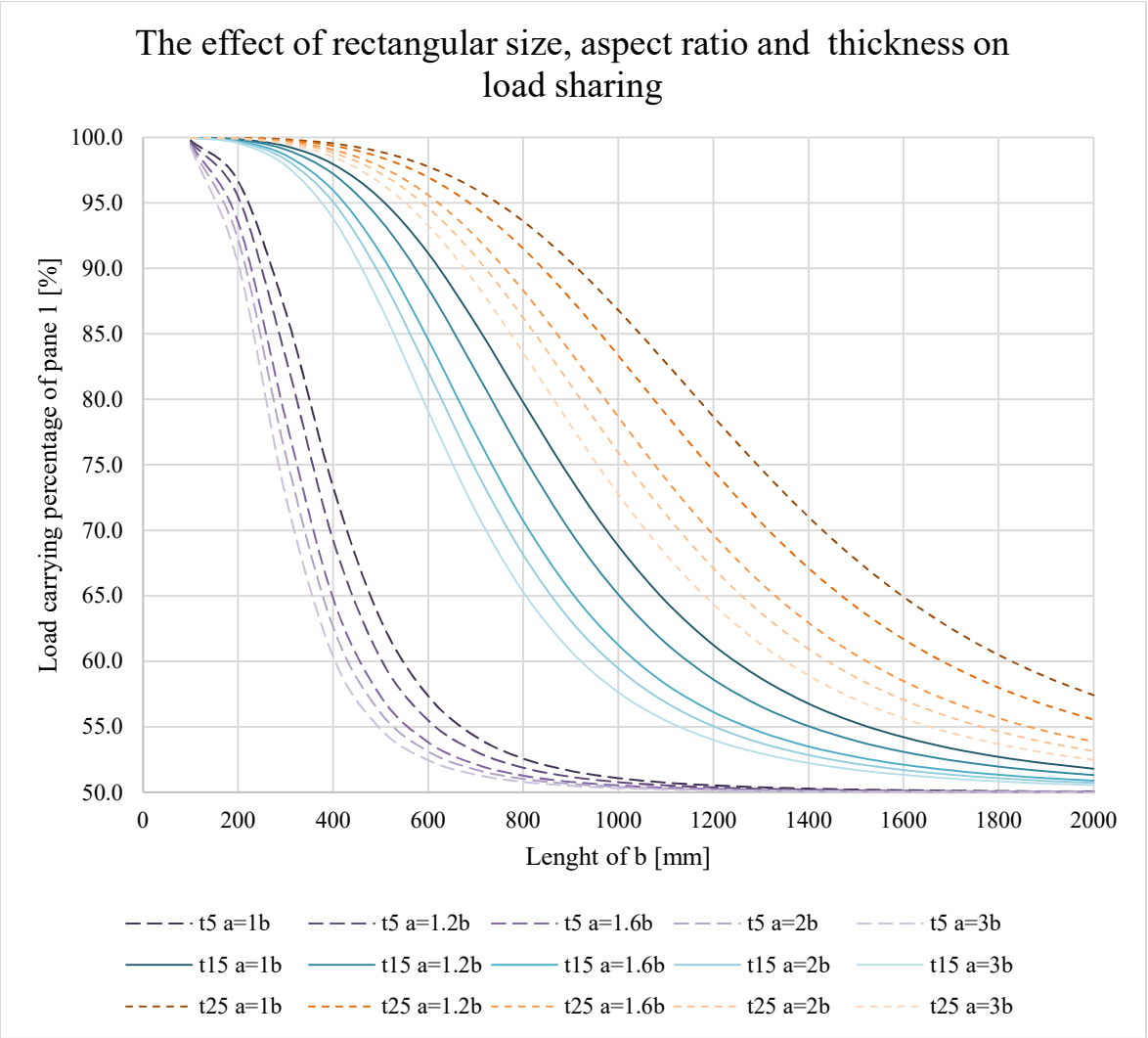

Figure 35. Load sharing percentage of pane 1 (Equation 11) with varying size, aspect ratio and thickness. "t5" means that h_1=h2=5 mm and so on. "b" is the length of shorter side.

The results show that larger the area, more equal the load sharing is between the glass panes. This is true for all the thicknesses and aspect ratios. When the glass panes are thinner and the aspect ratio is larger, the faster the load sharing converges close to 50 % when the size is increased. Hence, the conclusion is that the significance of load sharing increases when the size of the window increases, but thicker the glass panes, slower the converge is.

The influence of the thickness configuration is studied next. First, a small window is chosen for a starting point. The thicknesses of the panes are changed from 1 mm to 25 mm that result in 625 samples. The load carrying percentage of the directly loaded pane is calculated for each sample with Equation 11. The results are presented in Figure 36. It should be noted that the graph includes thickness configurations in bottom left and top right corners that are not realistic (e.g. h_1=1mm and h_2=25mm etc.).

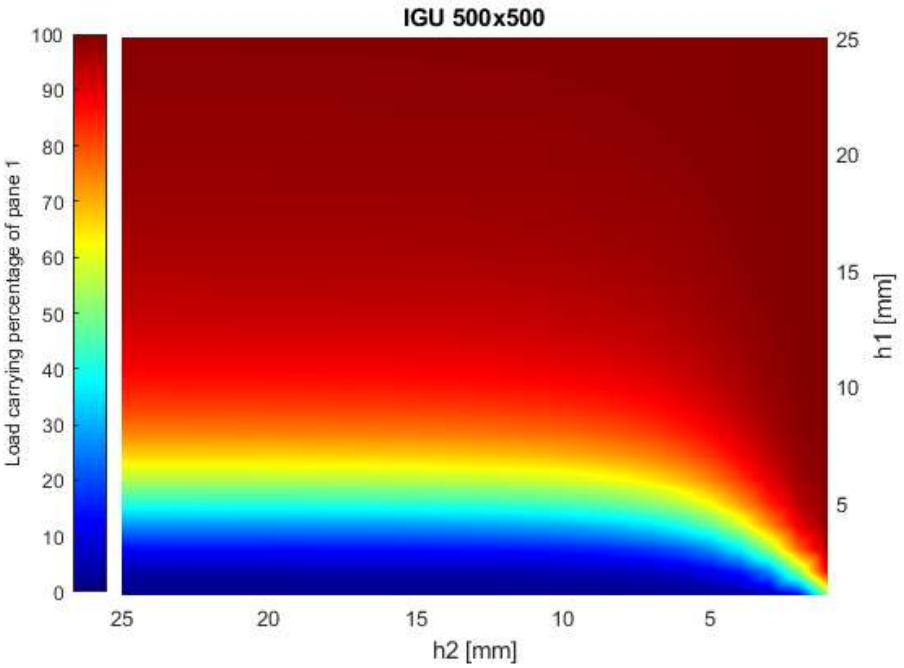

Figure 36. Load sharing percentage (Equation 11) of directly loaded pane with multiple thickness configurations (IGU size 500x500 mm, s=10 mm).

The colors from red to green show areas where the directly loaded pane carries more load than the indirectly loaded pane. Similarly, the colors from green to blue show areas where the indirectly loaded pane carries more load than the directly loaded pane.

It can be clearly seen that the graph is not symmetric. After some point, increasing the thickness of pane 2 does not significantly increase the contribution of that pane to the total load sharing. This can be observed where the “bright” lines have decreasing slope. When the slope is zero, increasing the thickness of the indirectly loaded panes does not affect the load sharing. The same calculation is done for a larger window. A medium size of 1280x800 mm is chosen. The results are presented in Figure 37.

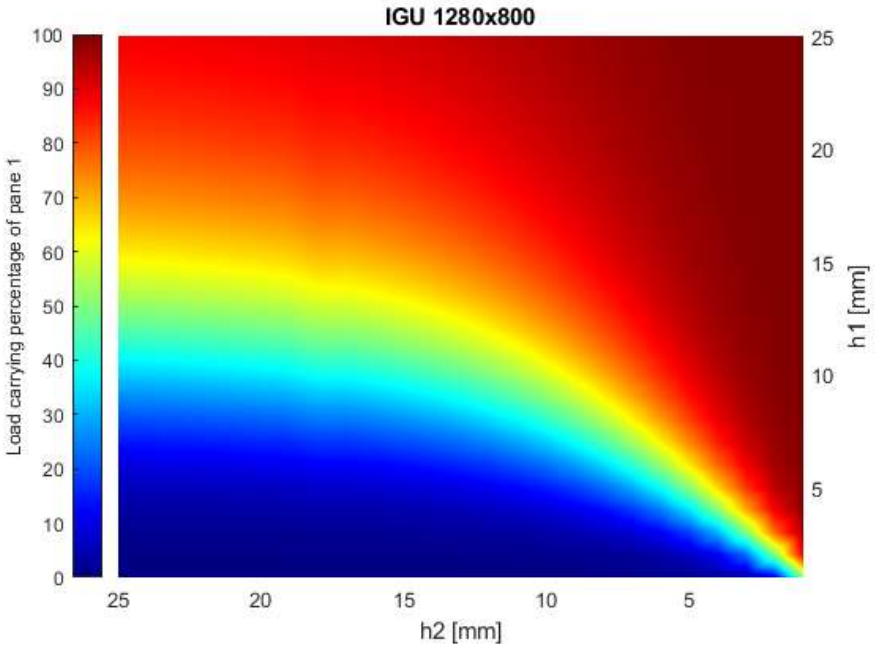

Figure 37. Load sharing percentage (Equation 11) of directly loaded pane with multiple thickness configurations (size 1280x800, s=10 mm).

The graph is more symmetrical. The implication is that the significance of the thickness of the indirectly loaded pane increased. The same calculation is done for a larger window. The results for 2560x1600 mm window are presented in Figure 38.

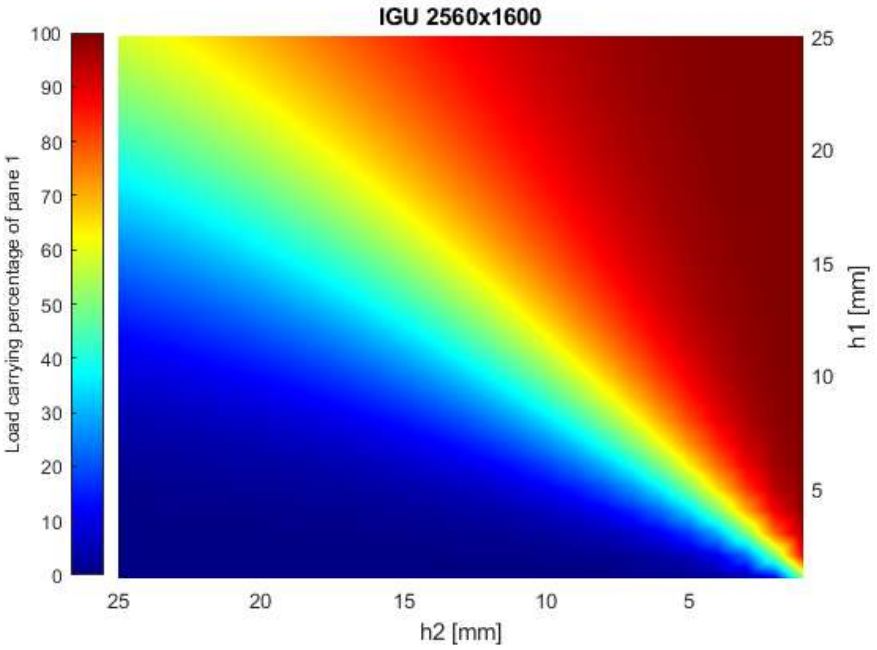

Figure 38. Load sharing percentage (Equation 11) of directly loaded pane with multiple thickness configurations (size 2560x1600, s=10 mm).

The graph is nearly symmetrical. The load sharing is around 50 % between the panes along the diagonal, where $h_1=h_2$. It should be noted that the directly loaded pane always carries more load if it has equal or larger thickness than the other pane.

From the results it can be concluded that in smaller window sizes the thickness of the indirectly loaded pane is less significant after the thickness of the first pane surpasses a certain threshold. The threshold is dependent on the size of the window but disappears once the window is large enough. The conclusion is intuitive since smaller the window, stiffer the glass pane is and hence is able to carry more load.

The effect of spacer thickness is studied next. Commercially available spacers often have thicknesses from 3 mm up to 25 mm depending on the material and the cross-section [23]. The spacer thickness is increased from 3 to 25 mm for 5 different glass thicknesses and 2 different window sizes. Recall the thickness configuration abbreviation from the first comparison graph (Figure 35). The results are presented in Figure 39 on terms of how much load the directly loaded pane carries (Equation 11).

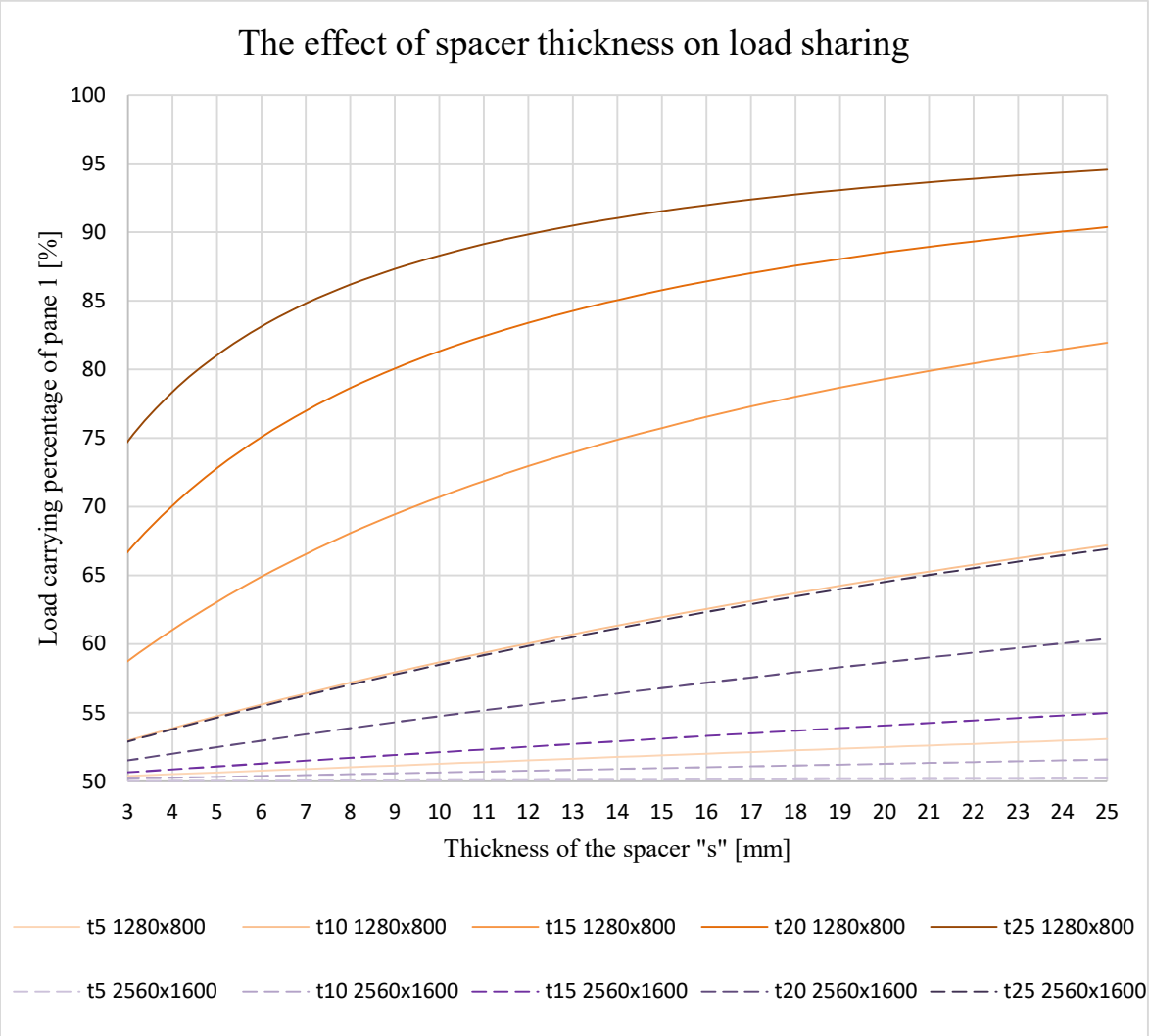

Figure 39. Load sharing percentage (Equation 11) of the directly loaded pane with increasing spacer thickness for 2 IGU sizes and 5 thickness configurations. "t5" means that h_1=h2=5 mm and so on.

The results show that the load sharing decreases as the space thickness increases. As the window size increases or the glass thickness decreases, the significance of the spacer thickness on the load sharing decreases. It can be concluded that increasing the spacer thickness is unbeneficial for the load sharing, especially for smaller windows with thick glasses.

5.5 Implementing climate loads

The climate loads should be considered as they are present for all the insulating glass units. The extreme situations are when the IGU is produced during wintertime and operated in summertime and vice versa. The climate loads are then the largest. Additionally, large altitude difference between the production and operation location induce pressure variation in the cavity. However, since the IGUs in cruise ships are located close to the sea level and presumably the IGUs are produced approximately at the same altitude, the altitude component may be neglected. The remaining winter and summer conditions suggested by DIN 18000-1 [60] are used as presented in Table 11.

Table 11. Combinations of actions [60].

Combination of actions	Temperature change ΔT [K]	Change in atmospheric pressure Δp [kPa]
"Summer"	+20	-2.0
"Winter"	-25	+4.0

The validated Ansys model and the analytical model are used to calculate deflection of both panes in DIGU. Additionally, MEPLA ISO is used for comparison. The superimposed pressure variation is calculated with Equation 10. In Ansys, the temperature body load is inserted using BF command while the atmospheric load is inserted as surface loads acting on both panes with opposite direction.

The climate loads are first considered individually and then superimposed. Finally, an external pressure is applied. The results are presented in Table 12. The IGU dimensions are not important for validation of the climate loads. The same dimensions are used as in chapter 5.6.

Table 12. The effect of climate loads in deflection, comparison between Ansys, BAM and MEPLA ISO (MI). "W" is winter condition and "S" is summer condition from [60] without altitude component, "p" is external uniform pressure. IGU dimensions are 2000x1400/10+20+10 mm. The model is simply supported around all its edges.

	Loading condition			w1 [mm]			w2 [mm]		
	ΔT [K]	Δp [kPa]	p [kPa]	Ansys	BAM	MI	Ansys	BAM	MI
	-25.0	0.0	0.0	+1.918	+1.926	+1.930	-1.918	-1.926	-1.930
	0.0	+4.0	0.0	+0.859	+0.888	+0.890	-0.859	-0.888	-0.890
W	-25.0	+4.0	0.0	+2.697	+2.814	+2.750	-2.697	-2.814	-2.750
S	+20.0	-2.0	0.0	-1.999	-1.974	-2.010	+1.999	+1.974	+2.010
W	-25.0	+4.0	0.1	+2.876	+3.052	+2.960	-2.537	-2.598	-2.500
S	+20.0	-2.0	0.1	-1.795	-1.736	-1.770	+2.179	+2.190	+2.220
W	-25.0	+4.0	1.0	**+4.388**	+5.129	+5.120	**-1.134**	-0.657	-0.680
S	+20.0	-2.0	1.0	**+0.023**	+0.405	+0.380	**+3.723**	+4.131	+4.160

The result show good agreement for all the loading cases except for the last two with 1.0 kPa external pressure (bolded). The Ansys model requires nonlinear analysis when using BF command with the HSFLD elements and therefore the geometric nonlinearities result in smaller deflections. Considering this, the model with climate loads is validated.

5.6 Design example

A thickness for single thermally toughened glass is calculated according to the rules and regulations for the classification of ships by Lloyd's Register (July 2019) [14]. The obtained

thickness is applied to an IGU construction so that the thicknesses of the panes are equal. The presented nonlinear FE Ansys model is used to calculate maximum deflection and maximum principal stresses of both panes. The results are compared to standard design stress criterion of 40 MPa. Finally, the Ansys model is used to a find optimal thickness that fulfils the stress criterion. The class prescribed thickness and the obtained optimal thickness are compared.

Consider an insulating glass unit with 2000x1400 mm glass panes with spacer thickness of 20 mm. The dimensions result in a glass pane that has roughly the same area as the Iona SkyDome panels [74] and the same aspect ratio as the default window sizes in ISO 3903 [18]. The chosen spacer thickness is common in building architecture. Three external pressure values are used according to the class rules: i) 2.5 kPa; ii) 7.5 kPa; iii) 15.0 kPa. The largest design pressure is defined for windows located near the waterline while the smallest is for windows located at the uppermost deck (Figure 41).

The thickness for single thermally toughened glass pane is calculated according to Equation 12. The aspect ratio is 1.43, hence β is 0.4422 and the resulting thicknesses are presented in Table 13.

Table 13. Thickness of single thermally toughened glass pane according to Lloyd's Register rules [14].

Pressure [kPa]	t_0 [mm]
2.5	7.3
7.5	12.8
15.0	18.0

Since there is no definition of insulating glass units in the class rules [14], the second glass pane of IGU has to be equally thick even though it is located on the inside of the structure. Other arrangements are presumable agreed on in real applications. However, at least the outer windowpane in IGU has to be according to the specification.

The characteristic failure strength specified in ISO 11336 [21] for thermally toughened glass is 160 MPa. With safety factor of 4, the design flexural stress is 40 MPa. As a reminder, the criterion is compared to the maximum principal stress on the top and bottom surfaces of both panes.

The stress criterion of 40 MPa is applied to Ansys model of single glass pane with E=70 MPa, ν=0.23 and the specified dimensions. The analysis is done with and without geometric nonlinearities. The maximum deflections and the maximum principal stresses are presented in Table 14.

Table 14. Maximum deflection and maximum principal stress for single thermally toughened glass pane (2000x1400 mm). BCs are as presented in Figure 22 and Figure 29 for linear and nonlinear Ansys analysis, respectively.

		Linear Ansys		Nonlinear Ansys	
p [kPa]	t_0 [mm]	w_{max} [mm]	σ_{p+} [MPa]	w_{max} [mm]	σ_{p+} [MPa]
2.5	7.3	29.2	41.4	17.2	23.5
7.5	12.8	16.2	40.4	13.9	35.5
15.0	18.0	11.7	40.9	11.1	39.8

The maximum principal stress from linear analysis surpasses the criterion slightly for each thickness. The class rules are based on linear assumptions, but clearly geometric nonlinearities are present in thinner glasses. The maximum principal stress from the nonlinear analysis is less than 40 MPa for all the thicknesses.

Next, an IGU is considered with the same specifications so that $h_1=h_2=t_0$. The nonlinear FE Ansys model that was validated in chapter 5.2 is used. The results are presented in Table 15.

Table 15. Maximum deflections and maximum principal stresses for IGU with equally thick glass panes. "LS" is the percentage of the total load that the indirectly loaded pane carries (Δp/p×100). Nonlinear Ansys analysis with BCs according to Figure 29.

p [kPa]	t_0 [mm]	$w1_{max}$ [mm]	$w2_{max}$ [mm]	$\sigma1_{p+}$ [MPa]	$\sigma2_{p+}$ [MPa]	LS [%]
2.5	7.3	11.4	10.9	16.2	15.5	48.4
7.5	12.8	8.4	7.0	21.6	17.8	44.8
15.0	18.0	7.0	4.5	25.1	16.0	38.7

The maximum principal stresses are significantly smaller than for single glass pane (Table 14). To concretize the benefit of load sharing, the same nonlinear FE Ansys model is used to find an optimal thickness ($h_1=h_2=t_0$) for each load case considering the 40 MPa stress criterion. The results are presented in Table 16.

Table 16. Maximum deflections and maximum principal stresses for IGU with optimized equally thick glass panes. "LS" is the percentage of the total load that the indirectly loaded pane carries (Δp/p×100). Nonlinear Ansys analysis with BCs according to Figure 29.

p [kPa]	t_0 [mm]	$w1_{max}$ [mm]	$w2_{max}$ [mm]	$\sigma1_{p+}$ [MPa]	$\sigma2_{p+}$ [MPa]	LS [%]
2.5	3.5	25.7	25.3	39.1	38.0	49.2
7.5	6.3	25.9	24.7	39.6	36.4	47.6
15.0	12.3	16.4	13.8	39.9	33.7	44.2

Comparing the results from Table 14 and Table 16 shows that the thickness can be reduced by 52 %, 51 % and 31 % for 2.5 kPa, 7.5 kPa and 15.0 kPa load cases, respectively, when the load sharing is considered.

So far, the effect of climate loads is not considered. The worst-case scenarios, winter and summer conditions, increase the maximum deflection and the maximum principal stress. It should be noted that the climate loads are not required by the classification societies. The results for the previously calculated optimal thicknesses including the climate loads are presented in Table 17.

Table 17. Maximum deflections and maximum principal stresses for IGU with optimized equally thick glass panes, including the climate loads from [60] without altitude component. Nonlinear Ansys analysis with BCs according to Figure 29.

p [kPa]	ΔT [K]	Δp [kPa]	t_0 [mm]	$w1_{max}$ [mm]	$w2_{max}$ [mm]	$\sigma1_{p+}$ [MPa]	$\sigma2_{p+}$ [MPa]
2.5	+20.0	-2.0	3.5	24.2	26.7	34.5	42.7
2.5	-25.0	+4.0	3.5	27.4	23.2	45.1	31.5
7.5	+20.0	-2.0	6.3	24.5	26.2	35.6	40.3
7.5	-25.0	+4.0	6.3	27.8	22.6	44.8	31.0
15.0	+20.0	-2.0	12.3	14.9	15.4	36.3	37.5
15.0	-25.0	+4.0	12.3	18.4	11.3	44.2	27.9

The effect of climate loads can be observed from the results. The maximum deflection and the maximum principal stress of the indirectly loaded pane increase in the summertime

(initial pillow shape). Similarly, the same happens for the directly loaded pane during wintertime (initial concave shape). The increase of the maximum principal stress is in order of 5 MPa for all the cases. As mentioned in chapter 3.1, the climate loads are only critical for small windows that exhibit large lateral stiffness. However, the effect is large enough to surpass the stress criterion and hence the thickness should be increased.

It should be noted that the maximum principal stress is at the corners of the IGU (Figure 40). This is because of the boundary conditions and large deflections. Real glass pane corners have a radius, but even then the stress concentration accumulates close to the corners.

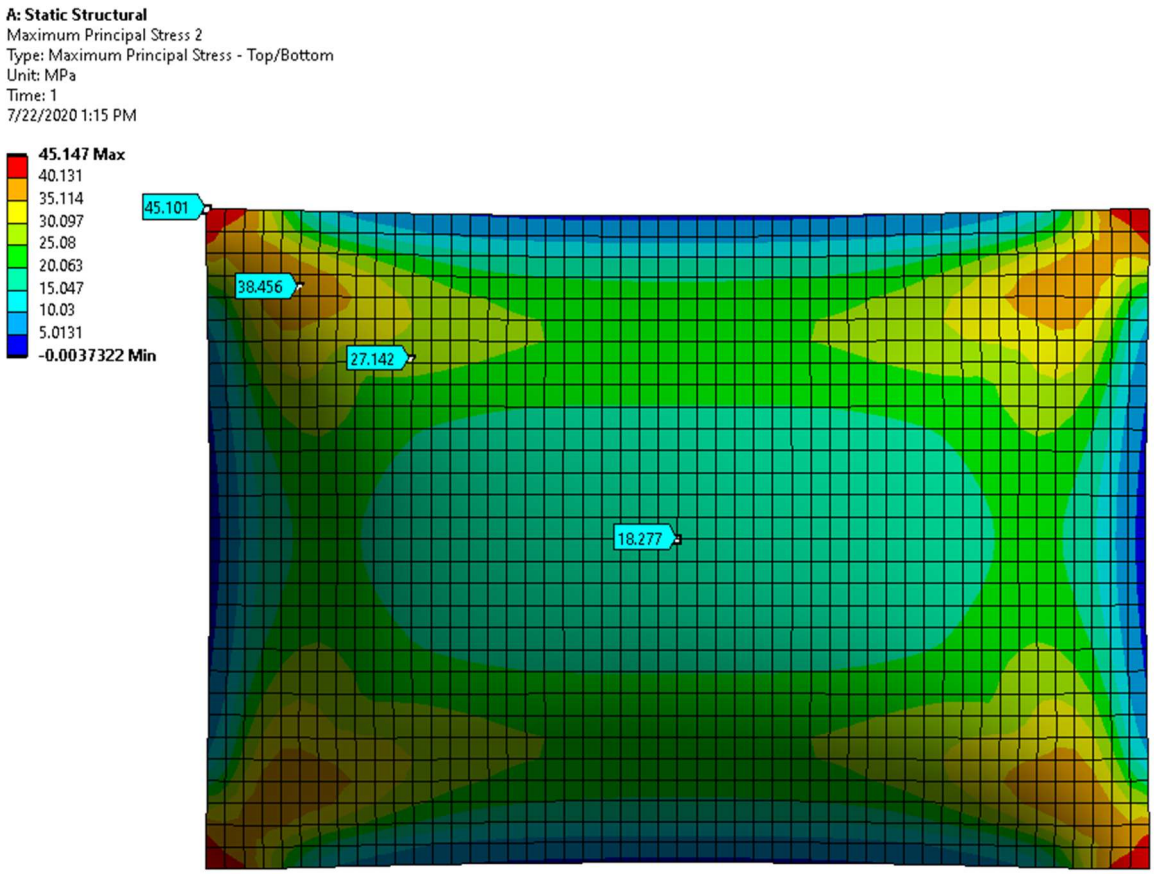

Figure 40. IGU (2000x1400/3.5+20+3.5 mm) maximum principal stress (top/bottom) of pane 1 for 2.5 kPa external load, including the climate loads as presented in Table 17, row 2. The deformation scale factor is set 22 for demonstrating the deformation of the edges. Nonlinear analysis results from Ansys.

6 Discussion

Majority of ship windows are insulating glass units (IGUs). The IGUs consist of two glass panes separated by a hermetically sealed gas. The gas transfers loads between the glass panes which increases the load carrying capacity of the IGU [55], also known as load sharing. However, the classification societies [14, 15, 16] prescribe design criteria only for monolithic glasses or laminated glasses, neglecting the load sharing effect. Hence, the current design criteria may lead to thicker glass constructions than necessary.

The presented Finite Element model can be used to calculate the response of an insulating glass unit. The response may be calculated in linear or nonlinear analysis. Linear analysis is sufficient for small deflections ($w_{max} < t/2$). In such case, the presented Finite Element model or existing analytical methods [55, 65] can be used on linear basis. Good agreement between the methods was found in terms of maximum deflection (relative error < 0.1%). The analytical methods are faster to use but they are restricted to rectangular or triangular glass shape and simply supported boundary condition. However, the glasses in ships are not limited to these conditions. Therefore, Finite Element Method may be justified.

If the glass structures are located closer to the waterline [14], or in case of an extreme event [6, 7], increased loads can be encountered. They cause large deflections of thin and large glass panes, i.e. geometric nonlinearity can be observed [20]. Then, it is necessary to evaluate the response on nonlinear basis. Good agreement was found between the presented model in nonlinear analysis and experimental results from open scientific literature [24]. The relative error in center-of-pane deflection for the maximum load (7.0 kPa) was less than 12 %. One source for error can be in the boundary conditions.

Glass connections can be designed to allow for in-plane translation (sliding) of the pane, or to resist it (Appendix 7). The presented model was used calculate both of these limit cases. The experimental results placed in between them, but closer to the unrestrained limit, as expected. Therefore, using the boundary condition without in-plane restrains is a conservative approach considering that in real-life applications the boundary conditions are indeed between these two limits. Especially if glued connections are used where the window is bonded to surrounding structure with some adhesive material (Appendix 7). These adhesive materials are also used in some windows onboard a ship [4, 5].

The boundary conditions and the geometric nonlinearities also affect the pressure variation of the gas. The pressure variation was nonlinear when the in-plane translations were restrained. On the other hand, it was linear when the in-plane translations were unrestrained. The nonlinearity appeared roughly after external pressure was larger than 4.0 kPa. These findings are important as the effect of geometric nonlinearity on the load sharing has not been studied [55]. The results indicate that the pressure variation can be determined on linear basis with the analytical method [55], if the load is small or the in-plane translations are unrestrained. In fact, ship windows often fulfil these conditions.

Additionally, the ship windows are designed to be large. This enables the immersion with the marine environment, which is important for the passengers [2]. The parametric study shows that load sharing is especially important for large insulating glass units. The load sharing increases as the glass pane compliance increases (area increases and thickness decreases). The same effect is observed when spacer thickness is decreased. These results are in line with [55].

However, the main reason to use insulating glass units is their ability to reduce heat losses [17]. The heat loss reduction is enhanced when the thickness of the spacer is increased [75]. At the same time, the noise insulation [76] and the fire safety [77] are enhanced. Therefore, the spacer design is rightfully driven by these design criteria rather than the load sharing. Especially when the spacer thickness on the load sharing is only critical for small windows, which most of the ship windows are not.

Similarly, the internal pressure loads from the climate loads are critical only for small windows [57]. However, they are often considered in the design process as they are present for all the insulating glass units. The climate loads can be included in the presented Finite Element model. Their implementation was validated by the analytical methods [55, 65]. The implication of the climate loads on the deflection and stress of an insulating glass unit was demonstrated in a design example.

An insulating glass unit with large but reasonable dimensions was considered. The thickness of the glass panes was calculated according to Lloyd's Register classification rules [14] for three different design pressure. Similarly, the thickness of the panes was calculated using the presented Finite Element model with unrestrained boundary condition on nonlinear basis, so that standard stress criterion of 40 MPa was fulfilled. The obtained thicknesses were compared.

The result indicate that the thickness of the glass panes can be reduced by up to 52 % when the load sharing is considered. The load sharing appeared to be more beneficial for thinner glass panes where the geometric nonlinearities were more pronounced. The climate loads according to standard DIN 18001-1 [60] increased the maximum principal stress approximately by 5 MPa. However, considering the climate loads is not required by the classification societies. Furthermore, it might not be reasonable for ship windows to use the extreme conditions from DIN 18001-1 [60]. More realistic climate loads could be obtained considering the ship's operation route.

The thickness reduction is significant when considering large insulating glass structures in cruise ships. For example, the Iona SkyDome has an area of 970 m² [74]. The weight of the glass panes could potentially be reduced to half. At the same time, the stability of the ship is increased as the SkyDome is located on the top deck. The thickness reduction is possible as long the glass panes are compliant, and the gas remains sealed.

However, some leaking of the gas occurs in small quantities. Insulating glass units conforming EN 1279-5 [78] are assumed for 25 years in service allowing annual gas leaking rate of 1% due natural ageing [79]. The gas can also leak due to actions on the glass panes [80]. If the edge seal system ruptures and the gas is able to escape quickly, it can be expected to have a sensible effect on the response. However, at least to author's knowledge, no research on this matter has been conducted. Any extensive leaking can be visually observed as condensation inside the unit. This gives a clear indication for maintenance.

It is beyond the scope of this study to include the effect laminated glass (LG) and the edge seal system on the response of the IGU. The stiffness of the interlayer dominates the flexural behavior of laminated glass [81]. The stiffness is dependent on the loading time and the temperature. Therefore, calculating the cavity volume change with LG is complicated. At

the same time, the modelling of LG has direct impact on the load sharing. Laminated glass can tentatively be represented with deflection-effective thickness in the presented model (Appendix 8).

Laminated glasses in ships often have ionomer interlayers that have excellent mechanical properties and are less sensitive to temperature changes and load durations [49]. With such properties, the LG acts more and more in a monolithic manner, which increases its performance and decreases the modelling complexity. Therefore, one might neglect the interlayer completely or use a part of its thickness in the design for simplification.

If the interlayer is assumed softer or neglected completely for presumably conservative results, the actual construction is stiffer than analyzed for. Consequently, the deflection of the panes due to internal pressure loads are smaller than expected. This results in higher stresses on the glass panes and the edge seal system than expected. The increased stress may be significant for the spacer and the sealings which shows that this approach is not conservative.

7 Conclusions

By analyzing the response of an insulating glass unit (IGU) with the presented Finite Element (FE) model, this thesis has shown that the current glass design criteria by different classification societies [14, 15, 16] are insufficient. Firstly, the equations for the glass pane thickness determination are based on linear assumptions. Secondly, the load sharing effect in insulating glass units is not considered. As a consequent, the glass panes are designed thicker or smaller than necessary. This increases the weight of the glass structures or hinders the immersion with the marine environment, respectively.

The presented FE model proved to be effective in evaluating the design criteria for thickness determination of glass panes in IGUs. It demonstrated how much thinner the glass panes can be designed when the load sharing effect is considered. It appeared to be the most effective when the geometric nonlinearities are pronounced, i.e. when thin glass panes and/or large loads are considered. Therefore, the linear assumptions are not always sufficient.

The nonlinearities can be included when using Finite Element Method (FEM). At the same, other restrictions from the analytical framework are also removed. These include limited glass shapes and boundary conditions. The boundary conditions had significant effect on the deflection of the panes and on the gas pressure variation in the performed nonlinear analyses. Therefore, using FEM was justified.

The obtained results from the linear and nonlinear FE analyses indicate that the presented model can be used in the design process. Additionally, it was found that pressure variation of the gas can be determined using an analytical method, even if geometric nonlinearity is observed in the glass panes. This is possible in cases where the boundary condition allows for sliding (in-plane movement) of the panes, or when the applied load is relatively small. This contributes to new knowledge and it implies that only one glass pane of an IGU has to be modelled, which decreases the FE modelling complexity.

The findings of this study are important as very little information is currently available in the open scientific literature on FE modelling of insulating glass units. However, the validation of the Finite Element model was limited to one set of experimental results. Future work is needed to obtain more experimental results for insulating glass units with different boundary conditions. This is required for gaining confidence in using the presented model and for determining the actual boundary conditions that ship windows have.

The literature review clearly illustrates how much research has been made for structural glass, but it also shows how much more there is to be done. Glass as a material requires very specific knowledge as it differs vastly from conventional building materials, e.g. from steel. Because glass is brittle material and does not have single strength value, often large safety factors are used which result in highly conservative constructions. However, with good engineering, the windows can be designed more economically, yet safely.

References

[1] C. W. Bostick, “Architectural trends thru the looking glass,” in *Glass performance days*, Tampere, Finland, June, 2009.

[2] S. McCartan, L. Moody and D. McDonagh, “Luxification and Design-Driven Innovation in Superyacht Design,” in *RINA Conference: Design, Construction & Operation of Super & Mega Yachts*, Genoa, 5-6 May 2011.

[3] C. Hughes, “New P&O Iona SkyDome Revealed,” BeyondCruise, 24 August 2020. [Online]. Available: https://beyondcruise.com/news/new-po-iona-skydome-revealed. [Accessed 28 May 2020].

[4] W. Fricke and B. Gerlach, “Effect of large openings without and with windows on the shear stiffness of side walls in passenger ships,” *Ships and Offshore Structures,* vol. 10, no. 3, pp. 256-271, 2015.

[5] B. Wiegard, S. Ehlers, O. Klapp and B. Scheider, “Bonded window panes in strength analysis of ship structures,” *Ship Technology Research,* vol. 65, no. 2, pp. 102-121, 2018.

[6] B. Gerlach, W. Fricke, M. Guiard, D. F. Gonzáles and M. Abdel-Maksoud, “Failure prediction of ship windows subjected to wave impacts,” *Ship Technology Research,* vol. 62, no. 3, pp. 159-172, 2015.

[7] E. M. Bitner-Gregersen and O. Gramstad, “Rogue waves - impact on ship and offshore structures,” in *DNV GL Strategic research & Innovation position paper*, 2015.

[8] B. Gerlach and W. Fricke, “Experimental and numerical investigation of the behavior of ship windows subjected to quasi-static pressure loads,” *Marine Structures,* vol. 46, pp. 255-272, 2016.

[9] G. Vergassola and D. Boote, “A simplified approach to the dynamic effective thickness of laminated glass for ships and passenger yachts,” *International Journal on Interactive Design and Manufacturing,* vol. 14, pp. 123-135, 2020.

[10] B. Van Antwerpen, D. d'Udekem and C. Weißenborn, "Vibro-Acoustic simulation of structure-borne induced radiation of ship windows," in *Proceedings of the International Conference on Acoustics NAG/DAGA*, Rotterdam, 2009.

[11] F. Verbaas, “From simple windows to structural material - Application of glass on board, an update (Part 1),” *Schip en Werf de Zee,* vol. 136, pp. 268-273, 2016.

[12] F. Verbaas, “From simple window to structural material - Application of glass on board, an update (part 2),” *Schip en Werf de Zee,* vol. 136, pp. 244-247, 2016.

[13] F. Verbaas, “Foundations for a code for maritime structural design of glass components,” in *24th International HISWA Symposium on Yacht Design and Yacht Construction*, Amsterdam, 2016.

[14] Lloyd's Register, “Rules and Regulations for the Classification of Ships,” London, 2019.

[15] *Rules for classification: Ships - DNVGL-RU-SHIPS Pt.3 Ch.12. Edition January 2017.*

[16] *RINA Rules 2019. Pt B, Ch 9, Sec 9. Arrangement of hull and superstructure openings.*

[17] M. Haldimann, A. Luible and M. Overend, Structural Use of Glass, Zürich, Switzerland: IABSE-AIPC-IVBH, 2008.

[18] “ISO 3903:2012. Ships and marine technology - Ships' ordinary rectangular windows,” International Organization for Standardization, Vernier.

[19] “ISO 21005:2018. Ships and marine technology - Thermally toughened safety glass panes for windows and side scuttles,” International Organization for Standardization, Vernier.

[20] B. Gerlach, "Structural Behavior of Ship Windows," *The German Society for Maritime Technology,* pp. 85-103, 2016.

[21] “ISO 11336-1: 2012. Large yachts - Strength, weathertightness and watertightness of glazed openings. Part 1: Design criteria, materials, framing and testing of independent glazed openings,” International Organization for Standardization, Geneva.

[22] “SFS-EN 1288-3:2000. Glass in Building. Determination of the bending strength of glass. Part 3: Test with specimen supported at two points (four point bending),” Finnish Standards Association, Helsinki.

[23] S. Bergh van den, R. Hart, B. P. Jelle and A. Gustavsen, “Window spacers and edge seals in insulating glass units: A state-of-the-art review and future perspectives,” *Energy and Buildings,* vol. 58, pp. 263-280, 2013.

[24] S. McMahon, S. H. Norville and S. M. Morse, “Experimental investigation of load sharing in insulating glass units,” *Journal of Architectural Engineering,* vol. 24 04017038, 2018.

[25] M. K. Feldmann, "Guidance for European Structural Design of Glass Components," Luxemburg, 2014.

[26] *AS 1288-2006 Glass in buildings - Selection and installation,* Sydney: Standards Australia.

[27] *ASTM E1300-16. Standard Practice for Determining Load Resistance of Glass in Buildings. ASTM International. West Conshohocken, PA. 2016.*

[28] *SFS-EN 16612:2019 Glass in building. Determination of the lateral load resistance of glass panes by calculation,* Helsinki: Finnish Standard Association.

[29] *DIN 18008-2:2010-12 Glass in building - Design and construction rules - Part 2: Linearly supported glazings,* Berlin: Beuth Verlag GmbH.

[30] S. Chen, M. Zang, D. Wang, S. Yoshimura and T. Yamada, “Numerical analysis of impact failure of automotive laminated glass: A review,” *Composites Part B,* vol. 122, pp. 47-60, 2017.

[31] C. Bedon, X. Zhang, F. Santos, D. Honfi, M. Kozlowski, M. Arrigoni, L. Figuli and D. Lange, "Performance of structural glass facades under extreme loads - Design methods, existing research, current issues and trends," *Construction and Building Materials,* vol. 163, pp. 921-937, 2018.

[32] K. Osnes, J. K. Holmen, O. S. Hopperstad and T. Børvik, "Fracture and fragmentation of blast-loaded laminated glass: An experimental and numerical study," *International Journal of Impact Engineering,* vol. 132 103334, 2019.

[33] S. Dey, O. S. Hopperstad, T. Børvik and K. Osnes, “On the dynamic response of laminated glass exposed to impact before blast loading,” *Experimental Mechanics,* vol. 59, pp. 1033-1046, 2019.

[34] B. Weller, K. Härth, S. Tasche and S. Unnewehr, Glass in Building: Principles, Applications and Examples, München: Birkhäuser Verlag AG, 2009.

[35] F. Oikonomopoulou, T. Bristogianni, L. Barou, F. A. Veer and R. Nijsse, "The potential of cast glass in structural applications. Lessons learned from large-scale castings and state-of-the art load-bearing cast glass in architecture," *Journal of Building Engineering,* vol. 20, pp. 213-234, 2018.

[36] *SFS-EN 572-2: 2012 Glass in building. Basic soda lime silicate glass products. Part 2: Float glass,* Helsinki: Finnish Standards Association, p. 15.

[37] S. Takeda, "Oxygen and silver diffusion into float glass," *Journal of Non-Crystalline Solids,* vol. 352, pp. 3910-3913, 2006.

[38] J. A. Howell, J. R. Hellmann and C. L. Muhlstein, "Nanomechanical properties of commercial float glass," *Journal of Non-Crystalline Solids,* vol. 354, pp. 1891-1899, 2008.

[39] E. L. Bourhis, Glass: Mechanics and Technology, 2 ed., John Wiley & Sons, Incorporated, 2014.

[40] *SFS-EN 572-1:2012 + A1:2016 Glass in building. Basic soda-lime silicate glass products. Part 1: Definitions and general physical and mechanical properties,* Helsinki: Finnish Standards Association, p. 11.

[41] *SFS-EN 12150-1:2015 +A1:2019 Glass in building. Thermally toughened soda lime silicate safety glass. Part 1: Definition and description,* Helsinki: Finnish Standards Association, p. 35.

[42] *SFS-EN 14179-1:2016 Glass in building. Heat soaked thermally toughened soda lime silicate safety glass. Part 1: Definition and description,* Helsinki: Finnish Standards Association .

[43] *SFS-EN 1863-1:2012 Glass in building. Heat strengthened soda lime silicate glass. Part 1: Definition and description,* Helsinki: Finnish Standard Association.

[44] S. Karlsson and B. Jonson, "The technology of chemical glass strengthening - a review," *European Journal of Glass Science and Technology Part A,* vol. 51, pp. 41-54, 2010.

[45] *SFS-EN 12337-1:2000 Glass in building. Chemically strengthened soda lime silicate glass. Part 1: Definition and description,* Helsinki: Finnish Standards Association.

[46] M. Overend, C. Butchar, H. Lambert and M. Prassas, "The mechanical performance of laminated hybrid-glass units," *Composite Structures,* vol. 110, pp. 163-173, 2014.

[47] P. Foraboschi, “Hybrid laminated-glass plate: Design and assessment,” *Composite Structures,* vol. 106, pp. 250-263, 2013.

[48] J. Xu and Y. Li, Impact Behavior and Pedestrian Protection of Automotive Laminated Windshield, Beijing: Science Press Beijing and Springer Nature Singapore Pte Ltd, 2018.

[49] M. Martín, X. Centelles, A. Solé, C. Barreneche, I. A. Fernández and L. F. Cabeza, "Polymeric interlayer materials for laminated glass: A review," *Construction and Building Materials,* vol. 230 116897, 2020.

[50] *SFS-EN ISO 12543-2: 2011 Glass in building. Laminated glass and laminated safety glass. Part 2: Laminated safety glass,* Helsinki: Finnish Standards Association, p. 10.

[51] F. A. Veer, P. C. Louter and F. P. Bos, "The strength of annealed, heat-strengthened and fully tempered float glass," *Fatigue & Fracture of Engineering Materials & Structures,* vol. 32, pp. 18-25, 2009.

[52] B. Demchyna and T. Osadchuk, "Flexural strength of glass using Weibull statistic analysis," *Journal of Achievements in Materials and Manufacturing Engineering,* vol. 87, no. 2, pp. 49-61, 2018.

[53] A. Vedrtnam and S. Pawar, "Laminated plate theories and fracture of laminated glass plate - A review," *Engineering Fracture Mechanics,* vol. 186, pp. 316-330, 2017.

[54] M. Teotia and R. K. Soni, "Applications of finite element modelling in failure analysis of laminated glass composites: A review," *Engineering Failure Analysis,* vol. 94, pp. 412-437, 2018.

[55] L. Galuppi and G. Royer-Carfagni, "Betti's analytical method for the load sharing in double glazed units," *Composite Structures,* vol. 235 111765, 2020.

[56] "How to make a sealed unit," Thermoseal Group, [Online]. Available: https://bit.ly/30JmFqQ. [Accessed 11 August 2020].

[57] S. Buddenberg, P. Hof and M. Oechsner, "Climate loads in insulating glass units: comparison of theory and experimental results," *Glass Structures & Engineering,* vol. 1, pp. 301-313, 2016.

[58] A. Rose, "Pressure release of insulating glass units (IGU)," in *Rosenheim Window & Facade Conference 2016*, Rosenheim, 2016.

[59] F. Le Blancq, "Diurnal pressure variations: the atmospheric tide," *Weather,* vol. 66, pp. 306-307, 2011.

[60] *DIN 18008-1: 2010. Glass in building - Design and construction rules - Part 1: Terms and general bases,* Berlin: Beuth Verlag GmbH.

[61] Z. Respondek and I. Major, "Study of deflection in insulating glass units under climatic loads simulation," in *IOP Conf. Series: Materials Science and Engineering 603 032060*, 2019.

[62] G. C. V. Vallabhan and G. D. Chou, "Interactive nonlinear analysis of insulating glass units," *Journal of Structural Engineering,* vol. 112, no. 6, pp. 1313-1326, 1986.

[63] J.-D. Wörner, X. Shen and B. Sagmeister, "Determination of load sharing in insulating glass units," *Journal of Engineering Mechanics,* vol. 119, no. 2, pp. 386-392, 1993.

[64] S. Timoshenko and J. Goodier, Theory of Elasticity, New York: McGraw-Hill, 1970.

[65] "MEPLA Software for Structural Glass Design," 6 April 2020. [Online]. Available: https://www.mepla.net/en/mepla_iso. [Accessed 5 May 2020].

[66] "Ansys Mechnical APDL 2020 R1. Element Reference. Chapter 7: Element Library - SHELL181".

[67] T. Nelson and E. Wang, "Reliable FE-Modeling with ANSYS," in *Proceedings of the international ANSYS conference*, Pittsburgh, 2004.

[68] "Ansys. Mechanical APDL 2020 R1. Element Reference - Chapter 7: Element Library 3-D Hydrostatic Fluid".

[69] S. Imaoka, "Hydrostatic Fluid Element at ANSYS 13.0," ANSYS Inc., 2010.

[70] "Ansys. Mechanical APDL 2020 R1. Technology Demonstration Guide. Chapter 24: Hydrostatic Fluid Analysis of an Inflating and Rolling Tire".

[71] “Ansys. Mechanical APDL 2020 R1. Theory Reference. Chapter 13: Element library. 13.242. HSFLD242 - 3D Hydrostatic Fluid”.

[72] D. Velchev and I. V. Ivanov, “A finite element for insulating glass units,” in *Challenging Glass 4 & COST Action TU0905 Final Conference*, Lausanne, Switzerland, 2014.

[73] *Ansys Mechanical APDL 2020 R1. Theory Reference. Chapter 14: Analysis tools - 14.11. Newton-Raphson Procedure.*

[74] “IONA SKYDOME with FRENER & REIFER,” FRENER REIFER, [Online]. Available: https://www.frener-reifer.com/news-en/iona-skydome/. [Accessed 8 July 2020].

[75] P. Sadooghi and N. P. Kherani, “Thermal analysis of triple and quadruple windows using partitioning radiant energy veils with different physical and optical properties,” *Solar Energy,* vol. 174, pp. 1163-1168, 2018.

[76] N. Garg, A. Kumar and S. Maji, “Parametric sensitivity analysis of factors affecting sound insulation of double glazing using Taguchi method,” *Applied Acoustics,* vol. 74, pp. 1406-1413, 2013.

[77] Y. Wang, K. Li, Y. Su, W. Lu, Q. Wang, J. Sun, L. He and K. Liew, "Determination of critical breakage conditions for double glazing in fire," *Applied Thermal Engineering,* vol. 111, pp. 20-29, 2017.

[78] *SFS-EN 1279-5:2018 Glass in building. Insulating glass units. Part 5: Product standard,* Helsinki: Finnish Standards Association.

[79] *SFS-EN 1279-3:2018 Glass in building. Part 3: Long term test method and requirements for gas leakage rate and for gas concentration tolerances,* Helsinki: Finnish Standards Association.

[80] M. D. Knorr, J. Wieser, G. Geertz, S. Buddenberg, M. Oechsner and W. Wittwer, “Gas loss of insulating glass units under load: internal pressure controlled permeation test,” *Glass Structures & Engineering,* vol. 1, pp. 289-299, 2016.

[81] L. Galuppi, G. Manara and G. Royer Carfagni, "Practical expressions for the design of laminated glass," *Composites: Part B,* vol. 45, pp. 1677-1688, 2013.

[82] “Trofisol - World of Interlayers: SentryGlas,” [Online]. Available: https://www.trosifol.com/products/architecture/trosifolr-structural-security/sentryglasr/. [Accessed 5 May 2020].

[83] “Laminated Glass, Noviflex Interlayer - AGP Plastics,” 2020. [Online]. Available: https://www.agpplastics.com/laminated-glass/. [Accessed 5 May 2020].

[84] J. Kuntsche, M. Schuster and J. Schneider, "Engineering design of laminated safety glass considering the shear coupling: a review," *Glass Structures & Engineering,* vol. 4, pp. 209-228, 2019.

[85] "TPU Safety Glazing Krystalflex Brochure," Huntsman, [Online]. Available: https://huntsman-pimcore.equisolve-dev.com/Documents/TPU_Safety_Glazing_Krystalflex_Brochure.pdf. [Accessed 4 August 2020].

[86] *SFS-EN 16613:2019 Glass in building. Laminated glass and laminated safety glass. Determination of interlayer viscoelastic properties,* Helsinki: Finnish Standards Association.

[87] L. Galuppi and G. Royer-Carfagni, “The post-breakage response of laminated heat-treated glass under in plane and out of plane loading,” *Composites Part B,* vol. 147, pp. 227-239, 2018.

[88] L. Galuppi and G. Royer-Carfagni, “A homogenized model for the post-breakage tensile behavior of laminated glass,” *Composite Structures,* vol. 154, pp. 600-615, 2016.

[89] M. Arıcı, H. Karabay and M. Kan, “Flow and heat transfer in double, triple and quadruple pane windows,” *Energy and Buildings,* vol. 86, pp. 394-402, 2015.

[90] Z. Respondek, “Heat transfer through insulating glass units subjected to climatic loads,” *Materials,* vol. 13, article 286, 2020.

[91] R. Hart, H. Goudey, D. Arasteh and D. C. Curcija, “Thermal performance impacts of center-of-glass deflections in installed insulating glazing units,” *Energy and Buildings,* vol. 54, pp. 453-460, 2012.

[92] I. Ivanov, D. Velchev, N. Penkova, K. Krumov and V. Iliev, “Stress analysis of insulating glass units under transient thermal loadings,” *Journal of Chemical Technology and Metallurgy,* vol. 53, no. 6, pp. 1095-1102, 2018.

[93] S. D. Rezaei, S. Shannigrahi and S. Ramakrishna, “A review of conventional, advanced, and smart glazing technologies and materials for improving indoor environment,” *Solar Energy Materials & Solar Cells,* vol. 159, pp. 26-51, 2017.

[94] A. A. Husain, W. Z. W. Hasan, S. Shafie and M. N. Hamidon, “A review of transparent solar photovoltaic technologies,” *Renewable and Sustainable Energy Reviews,* vol. 94, pp. 779-791, 2018.

[95] R. Tällberg, B. P. Jelle, R. Loonen, T. Gao and M. Hamdy, “Comparison of the energy saving potential of adaptive and controllable smart windows: A state-of-the-art review and simulation studies of thermochromic, photochromic and electrochromic technologies,” *Solar Energy Materials and Solar Cells,* vol. 200 109828, 2019.

[96] *SFS-EN ISO 717-1:2013 Acoustics. Rating of sound insulation in buildings and of building elements. Part 1: Airborne sound insulation,* Helsinki: Finnish Standards Association.

[97] "Trofisol - World of Interlayers: Product Brochures," Kuraray CO., LTD, 2019. [Online]. Available: https://bit.ly/3cJctCf. [Accessed 18 May 2020].

[98] K. Miskinis, V. Dikavicius, R. Bliudzius and K. Banionis, “Comparison of sound insulation of windows with double glass units,” *Applied Acoustics,* vol. 92, pp. 42-46, 2015.

[99] R. Assaf, G. Descombes, F. Guillemard, E. Elhachem and W. Larbi, "Experimental evaluation of sound transmission through single, double and laminated glazing," *AIP Conference Proceedigns 184, 020045,* 2017.

[100] "Trofisol - World of Interlayers: Trofisol Acoustis," Kuraray CO., LTD, [Online]. Available: https://www.trosifol.com/products/architecture/trosifolr-acoustic/. [Accessed 18 May 2020].

[101] A. N. Puzankov, D. L. Shchegolev, V. A. Tishkov and V. N. Bobylev, "Extra edge damping as a way to improve sound insulation of window structures," *International Journal of Acoustics and Vibration,* vol. 23, pp. 106-112, 2018.

[102] Y. Wang, Q. Wang, J. Sun, L. He and K. Liew, “Influence of fire location on the thermal performance of glass façades,” *Applied Thermal Engineering,* vol. 106, pp. 438-442, 2016.

[103] H. Emmons, “The Needed Fire Science,” *Fire Safety Science-Proceedings of the First International Symposium,* pp. 33-53, 1986.

[104] *SFS-EN 357:2004 Glass in building. Fire resistant glazed elements with transparent or translucent glass products. Classification of fire resistance,* Helsinki: Finnish Standards Association.

[105] Y. Wang, J. Sun, L. He, Q. Wang and D. Rush, "Experimental study on fallout behaviour of tempered glass façades with different frame insulation conditions in an enclosure fire," *Proceedings of the Combustion Institute ,* vol. 37, pp. 3889-3898, 2019.

[106] Y. Wang and J. Hu, "Performance of laminated glazing under fire conditions," *Composite Structures,* vol. 223 110903, 2019.

[107] Y. Wang, Q. Xie, Y. Zhang, Q. Wang and J. Sun, “Sensitivity analysis of influencing factors on glass façade breakage in fire,” *Fire Safety Journal,* vol. 98, pp. 38-47, 2018.

[108] X. Centelles, R. J. Castro and L. F. Cabeza, “Experimental results of mechanical, adhesive, and laminated connections for laminated glass elements - A review,” *Engineering Structures,* vol. 180, pp. 192-204, 2019.

[109] “Glazing Systems - Structural Glazing, Conventional Glazing and Walkable Glass,” Novum Structures, 2020. [Online]. Available: https://novumstructures.com/product-system/glazing-systems/. [Accessed 7 May 2020].

[110] M. Feldmann, D. Ungermann, B. Abeln, M. Baitinger and E. Preckwinkel, “Development of innovative steel-glass-structures in respect to structural and architectural design (INNOGLAST),” in *Research Project of the European Research Fund for Coal and Steel, No RFCS-CT-2007-00036, 2007-2010*.

[111] M. Santarsiero, C. Bedon and C. Louter, “Experimental and numerical analysis of thick embedded laminated glass connections,” *Composite Structures,* vol. 188, pp. 242-256, 2018.

[112] M. Santarsiero, C. Louter and A. Nussbaumer, “Laminated connections for structural glass applications under shear loading at different temperatures and strain rates,” *Construction and Building Materials,* vol. 128, pp. 214-237, 2016.

[113] P. Eversmann and A. Ihde, “Laminated Glass Connection Details: Towards Homogeneous Material joints in Glass,” in *Challenging Glass Conference Proceedings, [S.l], v. 6, p. 351-358, May 2018*.

[114] M. Fröling, "Strength design methods for glass structures," *Doctoral Thesis, Structural Mechanics,* 2013.

[115] L. Galuppi and G. Royer-Carfagni, "Enhanced Effective Thickness (EET) of curved laminated glass," *Annals of Solid and Structural Mechanics,* vol. 7, pp. 71-92, 2015.

[116] L. Galuppi and G. Royer-Carfagni, "Enhanced Effective Thickness for laminated glass beams and plates under torsion," *Engineering Structures,* vol. 206 110077, 2020.

[117] M. López-Aenlle and F. Pelayo, “Static and dynamic effective thickness in five-layered glass plates,” *Composite Structures,* vol. 212, pp. 259-270, 2019.

[118] M. López-Aenlle and F. Pelayo, "Dynamic effective thickness in laminated glass-beams and plates," *Composites: Part B,* vol. 67, pp. 332-347, 2014.

[119] G. Campione, G. Minafò and V. Rondello, "Approximate solution on large deflection of glass panels subjected to uniform pressure," *Journal of Engineering Mechanics,* vol. 141, no. 5: 04014152, 2015.

[120] “Contained fluid in an ANSYS® mechanical (worckbench) FEA model: working with HSFLD242 elements,” SimuTech Group, [Online]. Available: https://bit.ly/3iKp7oh. [Accessed 10 June 2020].

List of appendices

Appendix 1. Strength assessment of ship window according to Lloyd's Register

The required thickness for single thermally toughened glass pane according to Lloyd's Register [14] is

$$t_0 = b\sqrt{\frac{H_d\beta}{4000}} \tag{12}$$

where b is the length of shorter side of window [mm]
H_d is the design pressure head [m]
$\beta = 0.54A_R - 0.078{A_R}^2 - 0.17\ for\ A_R \leq 3$
$\beta = 0.75\ for\ A_R > 3$
A_R is the aspect ratio of window, a/b.

The equivalent thickness of laminated glass is

$${T_{L1}}^2 + {T_{L2}}^2 + \cdots + {T_{Ln}}^2 = {T_S}^2 \tag{13}$$

where n is the number of laminates
T_{Li} is the thickness of glass laminate
T_S is the thickness of toughened safety glass.

The design pressures are presented in Figure 41.

Window location	Design pressure head H_d in metres
Between the design waterline and a point $Z_{1,5}$ m above the waterline	Per BS MA 25: 1973
Between a point $Z_{1,5}$ m above the waterline and the deck immediately above (at $Z_{d1,5}$)	1,5
Over the next 2 'tween deck heights	$1,5 - f_w\left(\frac{Z_w - Z_{d1,5}}{H_{t1} + H_{t2}}\right)$
For subsequent decks to the top of the navigation bridge	0,25 sides and aft ends 0,75 house fronts
From the top of the navigation bridge to the uppermost deck, for house fronts	0,75 at top of navigation bridge 0 at uppermost continuous deck, with linear variation between, but not less than 0,25
From the top of the navigation bridge to the uppermost deck, at sides and aft ends	0,25

Symbols

f_w = 1,25 in way of sides and ends of superstructures

= 0,75 in way of house fronts

$Z_{1,5}$ = the vertical location in metres above the waterline at which the BS MA:25 pressure as given in Annex E of BS MA:25 (1973) is 1,5 t/m^2

$Z_{d1,5}$ = the vertical location in metres of the deck at which the pressure is 1,5 t/m^2 from *Table 2.11.1 Acceptable arrangements of glazing in lieu of portable storm covers/deadlights*

Z_w = the vertical location in metres above the waterline to the point under consideration

$H_{t1} + H_{t2}$ = sum of the appropriate 'tween deck heights in metres

Figure 41. Design pressure on windows according to LR [14].

Appendix 2. General properties of polymeric interlayers

The main interlayer materials are polyvinyl butyral (PVB), ionomer (SentryGlas® from the Trofisol™ product portfolio), ethylene-vinyl acetate (EVA) and thermoplastic polyurethane (TPU) [49]. The main features of each are presented in Table 18 and the mechanical properties in Table 19. It should be mentioned that SentryGlas® is a product by Kuraray Co., Ltd [82] and hardly any other ionomer interlayers exist with the exception of Noviflex® [83].

Table 18. The main features of different interlayers in laminated glasses [49].

Interlayer material	Features
PVB	Good mechanical and optical properties, good adhesion to glass with high light transmission, blocks UV radiation almost completely, multiple commercially available products for different purposes
Ionomer	Excellent mechanical properties for structural use, durable and high transparency, less sensitive to changes in temperature and load durations, good adhesion to glass and metals
EVA	Stress-crack resistance, high flexibility, toughness and elasticity associated with good impact strength, encapsulation material for silicon cells in photovoltaic modules
TPU	Good mechanical properties, resistant to UV radiation, abrasion and chemical degradation, used in hybrid components due to its high bonding strength

PVB is the most common interlayer material for laminated glasses. The market shares of the rest are smaller and therefore significantly fewer research results are available [84]. The nominal thickness of a single foil is 0.38 mm but typically two (0.76 mm) or four (1.52 mm) foils are used to form the interlayer [17]. A comprehensive review by Martín et al. [49] describes the polymeric interlayers, their mechanical aspects, ageing resistance and recyclability.

Table 19. Mechanical properties of typical commercial interlayers in laminated glasses.

Property	PVB[a]	Ionomer[a]	EVA[a]	TPU[b]
Density (kg/m³)	915-1070	950	970	1070
Tensile strength (MPa)	20.8-33.0	34.5	26.0	36
Elastic modulus (MPa)	2.36	300-480	7-9	3
Poisson's ratio (-)	0.5	0.442-0.500	0.47-0.49	-
Elongation at failure (%)	190	400	450	440

[a] according to [49]
[b] KRYSTALFLEX® PE399 from the company Huntsman [85]

The polymeric interlayers are viscoelastic materials. The physical properties are therefore temperature and loading time dependent (e.g. snow load vs. wind loads) [17]. The stiffness of the material decreases as the temperature and loading time increase. For example, laminated glasses subjected to sustained loads in four-point bending tests have shown progressive increase in deflection due to the interlayer creeping in multiple temperatures [49]. Furthermore, the glass transition temperature of the interlayer is important as it presents a temperature range in which significant decrease in stiffness is experienced [84]. The determination of viscoelastic properties is defined in EN 16613 [86], where the interlayers are divided to three families depending on their stiffness at some specified load case and temperature.

Additionally, non-fractured laminated glass exhibits shear transfer between the glass panes via the interlayer. The amount depends on the interlayer's shear stiffness, hence on temperature and time. Two limits cases are distinguished: full shear transfer and no shear transfer (Figure 42). Assuming either would result in unsafe or uneconomical design, respectively. The flexural behavior of laminated glass is dependent on the amount of shear transfer. In full shear transfer, the flexural rigidity would correspond to the total thickness of the laminated glass [81]. Similarly, the flexural rigidity in no shear transfer is the sum of the individual panes.

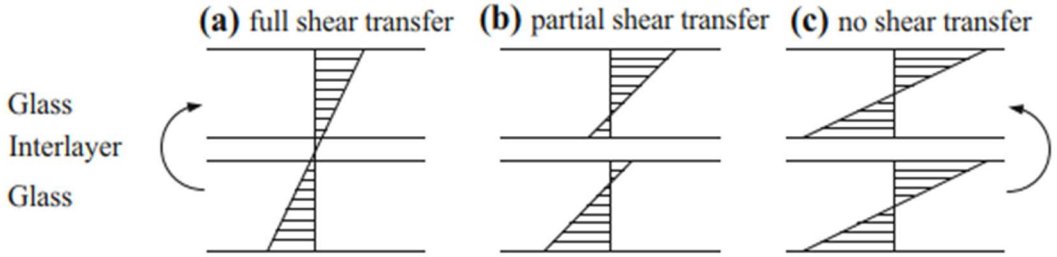

Figure 42. Shear transfer between glass panes in laminated glass and the corresponding stress distribution across the thickness [84].

Kuntsche et al. [84] studied the shear coupling and its usage. The study concluded that even small values of shear modulus lead to significant reduction of glass stresses. Therefore, partial shear transfer is preferred even though there is no consensus between different standards. EN 16612 [28] defines a shear transfer coefficient, ω, that depends on load case and the family of the interlayer. The stiffest interlayers have ω of 0.1-0.7 depending on the load case. However, no shear transfer is allowed for the permanent loads.

Appendix 3. Post-breakage behavior of laminated glass

Glass breaks without any inherent ductility and hence the interlayer in laminated glass is used to retain the fragments. The post-breakage capacity can be considered at structural system level or at individual structural element level. In applications where failing of an element poses a high local threat, e.g. overhead glazing, the latter is of an interest. Then only partial failure should be allowed. At structural system level, if individual element fails completely, the loads are redistributed to the adjacent elements [17]. A "fail-safe" concept is used that prescribe that if one or more elements fail, the overall stability of the structure must be maintained [25]. This is achieved by ensuring that any failed element is able to withstand the permanent loads and a part of the live loads.

Determining the post-breakage load carrying capacity of laminated glass is complicated as it is dependent on the glass-interlayer adhesion properties, the interlayer stiffness and the shape and size of the fragments [87]. Therefore, it is beneficial to use a stiff interlayer (e.g. ionomer) and glasses that break into large fragments (e.g. heat strengthened). A panel consisting only of fully tempered (small fragments) glass normally sags like a wet towel upon breaking and the residual capacity relies only on the tensile strength of the interlayer. In case of hybrid laminated glass, fully tempered glass should be located on the tension side [17].

Breaking due to out-of-plane bending and the corresponding residual capacity can be described in three stages (Figure 43): 1) both plies are intact; 2) the top ply carries the load while the bottom ply is broken; 3) both plies are broken but the top ply fragments lock together in compression while the tensile stress is sustained by the interlayer.

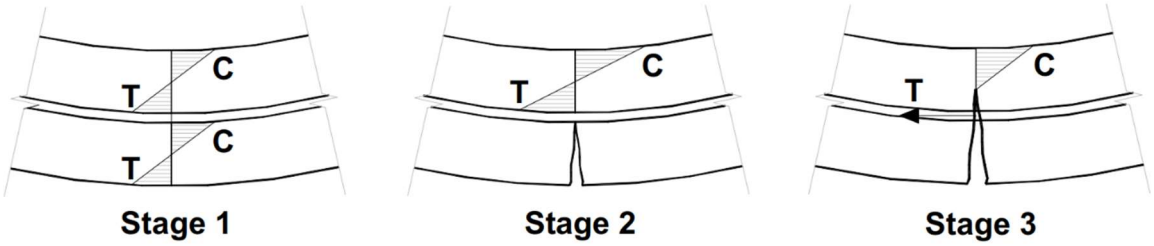

Figure 43. Post-breakage stress distribution of laminated glass in out-of-plane bending, the three stages [17].

Similar behavior can be observed during in-plane bending in addition of tension stiffening of the interlayer i.e. increase in the elastic modulus. This effect is caused by the adhesion of the interlayer with the broken shards and hence the degree of delamination plays an important role. The tension stiffening occurs in out-of-plane bending as well but in lesser proportions. In case of in-plane load (tensile), the residual capacity is governed only by the tension stiffening of the interlayer.

The response of a broken laminated glass can be estimated through homogenization if small fragments are assumed [88]. Based on this, the post-breakage behavior of laminated glasses can be evaluated using effective stiffness concept for the aforementioned loading cases [87].

Appendix 4. Thermal performance of IGU and energy saving applications

Thermal insulation is the most important property of an insulating glass unit. The performance is expressed with center of glass (COG) U-value or with thermal transmittance [75]. The thickness of the cavity is therefore one of the main influencing factors. Thicker the cavity, lower the U-value, better the insulation. For this reason, TIGUs have up to 67% better thermal performance over DIGUs [89]. Heat loss is increased if a double glazed unit takes a concave shape due to the climate loads e.g. in wintertime when temperature falls (Figure 11) [90]. This heat loss can be significant in cases where the initial cavity gap is smaller than optimal [91].

From structural point of view, the influence of the cavity temperature changes on the stresses in the glasses is insignificant. Daily changes in ambient temperature and solar radiation can cause stress concentrations on the edges of the glass that could lead to crack initiation [92]. However, risk of thermal breakage is normally only high for annealed glass. Maximum allowable temperature difference on the glass is around 40 °C, 100 °C and 200 °C for annealed glass, heat strengthened glass and fully tempered glass, respectively [17].

The temperature of the glass can further increase when some energy saving film or coating is applied to enhance the heat loss reduction. A comprehensive review by Rezaei et al. [93] describes all the window energy saving technologies. The summary of the work is presented in Figure 44.

Husain et al. [94] reviewed in detail the photovoltaic technologies that are used to harvest the solar energy. Tällberg et al. [95] reviewed the adaptive and controllable smart windows that include e.g. electrochromic technology that is used to dim airplane windows. The need for energy efficient technology is obvious but all the sophisticated technologies are still either expensive, hard to implement or not commercially available.

	Glazing technology	Benefit	Drawback
Static	Tinted glass	• Decreases glare	• Absorbs solar energy and releases heat into the building • Decreases visible transmittance
	Reflective coating	• Decreases glare • Reflects NIR radiation	• Decreases visible transmittance
	Low-E and solar control coating	• Reflects NIR or IR radiation • Reduces heat reradiation by the window	• Decreases *SHGC* (should be high for cold climates)
	Anti-reflective coating	• Enhances visible transmittance	• Increases *SHGC* (should be low for hot climates)
	Self-cleaning coating	• Visibility is maintained for longer time (due to self-cleaning)	–
	Aerogel	• Exceptionally low thermal conductivity • Glare reduction	• Translucent
	Multiple-pane glazing	• High insulating properties (low thermal conductivity, noise reduction) • Can be used to combine various technologies for desired properties	• Occupy considerable space (especially for triple and quadruple glazing) • Expensive
Passive	PCM	• Reduces building environment thermal fluctuation	• Translucent • Needs a chamber since it turns into liquid
	Thermochromic	• Reduces glare • Reflects NIR radiation • Reduces *SHGC*	• Low visibility • Solar modulation is not substantial • Activation temperature is high
Active	Electrochromic	• Solar modulation • Glare control	• Expensive • Limited modulation levels • Long response time relative to other active systems • Needs electrical energy for transparency modulation (very low) • Relatively Low *SHGC* for cold climates
	Spectrally tunable EC	• Independently modulation of NIR and visible spectra • *SHGC* may be controlled without affecting visible transmittance • Useful for various climates • Glare control	• Is not commercialized; however, first four drawbacks of conventional EC still hold
	PV EC	• Solar modulation • Glare control • Self-powered	• Very low visible transmittance
	Gasochromic	• Solar modulation • Glare control • Faster response time relative to EC • Simpler layer structure than EC	• Not commercialized yet • Needs special equipment (electrolyser) and electrical energy for operation
	SP	• Solar modulation • Glare control • Fast response time • Vast transparency levels	• Needs electrical energy for maintaining transparency levels (except fully tinted) • Electric power consumption is higher than EC but still low • Relatively low *SHGC* for cold climates • expensive
	LC	• Glare control • Becomes translucent (for privacy applications)	• Needs electric power for remaining transparent • Cannot modulate *SHGC*

Figure 44. Summary of energy saving technologies [93].

Appendix 5. Noise insulation performance of IGU

Insulating glass units provide sound insulation that is necessary for comfort in many applications. The sound insulation performance is described with Weighted Sound Reduction Index (R_w) and spectrum adaptation terms (C , C_{tr}) [96]. The adaptation terms are used include the different spectra of noise sources (C is for pink noise, $C_{tr}$is for road traffic noise) and always have negative value. The effectiveness of the insulation is thus given as R_w, $R_w + C_{tr}$ or $R_w + C$ depending on the application. Higher the resulting value, better the insulation. A comparison of achieved R_w between different configurations is presented in Figure 45.

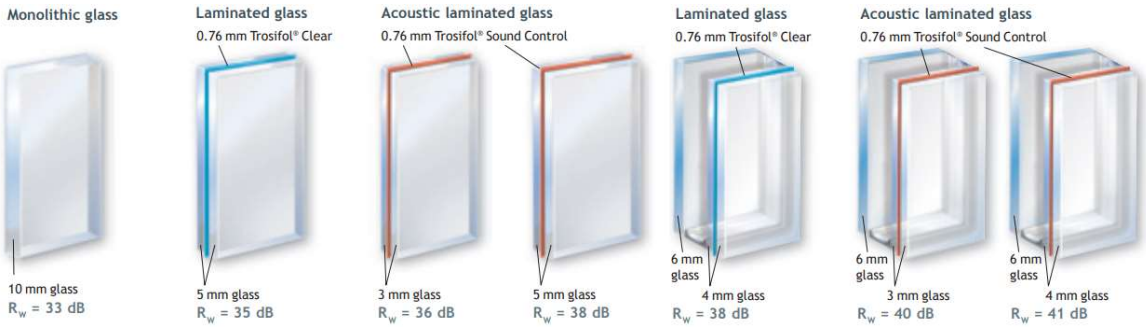

Figure 45. Comparison of Weighted Sound Reduction Index at some frequency between different configurations according to Trofisol™ product brochure [97].

In parametric study it was found that the thickness of the cavity had the most influence on the sound insulation [76]. Thicker the cavity, better the sound insulation. The thickness of the back pane had a little bit more contribution to the total sound insulation than the front glass pane. The effect of window frame and insulation were not studied but their effect on the sound insulation was highlighted.

Low frequency sounds are harder to attenuate. In an experimental study, DIGU consisting of two laminated glasses provided sound attenuation of 30 dB at 125 Hz while the same number for monolithic DIGU (monolithic/monolithic) and hybrid DIGU (monolithic/laminated) was obtained at 315 Hz and 250 Hz, respectively [98]. Therefore, using two laminated glasses in DIGUs is beneficial for better attenuation of low frequency noises. The insulation performance in DIGUs however drops at some low frequency range, called mass-air-mass frequency, where strong coupling of the panes occurs [99].

If the sound insulation performance is insufficient, three methods are identified for increasing it without adding significant mass: 1) adding a transparent film on the outer pane; 2) using a transparent acoustic interlayer between the glasses (e.g. Trofisol™ Sound Control [100]); 3) adding external non-transparent dampeners [101]. External dampeners however come with a visual impact and therefore acoustic interlayer would be a better solution. However, they are PVB type and not as good for structural applications as e.g. SentryGlas®. Hence a tradeoff has to be considered.

Appendix 6. Fire safety considerations of glasses

Glasses pose a vulnerable component for enclosed spaces in case of a fire. A broken window that falls off creates a new path for the fire to spread and an air entrance that accelerates the fire within the compartment [102]. A radiant heat source, i.e. a fire, increases the temperature of the glass that results in thermal expansion. If the thermal expansion of the glass is not uniform, local tension initiates crack growth that leads to failure [103]. This is practically true to all of the windows as the frame and the supports cover fully or partially the edges, or the radiant heat source is local.

Different performance indicators for fire resistance are defined in EN 357 [104]. The time to first crack occurrence is often used in the literature to compare the performance of different cases. Several experimental and numerical studies have been conducted to determine fire resistance.

Location of the fire and the support type influences the time to first crack occurrence. Point supported glass is more prone to breaking when the fire is close to the fixing. Linearly supported glass on the other hand breaks faster if the fire is located in the center of the glass [102].

The type of glass and the configuration have a considerable influence on the fire resistance. Annealed float glass breaks the fastest as it can withstand the least temperature differences (40 °C, see Table 4). A fully tempered glass can withstand much higher temperature differences, up to 380 °C [105]. The break time can be further increased using laminated glass [106] and insulating glass unit [77]. In those cases, the pane that is not directly heated survives longer because the thermal conductivity of the glass, the interlayer and the gas (in IGU) is low. Therefore, the fire resistance is improved. The significance of each factor is presented in Figure 46.

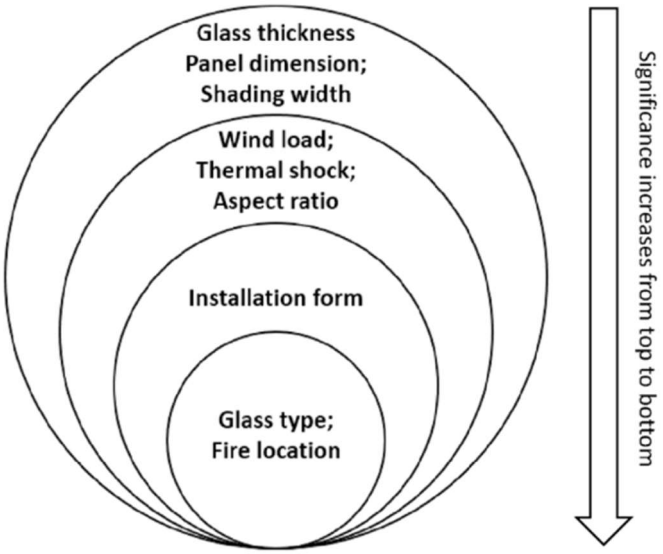

Figure 46. Significance of different factors influencing the fire safety of glasses [107]

Appendix 7. Glass connections

The glass connections are typically divided to two main groups: mechanical connections and adhesive connections [17]. The connection can also be a combination of these two. The support types are divided to linear and local supports (Figure 47). Some intermediate material is used to prevent direct contact between the glass and any harder material to prevent failure that could occur due to high stress concentration.

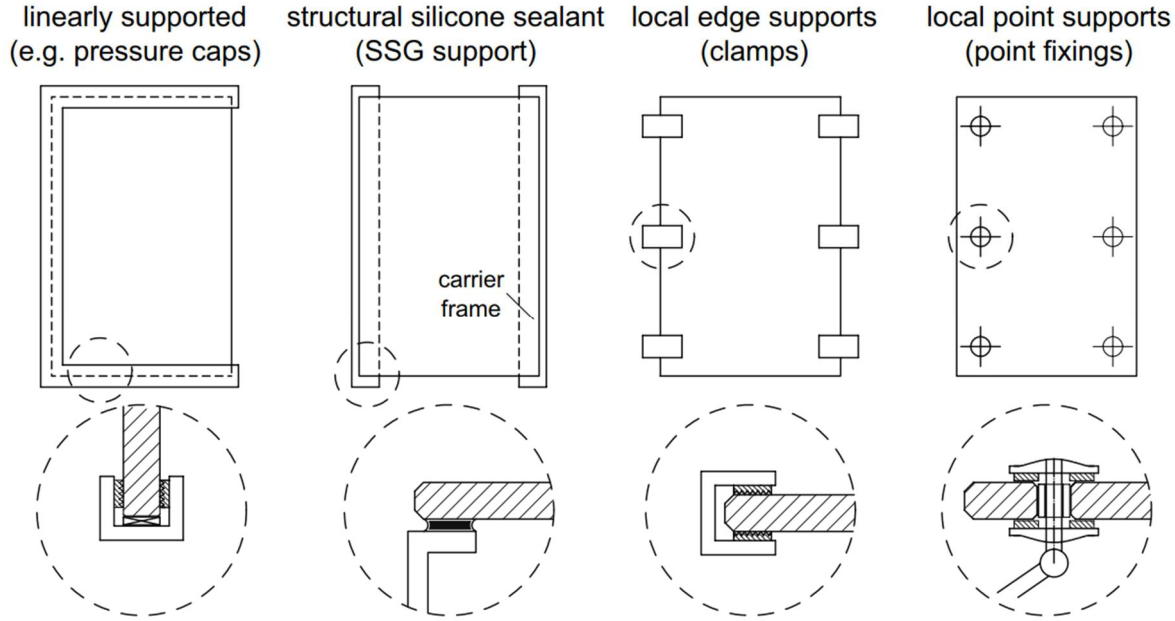

Figure 47. Principle sketch of common glass connection support types [17].

The trend in the glazing design has been to reduce the size of the supports while increasing their ability to transfer loads. This could lead to high local stresses even with the intermediate material, especially in small point supports. Thus, identifying the capabilities of the chosen connection and support type is important. A comprehensive review by Centelles et al. [108] describes the glass connections and their experimental results.

Mechanical connections are achieved by clamps and bolts, presented in Figure 48. The clamps are divided to low-friction clamps and friction-grip clamps depending how tightly they are fastened. Bolt connections are divided to through bolts and countersunk bolts.

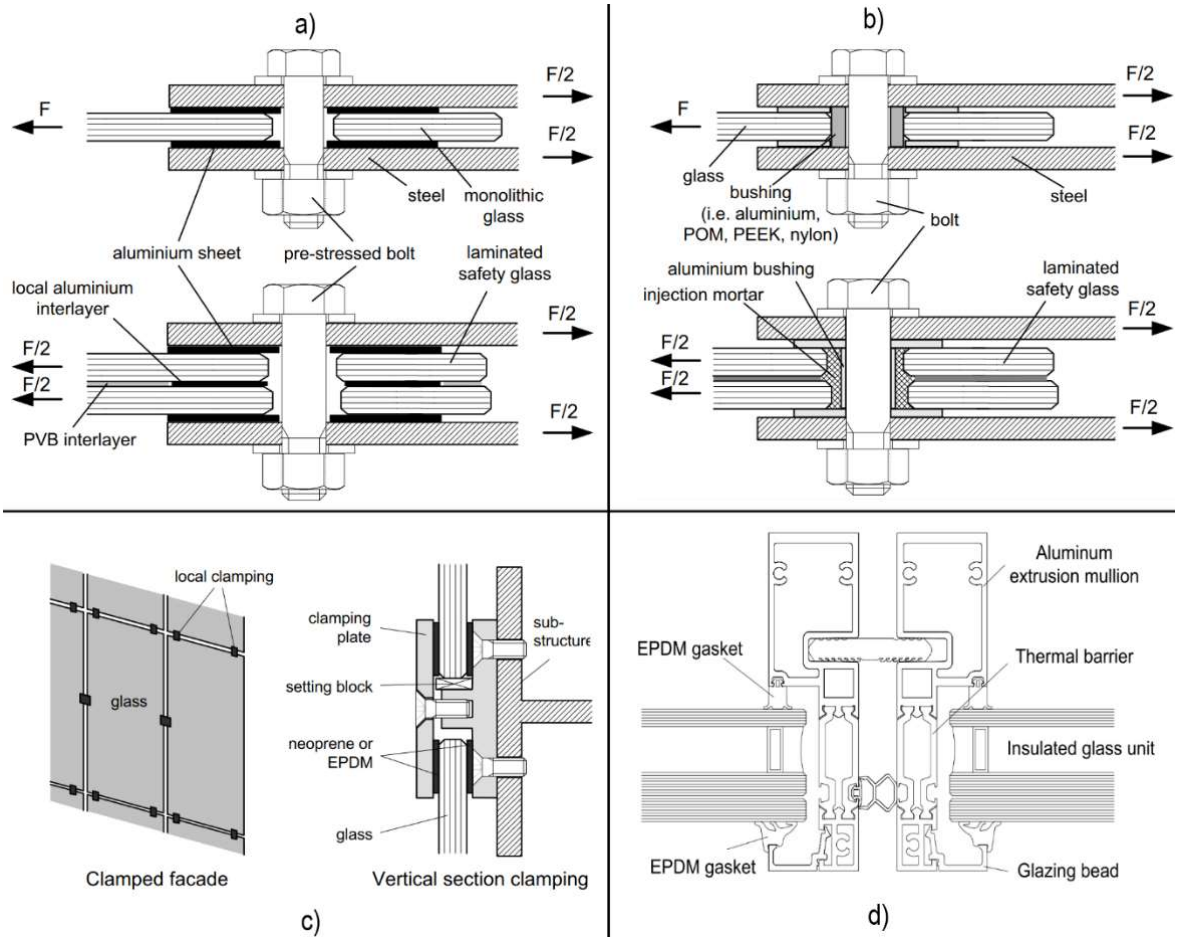

Figure 48. Principal sketches of different mechanical connections: a) friction-grip clamp; b) through bolt; c) low friction clamp (local); d) low friction clamp (linear) [17].

In low friction clamped connection the clamp merely holds the glass pane in place and is designed to resist loads perpendicular to the glass surface (case "c" and "d" in Figure 48). In vertical constructions the self-weight is transmitted to the frame by some block or intermediate material (setting block).

Friction-grip connections are tightly fixed to resist also in-plane loads (case "a" in Figure 48). In case of laminated glass, the interlayer between the glass panes has to be replaced by some other material in the vicinity of the connection because of the viscoelastic behavior (creeping) under long-term loading. See "local aluminium interlayer" in Figure 48.

Clamp supports can be either local (edge and corner) or linear and can be applied to any glass configuration (monolithic, laminated, insulating glass unit) [109].

Through bolt connections have similar lap joint construction as the friction-grip connection and therefore can be used to transmit in-plane loads (case "b" in Figure 48). Countersunk bolts are used reduce visual impacts of the structure i.e. no lap joint is used and hence not suitable for in-plane loads.

The advantage of clamped connections compared to bolted connections is that the pressure is distributed more evenly on the glass surface. Hence, the applied clamping results in lower stress concentrations. Moreover, several other parameters must be also

considered in bolted connections as they are susceptible to stress concentrations in the vicinity of the hole [17].

Adhesive connections, also called as glued connections, are an alternative to mechanical connections. The advantages over the mechanical connections are that the load is more uniformly distributed on to the glass surface, no holes are required, lesser visual impact is achieved, vibration damping is enhanced and better tolerance adjustment is allowed [108]. The disadvantages include lower strength and working temperature and weathering dependency. Two types of glued connection are used to obtain adhesion between glass and glass, metal or some other material:

- soft and rigid adhesives (epoxy resins, polyurethanes, acrylates, silicones)
- laminated connections (same as the interlayer material used in laminated glass).

Structural-silicone-sealant is a traditional soft connection used in architectural glazing. Being soft, it is able to reduce stress concentrations but cannot transfer high shear forces. Rigid adhesives provide stiffer and stronger adhesion and hence smaller supports can be used. The comparison of the most commonly used adhesives is presented in Table 20.

Table 20. General comparison of four common adhesives used in glued glass connections [110].

	Tension and shear strength	Stiffness	Ductility	Viscosity	Temperature resistance	Ageing behaviour	UV resistance	Transparency, colour
Epoxy resin	+ + +	+ + +	+	+ + +	+ +	+ +	+ +	+
Polyurethane	+ +	+ + +	+ +	+ +	+ +	+ +	+ +	+ +
Acrylate	+ +	+ +	+ +	+ +	+ +	+ + +	+ + +	+ + +
Silicone	+	+	+ + +	+	+ + +	+ + +	+ + +	+

The same interlayer material that is used to form the laminated glass, is used to create connection between glass and glass or some other material. Laminated connections have good mechanical properties with high transparency as these are normal demands for laminated glasses in general. The four most used materials are PVB, Ionomer, EVA and TPU (see section 2.2).

The interlayer can be used to bond a metal insert in the laminated glass to create an “embedded laminated connection” [111]. Similarly, a metal connector can be laminated on the surface of the glass [112]. Both of these provide a connection method that does not require drilling a hole in the glass because the bolt connection is in the metal element (Figure 49). In the future, fully transparent structures could possibly be built using laminated connections [113].

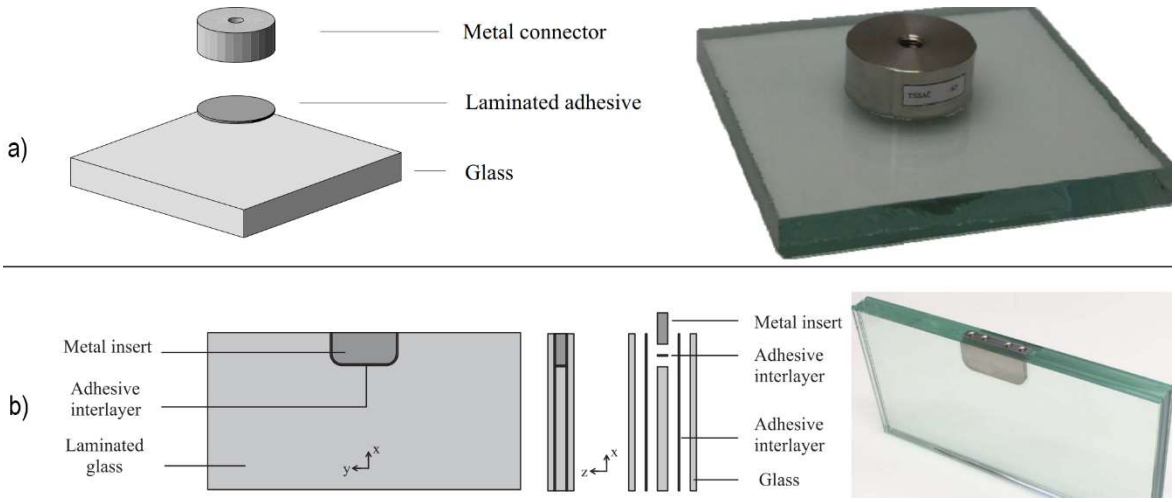

Figure 49. Examples of laminated connections: a) Metal connector on the surface [112]; b) embedded metal insert [111].

Appendix 8. Finite element modelling of laminated glass

Finite element (FE) method is commonly used to analyze the mechanical behavior of laminated glass structures.

Two common FE models for laminated glass are 3D solid model and layered shell model (2D). While the first is very accurate model as each 3D solid element has nodes in every direction, it is very expensive computationally because several elements are required across the thickness. The latter model is built layerwise using 2D shell elements with corresponding material properties. The model is significantly faster as there are fewer nodes. However, as the shell element is two dimensional, the transverse displacement is described by only one node i.e. stress distribution across the thickness cannot be expressed.

A solid-shell element has been found to give accurate displacement and stress results with computational efficiency [114]. It is a 3D solid element that has been modified for analyzing shell-like structures i.e. only one element is required thickness wise per layer. The advantage is that the stress distribution across the thickness can be calculated, unlike in shell elements. Even though faster methods and computations are developed, they can be inconvenient especially in the early design phase due to time limitations.

Practical approximations present an alternative method for modelling laminated glass [81]. Two concepts have been proposed in the recent years: effective thickness and effective Young's modulus. In both approaches, an equivalent monolithic glass is created that represents the laminated glass with regards to deformation and stresses. The effective properties are required as the strength and the stiffness of a laminated glass are less than of a monolithic glass with equal thickness.

In the first concept, deflection-effective thickness and stress-effective thickness are used to estimate the deflection and stresses, respectively, of a laminated glass. Galuppi et al. [81] proposed an enhanced effective thickness (EET) method for rectangular laminated glass plates that could be applied to most various static schemes and loading conditions. The results showed good agreement with the numerical methods. The same method has been applied to curved LG plates [115], LG plates under torsion [116] and LG plates with multiple layers [117]. Equivalent thickness calculation method for linearly supported uniformly loaded laminated glass is also presented in EN 16612 [28].

The effective Young's modulus is suggested as an alternative for the effective thickness. These two methods are equivalent i.e. they can be used interchangeably. However, the effective Young's modulus is more appealing when using finite element method as the thickness of the plate remains constant, while the modulus is changed depending on the time and temperature [118].

All the effective approaches typically neglect the viscoelasticity and the geometric non-linearity. An approximate solution for LG panel subjected to uniform pressure is presented by Campione et al. [119] that include the viscoelasticity and the geometric nonlinearity.

Three material models for the interlayer are commonly used: linear elastic, hyperelastic and viscoelastic model [30]. With small deformations, constant temperatures and short loading times, the linear elastic material model is typically sufficient. The viscoelasticity should be included for obtaining reliable numerical results as the interlayers are highly rate-, time- and temperature dependent [25]. The hyperelastic material models are suitable for small deformations and they can be extended for the rate dependencies.

For modelling the adhesion between the interlayer and the glass, the simplest and the most popular way is to assume perfect bonding i.e. they share the nodes in FE models. Penalty-based and intrinsic cohesive model are proposed (Figure 50) for representing the real adhesion. The cohesive model has been found to be very suitable for non-perfect bonding modelling [30].

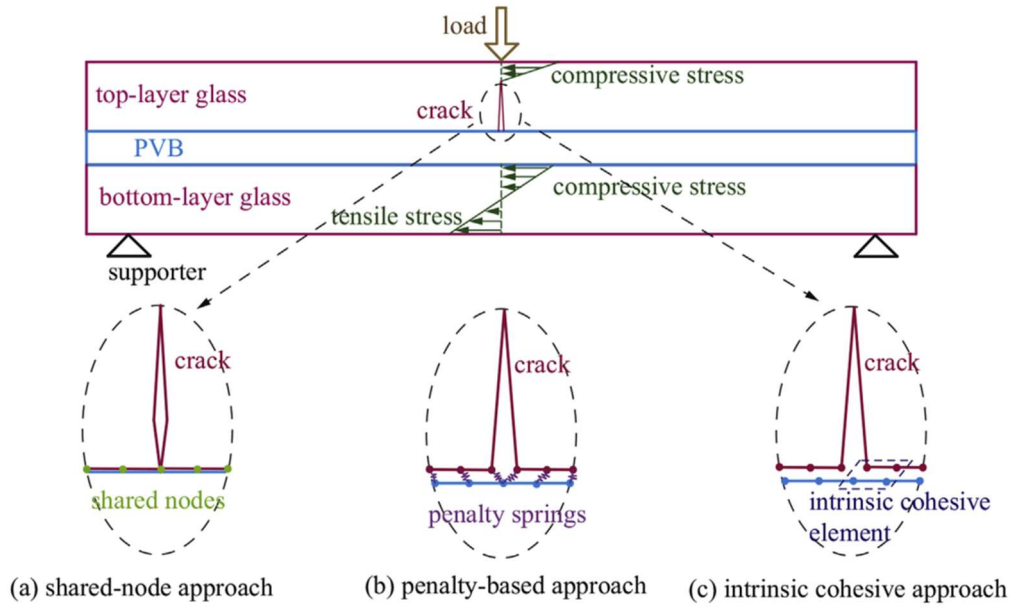

Figure 50. Modelling techniques for bonding of PVB interlayer and glass [30].

Appendix 9. Ansys routine for the hydrostatic fluid element

The hydrostatic elements are created under Analysis work tree using APDL command as seen below. The code is adapted from [120].

```
!Commands inserted into this file will be executed just prior to the ANSYS SOLVE command.
!These commands may supersede command settings set by Workbench.
!Active UNIT system in Workbench when this object was created:  Metric (mm, kg, N, s, mV, mA)
!NOTE:  Any data that requires units (such as mass) is assumed to be in the consistent solver unit system.
!See Solving Units in the help system for more information.


!   Commands inserted into this file will be executed just prior to the ANSYS SOLVE command.
!   These commands may supersede command settings set by Workbench.

!   Active UNIT system in Workbench when this object was created:  Metric (mm, kg, N, s, mV, mA)
!   NOTE:  Any data that requires units (such as mass) is assumed to be in the consistent solver unit system.
!               See Solving Units in the help system for more information.


fini
/prep7
*get,typemax,ETYP,,NUM,MAX              !max defined element type
*get,realmax,RCON,,NUM,MAX              !max defined real constant
*get,mat_max,MAT,,NUM,MAX               !max defined material
*get,nodemax,NODE,,NUM,MAX              !highest numbered node in model

!Create a new higher number for element type, real, and material

newnode=nodemax+1000                    !number for pressure node for HSFLD242
newnumber=typemax+1
*if,realmax,ge,newnumber,then
  newnumber=realmax+1
*endif
*if,mat_max,ge,newnumber,then
  newnumber=mat_max+1
*endif

!Define hydrostatic  fluid element

et,newnumber,HSFLD242                   !3-D Hydrostatic Fluid Element
keyopt,newnumber,1,0                    !Defines degrees of freedom for the hydrostatic fluid
                                        element  0 (default) to activate UX, UY, and UZ degrees
                                        of freedom on the surface nodes (I through P) and HDSP
                                        degree of freedom on the pressure node (Q).
keyopt,newnumber,5,0                    !Specifies how mass is computed for the hydrostatic fluid
                                        element Use KEYOPT(5) = 0 (default) to ignore the mass
                                        contribution from the fluid element.
keyopt,newnumber,6,0                    !Compressible 0, incompressible 1

n,newnode,630,6.5,380                   !Create new pressure node "Q"
type,newnumber
mat,newnumber
real,newnumber
r,newnumber,0.101                       !Reference pressure (real constant)
```

```
!Gas properties
TB,FLUID,newnumber,1,,GAS          !Fluid is gas
TBDATA,1,1.7e-9                    !Density of the gas kg/mm3
TOFFST,273.15                      !Specifies the temperature offset from absolute zero to zero.
TREF,20                            !Defines the reference temperature for thermal strain calculations. Temperature at time of sealing.
BF,newnode,TEMP,20                 !Assign a temperature to pressure node
!IC,newnode,HDSP,0.00              !Initial pressure (can be replaced by surface pressures)


cmsel,s,allnodes                   !Select nodes on interior
esln                               !Select elements that touch these nodes
ESURF,newnode                      !ESURF HSFLD242 elements over solid element faces

cmsel,s,negative
ESLN
esurf,pnode,reverse

allsel
fini
/SOLU
```

Once the simulation is completed, the hydrostatic pressure at the pressure node can be extracted by inputting APDL command in the result work tree as presented below.

```
!Commands inserted into this file will be executed immediately after the ANSYS /POST1 command.

!Active UNIT system in Workbench when this object was created:  Metric (mm, kg, N, s, mV, mA)
!NOTE:  Any data that requires units (such as mass) is assumed to be in the consistent solver unit system.
!See Solving Units in the help system for more information.


/post26
nsol,2,newnode,hdsp
prvar,2
```

Appendix 10. MEPLA ISO analysis report

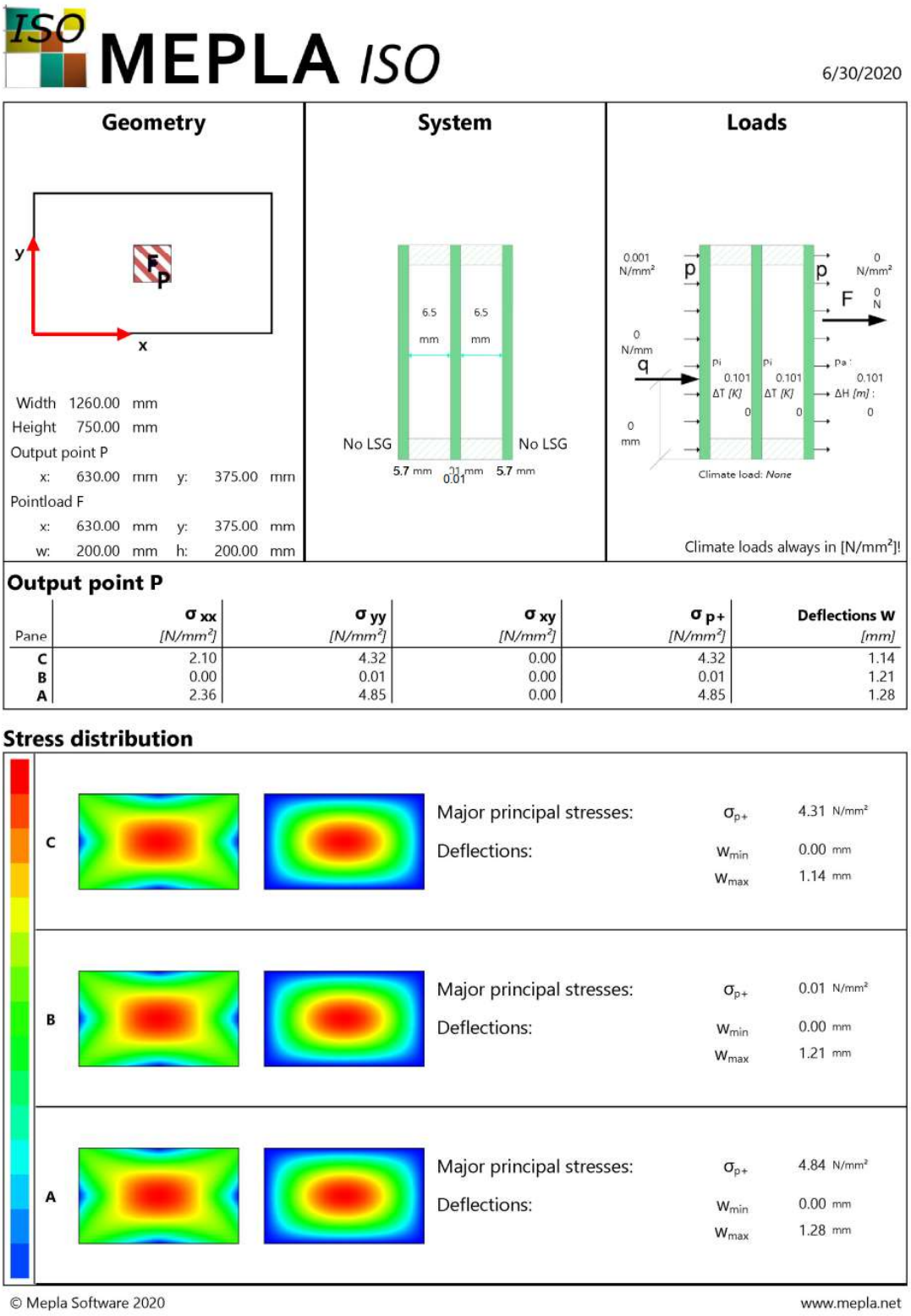

Figure 51. MEPLA ISO [65] report for SDS3 with 1 kPa uniform pressure. A is the directly loaded pane while C is the indirectly loaded. Pane B (middle pane) thickness is set to 0.01mm according to instructions by MEPLA ISO to study DIGUs.

Appendix 11. MATLAB routine for the analytical solution

```
clc; clear all; close all;

%Betti's Analytical Method (BAM) for rectangular IGU with sides a
%and b  corresponding to x and y direction, respectively, subjected
%to uniform pressure

% Initial parameters
a = 2000; % [mm] length of side in x-direction
b = 1400; % [mm] length of side in y-direction
A = a*b; % [mm²] Area of glass pane
h1 = 10; % [mm] thickness of pane 1 (directly loaded)
h2 = 10; % [mm] thickness of pane 2 (indirectly loaded)
s = 20; % [mm] thickness of the spacer (cavity thickness)
E = 70000; % [MPa=N/mm²] Young's modulus of glass
nu = 0.23; % [-] Poisson's ratio of glass
V0 = A*s; % [mm³] Reference volume of cavity at the time of sealing
p0 = 0.101325; % [MPa] Reference pressure of gas in cavity at the time
of sealing
D2 = E*h2^3/(12*(1-nu^2)); % [Nmm] flexural stiffness of pane 2
D1 = E*h1^3/(12*(1-nu^2)); % [Nmm] flexural stiffness of pane 1
T0 = 293.15; % [K] Reference temperature in the cavity at the time of
sealing
%293 means that temperature at time of sealing was 20 °C

p = 0.0000; % [MPa=N/mm²] Uniform pressure acting on pane 1
delta_t = 0; % [K] temperature variation of gas with respect to T0
delta_p =0.000; %[MPa] barometric pressure variation with respect to
p0
%negative delta_p value means that IGU takes pillow shape


% Point of interest in the domain
x = a/2; % [mm] x-point
y = b/2; % [mm] y-point


% Shape function of rectangular plate, simply supported, uniform
pressure
m = 1:2:31;
n = 1:2:31;
%x = 0; For calculating multiple results
 %for k = [1:31] For calculating multiple results
shape_xy = zeros(length(m),length(n));
shape_xytilde = zeros(length(m),length(n));

    for i = 1:length (m)
     for j = 1:length (n)
         for mi = 1:i
              for ni = 1:j

        shape_xy(i,j) = shape_xy(i,j) +
16*a^2*b^2/pi()^6*((sin(m(mi)*pi()*x/a)*sin(n(ni)*pi()*y/b))/(m(mi)*n(
ni)*(((m(mi))^2)*b^2+(n(ni))^2*a^2)^2));
        shape_xytilde(i,j) = shape_xytilde(i,j) +
64*a^2*b^2/pi()^8*(1/((m(mi))^2*(n(ni))^2*((m(mi))^2*b^2+(n(ni))^2*a^2
)^2));
```

```
            end
        end
    end
   end

 %x = x + 42; For calculating multiple results

%Pressure inside the cavity arising from the external load [MPa]
delta_ext = (h2^3 * shape_xytilde(length(m), length(n)) * p) /
((h1^3+h2^3) * shape_xytilde(length(m), length(n)) + (E/(12*(1-
nu^2)))*h1^3*h2^3*V0/(A^3*p0)); % [MPa]

%Pressure inside the cavity arising from temperature variation [MPa]
short = E/(12*(1-nu^2))*(h1^3*h2^3/(h1^3+h2^3));
short1 = E/(3*(1-nu^2))*(h1^3*h2^3/(h1^3+h2^3));
delta_temp = -0.5*(p0+short*V0/(A^3*shape_xytilde(length(m),
length(n)))-
sqrt(T0^2*(A^3*p0*shape_xytilde(length(m),length(n))+short*V0)^2+short
1*A^3*delta_t*T0*V0*p0*shape_xytilde(length(m),
length(n)))/(A^3*T0*shape_xytilde(length(m), length(n))));

%Pressure inside the cavity arising from barometric pressure variation
%[MPa]
delta_p3 = shape_xytilde(length(m),
length(n))/(shape_xytilde(length(m),
length(n))+short*(V0/(A^3*p0)))*delta_p;
delta_baro = delta_p3-delta_p;

%Superimposed pressure in the cavity
delta_p_tot = delta_ext + delta_temp+ delta_baro;
delta_p_p1 = p-delta_p_tot;

%Maximum deflection
w1max = (delta_p_p1/D1)*A^2*shape_xy(length(m), length(n)) % pane 1
[mm]
w2max = (delta_p_tot/D2)*A^2*shape_xy(length(m), length(n)) % pane
2[mm]
%end For calculating multiple results
```